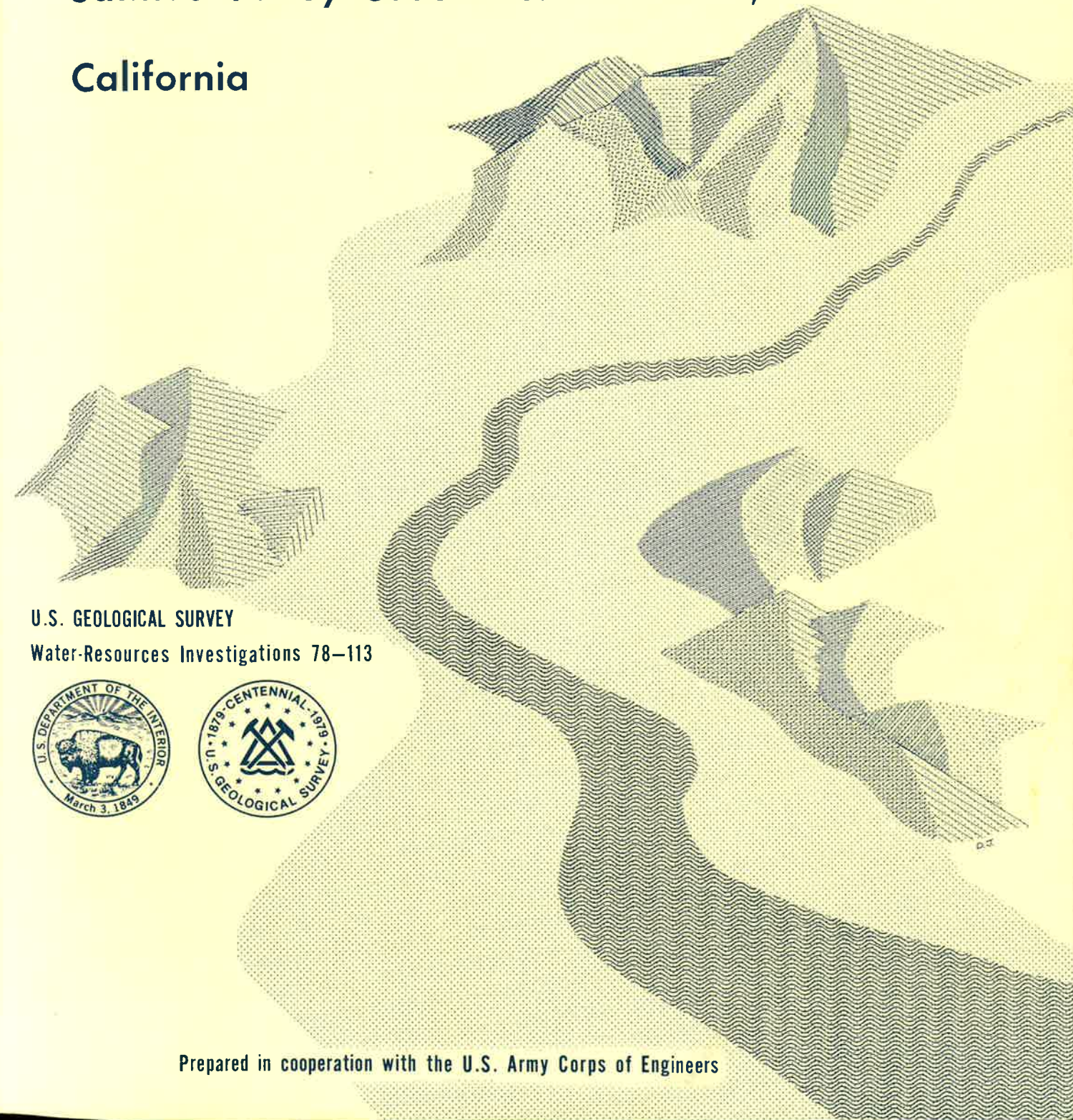


Two-Dimensional and Three-Dimensional  
Digital Flow Models for the  
Salinas Valley Ground-Water Basin,  
California



U.S. GEOLOGICAL SURVEY  
Water-Resources Investigations 78-113



Prepared in cooperation with the U.S. Army Corps of Engineers

TWO-DIMENSIONAL AND THREE-DIMENSIONAL DIGITAL FLOW MODELS  
OF THE SALINAS VALLEY GROUND-WATER BASIN, CALIFORNIA

By Timothy J. Durbin, Glenn W. Kapple, and John R. Freckleton

---

U.S. GEOLOGICAL SURVEY

Water-Resources Investigations 78-113

Prepared in cooperation with the  
U.S. Army Corps of Engineers



4003-05

November 1978

UNITED STATES DEPARTMENT OF THE INTERIOR

CECIL D. ANDRUS, Secretary

GEOLOGICAL SURVEY

H. William Menard, Director

---

OPEN-FILE REPORT

For additional information write to:

District Chief  
Water Resources Division  
U.S. Geological Survey  
345 Middlefield Road  
Menlo Park, Calif. 94025

CONTENTS

---

	Page
Conversion factors -----	XI
Abstract -----	1
Introduction -----	2
Purpose and scope -----	2
Well-numbering system -----	6
Acknowledgments -----	6
Description of the study area -----	7
Location and physiographic setting -----	7
Outline of ground-water hydrology -----	8
Areas of the ground-water basin -----	8
Ground-water movement -----	11
Water-level changes -----	11
Ground-water geology -----	15
Consolidated rocks -----	15
Basement complex -----	15
Older marine rocks -----	15
Semiconsolidated rocks -----	18
Younger marine rocks -----	18
Unconsolidated deposits -----	18
Paso Robles Formation -----	19
Alluvial fan deposits -----	20
River deposits -----	20
Windblown sand -----	21
Configuration of the ground-water basin -----	22
Base of the ground-water basin -----	22
Boundaries of the ground-water basin -----	24
Interacting hydrological models -----	25
Outline of the models -----	25
Model calibration -----	27
Small-stream model -----	27
Development of the model -----	27
Development of the governing equation -----	29
Use of the governing equation in the model -----	30
Model calibration -----	31
Application of model to estimate the mean ground-water recharge rate -----	33
Integration of flow-duration curve -----	33
Regionalized flow-duration curve -----	33
Mean discharge from ungaged tributaries -----	36
Mean ground-water recharge -----	41
Application of model to estimate the monthly mean tributary inflow rate -----	47

	Page
River model -----	49
Development of the model -----	49
Development of the governing equation -----	49
Use of the governing equation in the model -----	50
Model calibration -----	53
Two-dimensional ground-water model -----	62
Description of the model -----	62
Source and sink discharge -----	63
Agricultural and municipal pumpage -----	64
Ground-water recharge from irrigation-return water -----	64
Ground-water discharge from riparian vegetation -----	68
Ground-water recharge from small streams -----	71
Ground-water recharge from precipitation -----	71
Ground-water recharge from the Salinas River -----	72
Boundary conditions -----	72
Specified-head boundaries -----	73
Specified-discharge boundaries -----	73
No-flow boundary -----	73
Constant-discharge boundary -----	73
Initial conditions -----	74
System parameters -----	75
Transmissivity -----	75
Development of an approach to model calibration -----	75
Equivalent hydraulic conductivity -----	76
Spatial relations -----	76
Calibration results -----	78
Storage coefficient -----	81
Model verification -----	83
Source and sink discharge used for model verification -----	90
Agricultural and municipal pumpage -----	90
Natural ground-water recharge and discharge -----	92
Boundary and initial conditions -----	93
Verification results -----	93
Water levels -----	93
Streamflow -----	95
Extension of results to three-dimensional ground-water model -----	98
Three-dimensional ground-water model -----	98
Description of the model -----	98
Source and sink discharge -----	100
Agricultural and municipal pumpage -----	100
Ground-water recharge from irrigation-return water -----	100
Natural ground-water recharge and discharge -----	103
Boundary conditions -----	103
Specified-head boundaries -----	103
Specified-discharge boundaries -----	104
Initial conditions -----	104

	Page
Three-dimensional ground-water model--Continued	
System parameters -----	105
Hydraulic conductivity -----	105
Equivalent hydraulic conductivity -----	105
Ratio of horizontal to vertical hydraulic conductivity -----	106
Spatial relations -----	108
Calibration results -----	108
Specific storage -----	113
Spatial relations -----	113
Calibration results -----	116
Modeling errors -----	122
Sources of the deviation of model-generated water levels from measured water levels -----	122
Conceptual model -----	122
Computational scheme -----	122
System parameters -----	122
Input data -----	124
Initial conditions -----	124
Prototype water levels -----	125
Errors of prediction -----	126
Summary -----	127
References cited -----	130

ILLUSTRATIONS

	Page
Figure 1. Map showing location and hydrologic features of the Salinas River valley -----	4
2. Map showing ground-water areas of the Salinas Valley ground-water basin and potentiometric contours for autumn 1970 -----	In pocket
3. Graph showing cumulative distribution of specific capacities of wells for each area of the ground-water basin -----	9
4. Hydrographs for wells 14S/2E-3C1, 14S/3E-24N1, 17S/6E-21N1, and 20S/8E-5C1, showing autumn water-level measurements for the period 1931-75 -----	13
5. Graph showing cumulative departure of seasonal precipitation from mean annual precipitation for water years 1931-75 -----	14
6. Diagram showing generalized stratigraphic relations in the Salinas Valley -----	17
7. Map showing generalized geology of the Salinas Valley -----	In pocket
8. Map showing distribution and thickness of the confining unit overlying the 180-foot aquifer -----	22
9. Map showing altitude of the base of the ground-water basin -----	In pocket

	Page
Figure 10. Schematic diagram showing the data input to and output from the models used in the study and the interconnections between the models-----	26
11. Graph showing relation between flow width and discharge for selected small streams in the Salinas River drainage basin-----	32
12. Graph showing hypothetical flow-duration and potential-infiltration curves-----	34
13. Graph showing dimensionless flow-duration curves for selected stream-gaging stations in the Salinas River drainage basin-----	35
14. Graph showing regionalized flow-duration curve used for ungaged tributaries to the Salinas River-----	37
15. Map showing mean annual precipitation in the Salinas Valley-----	38
16. Graph showing relation between mean annual precipitation and mean annual runoff-----	40
17. Graph showing comparison of runoff computed by the precipitation-runoff relation and measured runoff-----	40
18. Map showing mean annual runoff in the Salinas Valley-----	42
19. Ground-water profiles computed by the two-dimensional ground-water model and thalweg profile along the Salinas River-----	51
20. Graph showing generalized relation between seepage discharge from a stream channel and depth to the regional water table-----	52
21. Graph showing relation between mean flow depth and discharge for the Salinas River-----	53
22. Graph showing relation between flow width and discharge for the Salinas River-----	54
23. Hydrograph showing monthly mean measured discharge for the Salinas River near Bradley-----	57
24. Hydrograph showing comparison of monthly mean discharge computed by the river model and monthly mean measured discharge for the Salinas River at Soledad-----	58
25. Hydrograph showing comparison of monthly mean discharge computed by the river model and monthly mean measured discharge for the Salinas River near Spreckels-----	59
26. Scattergram of monthly mean discharge computed by the river model and monthly mean measured discharge for the Salinas River at Soledad and near Spreckels-----	60
27. Map showing finite-element grid for the two-dimensional ground-water model and geographic distribution of agricultural pumpage for agricultural year 1970-----In pocket	
28. Graph showing monthly distribution of agricultural pumpage that was used in the two-dimensional ground-water model-----	66

	Page
Figure 29. Map showing finite-element grid for the two-dimensional ground-water model and geographic distribution of municipal pumpage for 1970-----In pocket	
30. Map showing finite-element grid for the two-dimensional ground-water model and geographic distribution of phreatophyte discharge-----In pocket	
31. Map showing finite-element grid for the two-dimensional ground-water model and geographic distribution of ground-water recharge from small streams and direct precipitation-----In pocket	
32. Graph showing relation between hydraulic conductivity of coarse-grained lithologies and depth below the water table-----	77
33. Map showing cumulative thickness of fine-grained lithologies-----In pocket	
34. Graph showing cumulative distribution of the deviation of the final hydraulic-conductivity estimates from the initial estimates that were used in the two-dimensional ground-water model-----	79
35. Map showing finite-element grid for the two-dimensional ground-water model and geographic distribution of hydraulic conductivity-----In pocket	
36. Map showing finite-element grid for the two-dimensional ground-water model, steady-state water-level contours generated by the model, and measured water-level contours for autumn 1970-----In pocket	
37. Graphs showing cumulative distribution, for each of the ground-water areas, of the deviation of steady-state water level generated by the two-dimensional ground-water model from measured water level for autumn 1970-----	80
38. Map showing finite-element grid for the two-dimensional ground-water model and geographic distribution of storage coefficient-----In pocket	
39. Graph showing cumulative distribution of the deviation of the final storage coefficient estimates that were used in the two-dimensional ground-water model from the initial estimates-----	82
40. Hydrographs showing comparison of water level generated by the two-dimensional ground-water model and measured water level for wells 14S/2E-34A1 and 15S/2E-1Q1 in the Pressure Area-----	84
41. Hydrographs showing comparison of water level generated by the two-dimensional ground-water model and measured water level for wells 14S/3E-15H3 and 14S/3E-16R1 in the East Side Area-----	85

	Page
Figure 42. Hydrographs showing comparison of water level generated by the two-dimensional ground-water model and measured water level for wells 17S/6E-19D1 and 18S/6E-25F1 in the Forebay Area -----	86
43. Hydrographs showing comparison of water level generated by the two-dimensional ground-water model and measured water level for wells 19S/7E-10P1 and 20S/8E-15H3 in the Upper Valley Area -----	87
44. Graph showing cumulative distribution, for each of the ground-water areas, of the deviation of the amplitude of seasonal fluctuations of water level generated by the two-dimensional ground-water model from the amplitude of measured water level -----	88
45. Map showing finite-element grid for the two-dimensional ground-water model, transient-state water-level contours generated by the model, and measured water-level contours for autumn 1971 -----	In pocket
46. Graph showing cumulative distribution, for each of the ground-water areas, of the deviation of transient-state water level generated by the two-dimensional ground-water model from measured water level for autumn 1971 -----	89
47. Graph showing annual agricultural pumpage for 1945 through 1970 that was used for the verification of the two-dimensional ground-water model -----	91
48. Graph showing annual municipal pumpage for 1945 through 1970 that was used for the verification of the two-dimensional ground-water model -----	92
49. Hydrographs showing comparison of water level generated by the two-dimensional ground-water model and measured autumn water level for 1945 through 1970 for wells 14S/2E-3C1, 14S/3E-24N1, 17S/6E-21N1, and 20S/8E-5C1 ---	94
50. Graph showing cumulative distribution, for each of the ground-water areas, of the deviation of transient-state water level generated by the two-dimensional ground-water model from measured water level for autumn 1970 -----	96
51. Hydrographs showing comparison of annual mean discharge computed by the river model and annual mean measured discharge for the Salinas River near Spreckels -----	97
52. Histograms of the vertical distribution of pumpage that was used in the three-dimensional ground-water model, for representative quarter townships in the Pressure Area ----	101
53. Histograms of the vertical distribution of pumpage that was used in the three-dimensional ground-water model, for representative quarter townships in the East Side Area ----	102
54. Graph showing cumulative distribution of the ratio of horizontal to vertical hydraulic conductivity for laboratory samples of alluvium from the San Joaquin Valley, Calif -----	107

	Page
Figure 55. Map showing finite-element grid for the three-dimensional ground-water model and geographic distribution of the hydraulic conductivity of coarse-grained lithologies -----	110
56. Map showing finite-element grid for the three-dimensional ground-water model and steady-state water-level contours generated by the model for the top layer of elements in the grid -----	In pocket
57. Map showing finite-element grid for the three-dimensional ground-water model and steady-state water-level contours generated by the model for the third layer of elements from the top in the grid -----	In pocket
58. Sections showing finite-element grid for the three-dimensional ground-water model and steady-state water-level contours generated by the model -----	In pocket
59. Graphs showing cumulative distribution of the deviation of steady-state water level generated by the three-dimensional ground-water model from measured water level for autumn 1970, for the East Side Area and the 180-foot and 400-foot aquifers in the Pressure Area -----	112
60. Map showing finite-element grid for the three-dimensional ground-water model and geographic distribution of specific storage -----	114
61. Hydrographs showing comparison of water level generated by the three-dimensional ground-water model and measured water level for wells 13S/2E-31L3 and 14S/3E-31F1 in the 180-foot aquifer of the Pressure Area -----	117
62. Hydrographs showing comparison of water level generated by the three-dimensional ground-water model and measured water level for wells 14S/2E-34A1 and 16S/4E-10R2 in the 400-foot aquifer of the Pressure Area -----	118
63. Hydrographs showing comparison of water level generated by the three-dimensional ground-water model and measured water level for wells 14S/3E-6R1 and 14S/3E-15P1 in the East Side Area -----	119
64. Graphs showing cumulative distribution of the deviation of the amplitude of seasonal fluctuations of water level generated by the three-dimensional ground-water model from the amplitude of measured water level, for the East Side Area and the 180-foot and 400-foot aquifers in the Pressure Area -----	120
65. Map showing finite-element grid for the three-dimensional ground-water model and transient-state water-level contours generated by the model for the top layer of elements in the grid -----	In pocket
66. Map showing finite-element grid for the three-dimensional ground-water model and transient-state water-level contours generated by the model for the third layer of elements from the top in the grid -----	In pocket

Figure 67. Sections showing finite-element grid for the three-dimensional ground-water model and transient-state water-level contours generated by the model-----In pocket	Page
68. Graphs showing cumulative distribution of the deviation of transient-state water level generated by the three-dimensional ground-water model from measured water level for autumn 1971, for the East Side Area and the 180-foot and 400-foot aquifers in the Pressure Area -----	121
69. Graph showing sensitivity of hydraulic heads computed by the two-dimensional ground-water model to changes in the storage-coefficient values used in the model -----	124
70. Graph showing sensitivity of hydraulic heads computed by the two-dimensional ground-water model to changes in the hydraulic-conductivity values used in the model -----	125

TABLES

Table 1. Estimated water budget for the Salinas Valley ground-water basin -----	Page
2. Geologic units of the Salinas Valley -----	10
3. Model parameters and their application in the models -----	16
4. Stream-gaging stations used in the development of regionalized flow-duration curve -----	28
5. Mean ground-water recharge rate and surface-water outflow rate to the Salinas River from small streams -----	36
6. Monthly mean tributary inflow rate to the Salinas River -----	44
7. Comparison of measured and computed annual mean discharge for the Salinas River at Soledad and the Salinas River near Spreckels -----	48
8. Mass balance for the Salinas River between Bradley and Spreckels -----	56
9. Mass balance for the Salinas River between Bradley and Soledad -----	61
10. Mass balance for the Salinas River between Soledad and Spreckels -----	61
11. Agricultural pumpage for agricultural years 1969-71 -----	62
12. Municipal pumpage for 1970 -----	65
13. Disposition of applied irrigation water and precipitation for 1944 -----	65
14. Areal distribution of and mean consumptive use of ground water by riparian vegetation along the Salinas River -----	67

CONVERSION FACTORS

The inch-pound system of units is used in this report. For readers who prefer metric units, the conversion factors for the terms used in this report are listed below:

<u>Multiply inch-pound unit</u>	<u>By</u>	<u>To obtain metric unit</u>
acre	0.4047	hectare
acre-ft (acre-foot)	.001233	cubic hectometer
acre-ft/yr (acre-foot per year)	.001233	cubic hectometer per year
ft (foot)	.3048	meter
ft/d (foot per day)	.3048	meter per day
ft/mi (foot per mile)	.1894	meter per kilometer
ft <sup>3</sup> /s (cubic foot per second)	.02832	cubic meter per second
gal/min (gallon per minute)	.003785	cubic meter per minute
(gal/min)/ft (gallon per minute per foot)	.2070	liter per second per meter
inch	25.40	millimeter
in/yr (inch per year)	25.40	millimeter per year
mi (mile)	1.609	kilometer
mi <sup>2</sup> (square mile)	2.590	square kilometer

TWO-DIMENSIONAL AND THREE-DIMENSIONAL DIGITAL FLOW MODELS  
OF THE SALINAS VALLEY GROUND-WATER BASIN, CALIFORNIA

---

By Timothy J. Durbin, Glenn W. Kapple, and John R. Freckleton

---

ABSTRACT

The Salinas Valley is a topographic and ground-water basin in central coastal California. The ground-water basin extends from Monterey Bay south-eastward along the Salinas River to San Ardo, a distance of 70 miles, and has a maximum thickness of 2,000 feet. Annual recharge to the ground-water basin, which is derived mostly from the Salinas River, is about 290,000 acre-feet. Annual discharge, which is mostly from pumpage but also includes the consumptive use of ground water by riparian vegetation along the Salinas River, is about 507,000 acre-feet. About 45 percent of the pumpage, or 217,000 acre-feet of water annually, returns to the ground-water system.

A group of interacting hydrologic models was developed for the Salinas Valley. These models include the small-stream model, river model, two-dimensional ground-water model, and three-dimensional ground-water model. The small-stream model simulates ground-water recharge from small streams that are tributary to the Salinas River. The river model simulates ground-water recharge from and surface-water discharge in the Salinas River. The two-dimensional and three-dimensional ground-water models simulate hydraulic head in the ground-water basin.

The ground-water models were calibrated by comparing water level computed by the models to the corresponding measured water level for both steady-state and transient-state simulations. For the steady-state simulation, which was used to calibrate transmissivity for the two-dimensional model and hydraulic conductivity for the three-dimensional model, the median deviation of the model-generated water level from measured water level was 6 and 5 feet for the two-dimensional and three-dimensional models, respectively. For the transient-state simulation, which was used to calibrate storage coefficient for the two-dimensional model and specific storage for the three-dimensional model, the median deviation of the model-generated water level (at the end of a 3-year calibration period) from measured water level was 6 feet for both models.



A 26-year simulation was used to verify the two-dimensional ground-water model. The median deviation of model-generated water level at the end of the verification period from measured water level was 6 feet, which is probably indicative of the predictive reliability for long-term simulations of both the two-dimensional and three-dimensional ground-water models.

Development of the ground-water-flow models was the first part of a two-part study. The second part will consist of the development of a two-dimensional ground-water-quality model.

## INTRODUCTION

### Purpose and Scope

The Salinas Valley is a large topographic and ground-water basin in the central coastal area of California (fig. 1). The term "Salinas Valley" is somewhat ambiguous in that different authors have used the term to designate different areas. The term is sometimes used to designate a large physiographic feature that extends along the Salinas River from Monterey Bay to near Santa Margarita. The term is also used in a more limited sense to designate the relatively flat lowlands along the Salinas River that extend from Monterey Bay to San Ardo. In this report, the term "Salinas Valley" designates the latter area, and the term "Salinas River valley" is used to designate the larger physiographic feature that extends from Monterey Bay to near Santa Margarita.

In the Salinas Valley, ground water has been the principal source of water for agricultural production, which is the economic base for the area. In 1970 about 180,000 acres were under cultivation. Although some dry farming is practiced in the valley, most of the acreage under cultivation is irrigated with ground water. Most irrigable land in Salinas Valley is in production, and the agricultural demand for ground water is for the most part stable (California Department of Water Resources, 1969). The total demand for water by agriculture is more or less commensurate with the total supply. Future water-resource problems for agriculture most likely will be related to the distribution of water within the valley and to water quality (California Department of Water Resources, 1969), but probably will not be related to the total available supply.

In addition to being an important agricultural area, Salinas Valley contains several growing urban areas. Salinas, the largest community in the valley, more than quadrupled its population in the 20-year period 1950 to 1970. In 1950 the population of Salinas was 14,000, in 1960 it was 29,000, and in 1970 it was 59,000 (U.S. Bureau of the Census, 1971). The 1970 population of other cities in the valley is as follows: Castroville, 3,200; Greenfield, 2,600; Gonzales, 2,600; King City, 3,700; Marina, 8,300; and Soledad, 6,800 (U.S. Bureau of the Census, 1971).

Water for the urban centers in Salinas Valley is obtained from ground water near the areas of demand. In 1970 residential, commercial, and industrial usage of ground water equaled about 5 percent of agricultural usage. The geographic areas with locally large urban demand for ground water are generally contiguous to areas with local agricultural ground-water supply problems, and the urban demand may tend to exacerbate the agricultural supply problems.

At the request of local public agencies, the U.S. Army Corps of Engineers is engaged in an investigation of the Salinas-Monterey Bay area urban water resources (U.S. Army Corps of Engineers, 1975). A major part of this effort is oriented toward formulating plans for managing the water resources of the area with respect to water supply, water quality, and wastewater. These plans are being developed for State and local consideration.

Possible alternative water-management plans that may be considered within the scope of the investigation by the Corps of Engineers include the regulation of surface-water inflow to the valley, alteration of the geographic distribution of ground-water pumpage and recharge, and utilization of wastewater. The construction of dams on tributaries of the Salinas River (Monterey County Flood Control and Water Conservation District, 1968a) would be one method of regulating surface-water inflow. Irrigation projects such as the Castroville Project (Monterey County Flood Control and Water Conservation District, 1974) and the East-Side Project (Monterey County Flood Control and Water Conservation District, 1968b) would alter the geographic distribution of ground-water pumpage. The land application of wastewater is a possible method for utilizing urban wastewater (Metcalf and Eddy, Engineers, 1976).

Each of these alternatives has a potential impact on the quantity and quality of ground water available for agricultural and urban uses. One of the major problems, however, in evaluating alternative management plans is lack of adequate information concerning the ground-water system. To assist in meeting the objectives of the investigation by the Corps of Engineers, the U.S. Geological Survey was asked by the Corps to develop digital models of the Salinas Valley ground-water basin. Within the overall scope of the request, digital ground-water-flow and ground-water-quality models were to be developed for use in evaluating water-management alternatives. This report describes the development of two-dimensional and three-dimensional ground-water-flow models. Work is in progress on the use of these models and on the development of a two-dimensional ground-water-quality model.

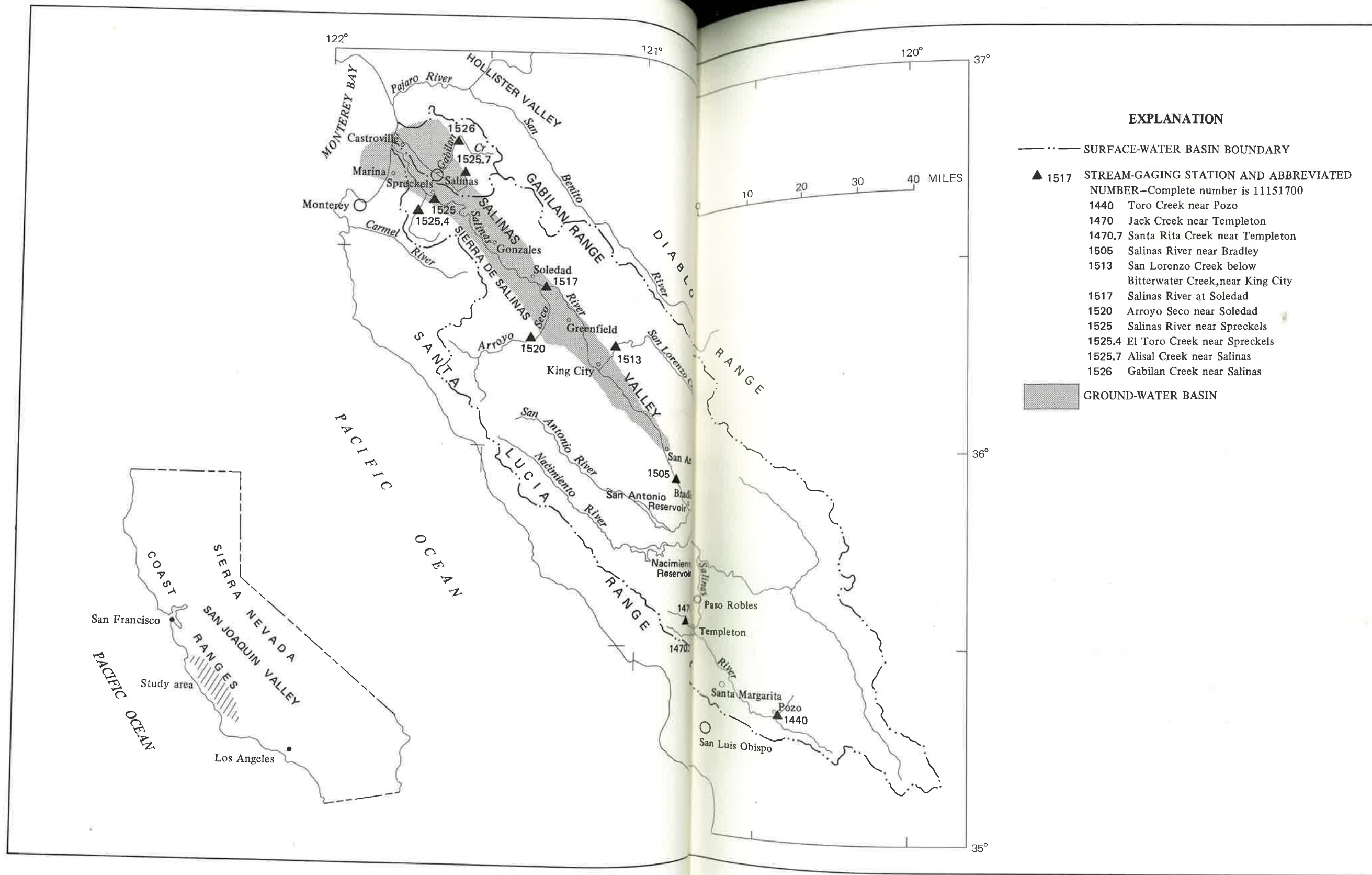


FIGURE 1.--Location and hydrologic features of the Salinas River valley.

FIGURE 1.--Continued

### Well-Numbering System

Wells are numbered according to their location in the rectangular system for subdivision of public land. For example, in the well number 14S/3W-15P1, that part of the number preceding the slash indicates the township (T.14 S.), the number and letter following the slash indicate the range (R. 3 W.), the number following the hyphen indicates the section (sec. 15), and the letter following the section number indicates the 40-acre subdivision of the section according to the lettered diagram below. The final digit is a serial number for wells in each 40-acre subdivision. The study area lies entirely in the southwest quadrants of the Mount Diablo base line and meridian.

D	C	B	A
E	F	G	H
M	L	K	J
N	P	Q	R

### Acknowledgments

Many persons and organizations contributed ideas and data to the study. Special acknowledgment is given to Loran S. Bunte, Jr., and R. L. Binder, Monterey County Flood Control and Water Conservation District, for the contribution of insights, advice, and data. Acknowledgment is also given to Gene L. Gerdes, California Department of Fish and Game; John Zulberti, California Division of Oil and Gas; Pacific Gas and Electric Co.; and U.S. Army Corps of Engineers for the contribution of data. George F. Pinder, Princeton University, and Genevieve Segol, University of Waterloo, provided computer programs and helped with the adaptation of those programs to the study.

## DESCRIPTION OF THE STUDY AREA

### Location and Physiographic Setting

The Salinas River valley is in the southern Coast Ranges of California, a geomorphic province (Jenkins, 1943) between the San Joaquin Valley and the Pacific Ocean. This province is characterized by a series of generally parallel mountain ridges that trend subparallel to the coast and dominate the gross topography of the area.

The Salinas River valley is the largest of the intermontane valleys of the southern Coast Ranges. It extends southward 120 mi from Monterey Bay to the vicinity of Santa Margarita (fig. 1). The study area is for the most part limited to the generally flat lowland tracts that extend from Monterey Bay to San Ardo, a distance of about 70 mi. These lowlands are about 10 mi wide at Monterey Bay, but their width gradually decreases southward to about 3 mi at San Ardo. South of San Ardo the valley opens into broad, deeply dissected upland tracts. The altitude of the valley floor ranges from sea level at Monterey Bay to 400 ft at San Ardo and to 1,200 ft at Santa Margarita.

The valley is drained by the Salinas River, which has a drainage area of about 5,000 mi<sup>2</sup> above Monterey Bay. On the southwest the drainage basin is separated from the Pacific Ocean by the Santa Lucia Range and from the Carmel River drainage basin by the Sierra de Salinas. The Santa Lucia Range extends from Monterey to San Luis Obispo, a distance of about 120 mi. The range is expressed physiographically by distinct northwestward-trending ridges, deep valleys, and prominent mountain peaks. The average ridge crest altitude is about 4,000 ft. The Sierra de Salinas is a northwestward-trending ridge, extending from near Salinas to the Arroyo Seco. The precipitous northeastern scarp of the Sierra de Salinas, which faces Salinas Valley, is dissected by short, steep canyons and high-gradient streams. Ridge-crest altitudes are about 3,700 ft.

On the northeast, the Salinas River drainage basin is separated from the San Joaquin Valley by the Diablo Range and from the San Benito River drainage by the Gabilan Range. The Diablo Range, which is 200 mi long and 30 mi wide, is the largest range in the southern Coast Ranges. Within the Salinas River drainage basin, the southeastern slope of the range is composed of broad valleys and gently rolling hills that rise to an average crest altitude of about 2,500 ft. The Gabilan Range is somewhat higher and has an average crest altitude of about 3,000 ft. The central summit surface is a system of broad ridges that connect isolated peaks. At the margin of Salinas Valley, the summit surface is dissected by steep canyons.

## Outline of Ground-Water Hydrology

The study includes the area between Monterey Bay and San Ardo (fig. 2) that is underlain by alluvial deposits. Ground water occurs in a generally continuous system of aquifers in these deposits. Locally the ground-water basin has as much as 2,000 ft of saturated sediments, but the average is less than 1,000 ft.

### Areas of the Ground-Water Basin

Four areas of the Salinas Valley ground-water basin have been designated (California Department of Water Resources, 1969). The names of these areas are Pressure Area, East Side Area, Forebay Area, and Upper Valley Area (fig. 2). The Forebay Area includes the Arroyo Seco Cone Area designated by the California Department of Public Works, Division of Water Resources (1946), which is no longer considered as a separate area (California Department of Water Resources, 1969). Ground water moves among the areas, and they do not represent subbasins of the Salinas Valley ground-water basin. Instead, they simply form a convenient frame of reference for the study of the ground-water basin. The area designations correspond to "subareas" in the literature and local usage.

One characteristic that distinguishes the areas is the degree of ground-water confinement. The Pressure Area comprises a system of confined and semiconfined aquifers that extend from about 6 mi offshore beneath Monterey Bay to Gonzales. The Pressure Area is characterized in the subsurface by two quasi-continuous clay layers that divide the upper part of the ground-water basin into two aquifers. The upper aquifer has been designated the 180-foot aquifer, and the lower one the 400-foot aquifer, where the number is in reference to the average depth to water-bearing strata (California Department of Public Works, Division of Water Resources, 1946). Ground water in the East Side Area is semiconfined. Ground water occurs in lenses of sand and gravel that are interbedded within massive deposits of finer grained material. Ground water in the Forebay and Upper Valley Areas is mostly unconfined.

A second characteristic that distinguishes the areas is the specific capacity of wells. Values of specific capacity are smallest in the northwestern part of the valley and tend to increase from Monterey Bay southeastward (fig. 3). The median specific capacity of wells is 25 (gal/min)/ft of drawdown in the East Side Area, 60 (gal/min)/ft of drawdown in the Pressure Area, 100 (gal/min)/ft of drawdown in the Forebay area, and 150 (gal/min)/ft of drawdown in the Upper Valley Area. The specific capacities of individual wells within each of the areas are quite variable. In the Upper Valley Area, specific capacities range from 5 to 700 percent of the median value. In the other areas, specific capacities generally range from 5 to 400 percent of the respective median values.

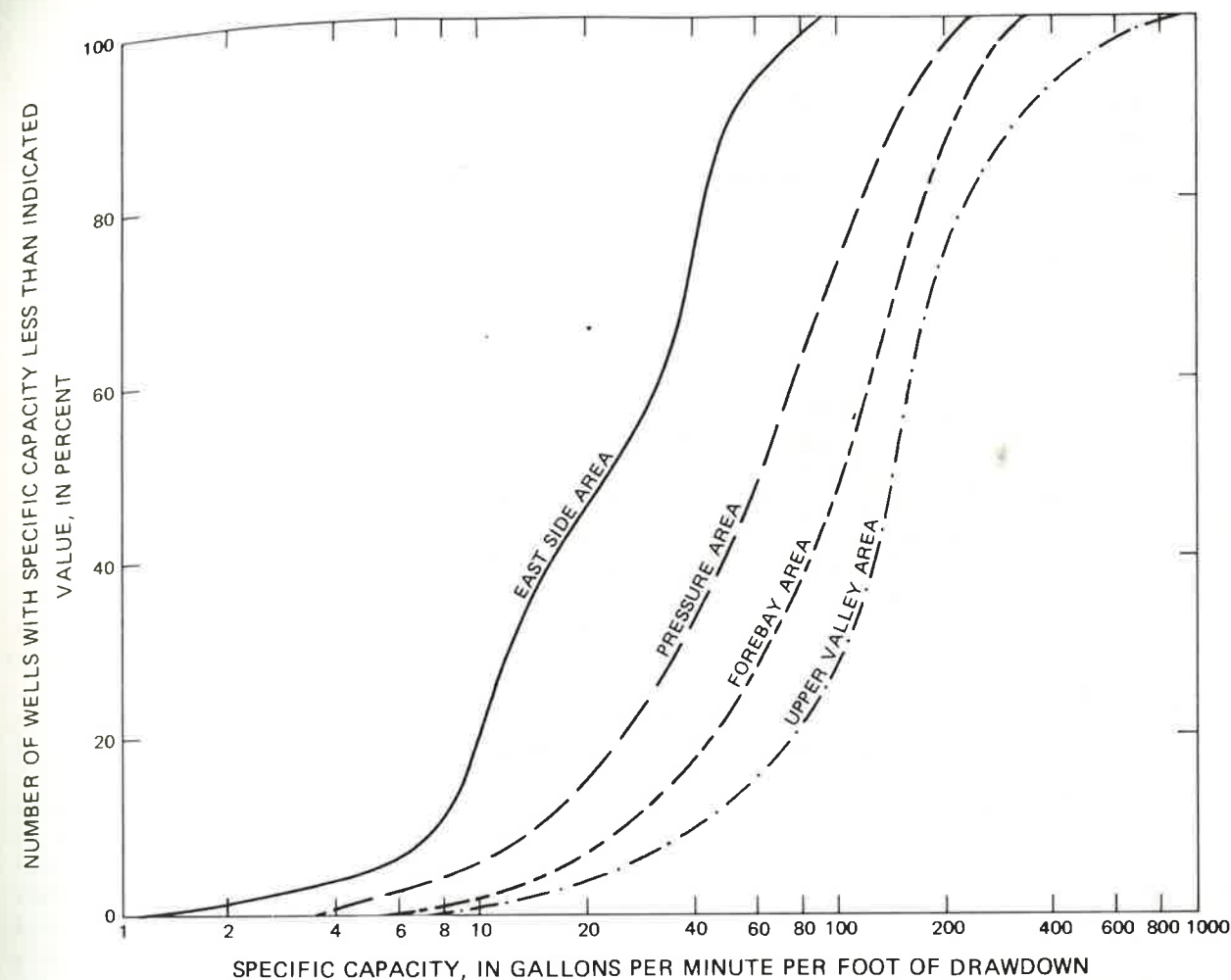


FIGURE 3.--Cumulative distribution of specific capacities of wells for each area of the ground-water basin.

A third characteristic that distinguishes the areas is the source of ground-water recharge. Infiltration from the channel of the Salinas River is the principal source of ground-water recharge for the Salinas Valley ground-water basin. At the 1970 pumping rate, the river supplied about 50 percent of ground-water recharge (excluding irrigation return water), or about 156,000 acre-ft/yr (table 1). The Salinas River directly recharges the Pressure, Forebay, and Upper Valley Areas. Indirectly it recharges the East Side Area by the movement of ground water across area boundaries.

TABLE 1. - Estimated water budget for the Salinas Valley ground-water basin (based on the assumption that the ground-water basin is in equilibrium with the 1970 pumping rate and the long-term average natural recharge rate)

Budget item	Rate of inflow or outflow (acre-ft/yr)
<b>Inflow</b>	
Recharge from Salinas River-----	156,000
Recharge from tributaries to Salinas River-----	96,000
Subsurface inflow -----	21,000
Seawater intrusion -----	11,000
Direct recharge from precipitation -----	6,000
Irrigation return water -----	217,000
Total inflow -----	507,000
<b>Outflow</b>	
Pumping -----	482,000
Consumptive use of ground water by riparian vegetation-----	25,000
Total outflow -----	507,000

Tributaries of the Salinas River that drain the highlands contiguous to the ground-water basin are also important sources of ground-water recharge. Infiltration from the channels of these streams supplies about 30 percent of ground-water recharge (excluding irrigation water) or about 96,000 acre-ft/yr. All the areas receive recharge from this source. The Arroyo Seco is the largest tributary of the Salinas River north of San Ardo, and this stream supplies about 73,000 acre-ft/yr of ground-water recharge to the Forebay Area.

Ground-water inflow from outside the ground-water basin is an important source of recharge to the Upper Valley Area. This inflow represents about 10 percent of recharge to the Salinas Valley ground-water basin, or about 21,000 acre-ft/yr.

A source of recharge to the Pressure Area, albeit an undesirable source is seawater intrusion. In 1970 the rate of seawater intrusion was about 11,000 acre-ft/yr.

## Ground-Water Movement

As mentioned earlier, ground water in the Salinas Valley ground-water basin moves among the four areas of the ground-water basin. The general direction of ground-water movement is down the valley, from San Ardo toward Monterey Bay. The average hydraulic gradient is 6 ft/mi (fig. 3) and closely follows the gradient of the Salinas River, because percolation from or to the river tends to maintain ground-water levels near the river to within a few feet above or below the river thalweg.

In many areas of the Salinas Valley ground-water basin, pumping of wells imparts an identifiable cross-valley gradient component to the potentiometric surface. Ground water moves from the river toward areas of pumping. This phenomenon is especially apparent in the area between Gonzales and Salinas. In this reach the Salinas River is asymmetrically located near the southwest side of the valley. At Gonzales, water levels in wells near the northeast side of the valley are about 30 ft lower than on the southwest side. At Salinas the cross-valley water-level differential is as much as 60 ft, and water-level altitudes in the East Side Area are as much as 50 ft below sea level.

Water levels in much of the Pressure Area are also below sea level during a large part of each year. In autumn 1970, water levels in the area between Salinas and Monterey Bay were, for the most part, more than 5 ft below sea level. As a result, at Monterey Bay the direction of ground-water movement is inland and seawater intrusion is occurring (California Department of Water Resources, 1970, 1973, and 1975). Intrusion was first noticed in the late 1930's (California Department of Public Works, Division of Water Resources, 1946) when some wells in the 180-foot aquifer were abandoned because of high chloride. The degradation of the 180-foot aquifer led to the development of the deeper 400-foot aquifer as an alternative source of ground water; however, seawater intrusion is now also occurring in the 400-foot aquifer. In 1970 the area with chloride greater than 500 mg/L (milligrams per liter) extended about 4 mi inland in the 180-foot aquifer and about 2 mi inland in the 400-foot aquifer (Monterey County Flood Control and Water Conservation District, 1970).

## Water-Level Changes

Water-level changes are the response of the ground-water basin to changes in discharge (largely pumping) and recharge. Ground-water pumping from the valley has been increasing since 1900, which, effectively, was the beginning of ground-water usage in Salinas Valley. In response to increased pumping, ground-water levels declined. Since about 1960, however, ground-water levels have, for the most part, stabilized or partially recovered in response to increased ground-water recharge that resulted from the partial regulation of surface-water inflow to the valley.

Long-term changes in pumping have resulted from changes in the crop acreage under irrigation and from changes in population. In 1902 about 7,500 acres were under irrigation (Hamlin, 1904). By 1945 the irrigated area had increased to 125,000 acres (California Department of Public Works, Division of Water Resources, 1946), and by 1970 it had increased to 180,000 acres. Based on the extrapolation of 1945 average unit area applications of irrigation water, agricultural pumpage in 1902 was probably 21,000 acre-ft. Pumpage in 1945 was about 350,000 acre-ft (California Department of Public Works, Division of Water Resources, 1946). In 1970 it was about 460,000 acre-ft. From population estimates (U.S. Bureau of the Census, 1971), urban pumpage was 2,000 acre-ft in 1902, 5,000 acre-ft in 1940, and 22,000 acre-ft in 1970.

Long-term effects on ground-water recharge began with the construction of dams on the Nacimiento River in 1956 and on the San Antonio River in 1967. Prior to the construction of these dams, the Salinas River, which is the principal source of ground-water recharge, usually dried up during the summer and ceased contributing ground-water recharge. The reservoirs created by the dams, which have a combined capacity of 700,000 acre-ft, are operated to sustain summer flow in the Salinas River. Concomitantly, ground-water recharge from the river has increased.

Figure 4 shows water-level hydrographs for four wells--one in each of the four areas of the ground-water basin. The hydrographs show autumn water levels for 1931 through 1975 reflecting the combined influences of ground-water pumping and recharge. For 1931 through 1958, water levels in the wells generally declined in response to the expansion of irrigated acreage. The greatest water-level decline during this period occurred in the East Side Area. After 1958, water levels rose in the wells in the Forebay and Upper Valley Areas in response to the maintenance of summer flow in the Salinas River. After about 1970 the water level in each of the wells was fairly stable.

Superimposed on the long-term effects, on water levels, of long-term changes in pumping and recharge are the short-term effects of climatic factors. Water levels tend to decline during periods of below-average precipitation and to rise during periods of above-average precipitation. Farmers in the Salinas Valley rely on precipitation to meet part of the soil-moisture requirement of crops. In years with below-average precipitation, farmers compensate for the lack of natural soil moisture with increased ground-water pumping for irrigation. In wet years, pumping is correspondingly decreased. Similarly, ground-water recharge is affected by year-to-year variations in precipitation. Recharge decreases in dry years and increases in wet years, although this effect is somewhat dampened by the regulation of flow in the Salinas River.

Figure 5 is a graph of the cumulative departure of seasonal precipitation for the period 1931-75. The cumulative departure for a given year is obtained average annual precipitation for the inclusive prior years. Segments of the graph that slope upward indicate periods of above-average seasonal precipitation, while segments of the graph that slope downward indicate periods of below-average seasonal precipitation.

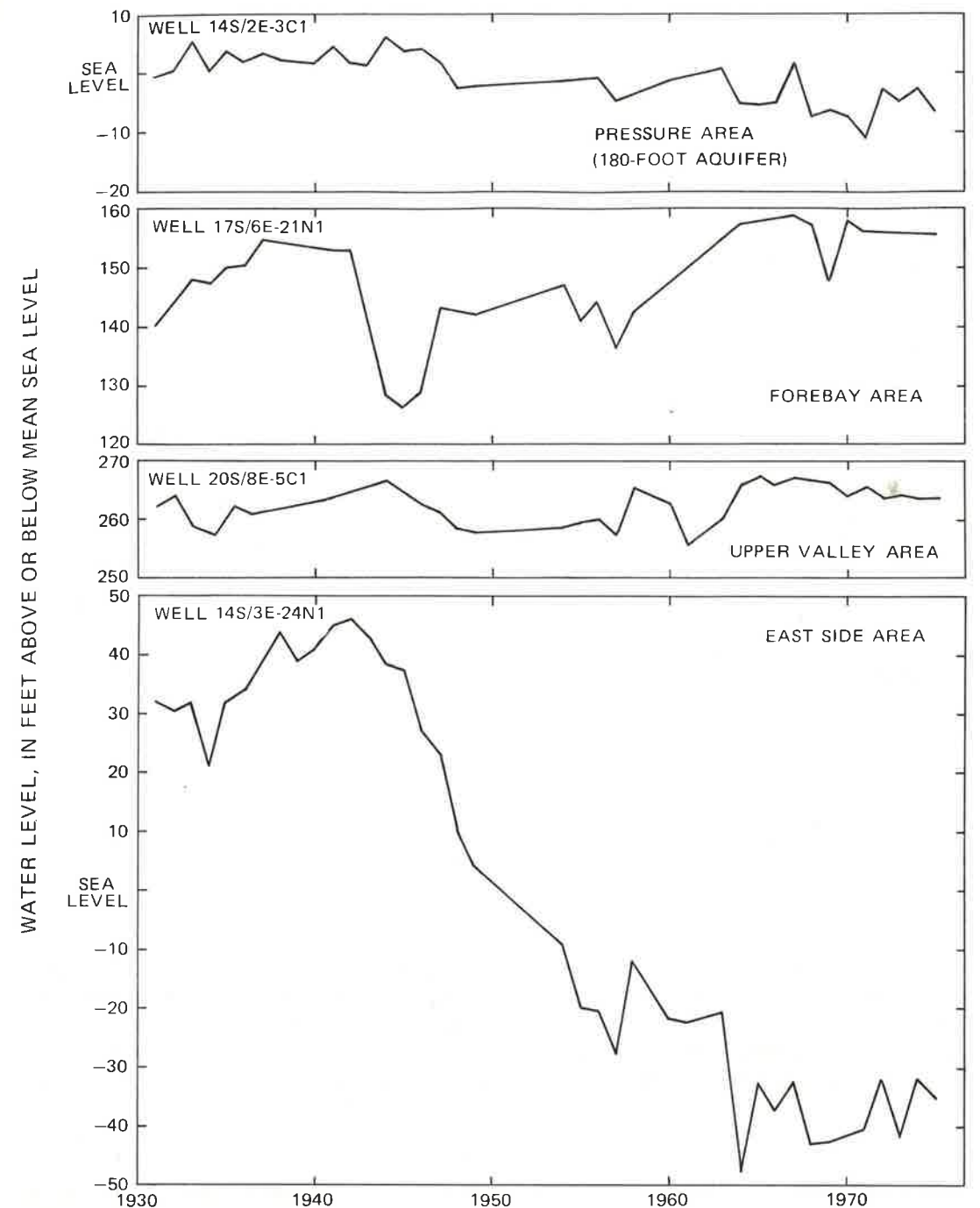


FIGURE 4.--Hydrographs for wells 14S/2E-3C1, 14S/3E-24N1, 17S/6E-21N1, and 20S/8E-5C1, showing autumn water-level measurements for the period 1931-75. Each well represents one of the four areas of the Salinas Valley ground-water basin. Water-level data from California Department of Public Works, Division of Water Resources (1949, 1950), and Monterey County Flood Control and Water Conservation District (1959-67, 1968-75).

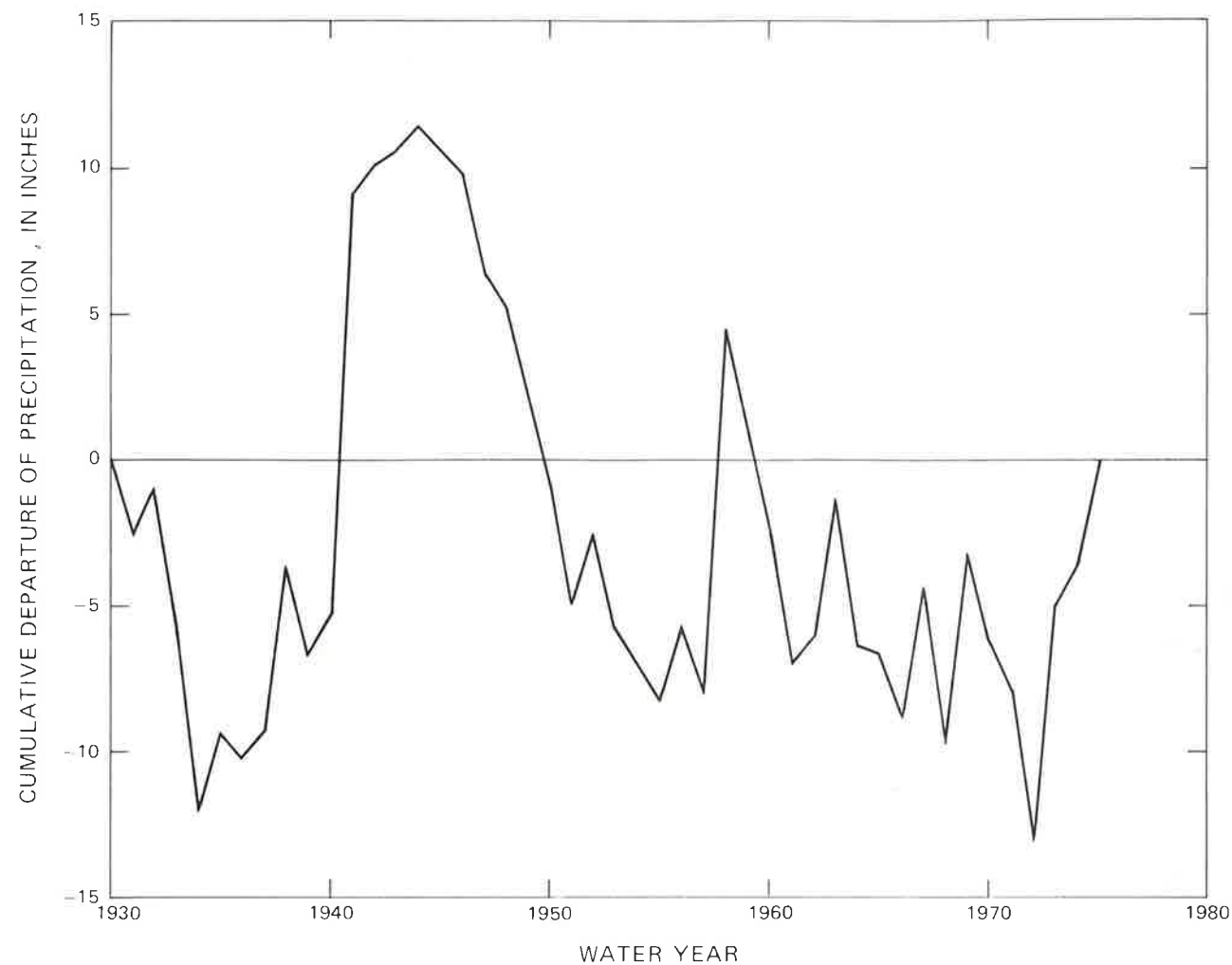


FIGURE 5.--Cumulative departure of seasonal precipitation from mean annual precipitation for water years 1931-75. The water year is the 12-month period ending September 30 and is designated by the calendar year in which it ends. Based on precipitation data from U.S. Weather Bureau (1955, 1965, and 1961-65) and Environmental Data Service (1966-75).

A comparison of the cumulative-departure graph with the water-level hydrographs for the four wells (fig. 4) generally indicates the correlation of the valley's water levels to dry periods with water-level declines and to wet periods with water-level rises. During the extended dry period from 1945 through 1951, water levels in many of the wells either declined after a period of rise or accelerated after a period of existing decline. A dry period also occurred from 1959 through 1962. During this period the water-level response was similar to the response for 1945 through 1951. A 2-year wet period occurred in 1940-41, and water levels rose in many of the wells that had water-level measurements for those years.

## Ground-Water Geology

On the basis of their capacity to store and yield ground water, the rocks in the Salinas Valley area are divided into three classes: (1) Those that are consolidated and yield water only from fractures, or fully indurated, and yield water to wells in such small quantity that the development of wells in these rocks is not ordinarily feasible; (2) those that are semiconsolidated, or moderately indurated, but have connected interstices that may yield some water to wells; and (3) those that are unconsolidated and have connected interstices that may yield appreciable quantities of water to wells. Table 2 contains the geologic units of the Salinas Valley and their general lithologic character and water-bearing properties. Figure 6 shows their generalized stratigraphic relations, and figure 7 shows the areal distribution of the units.

### Consolidated Rocks

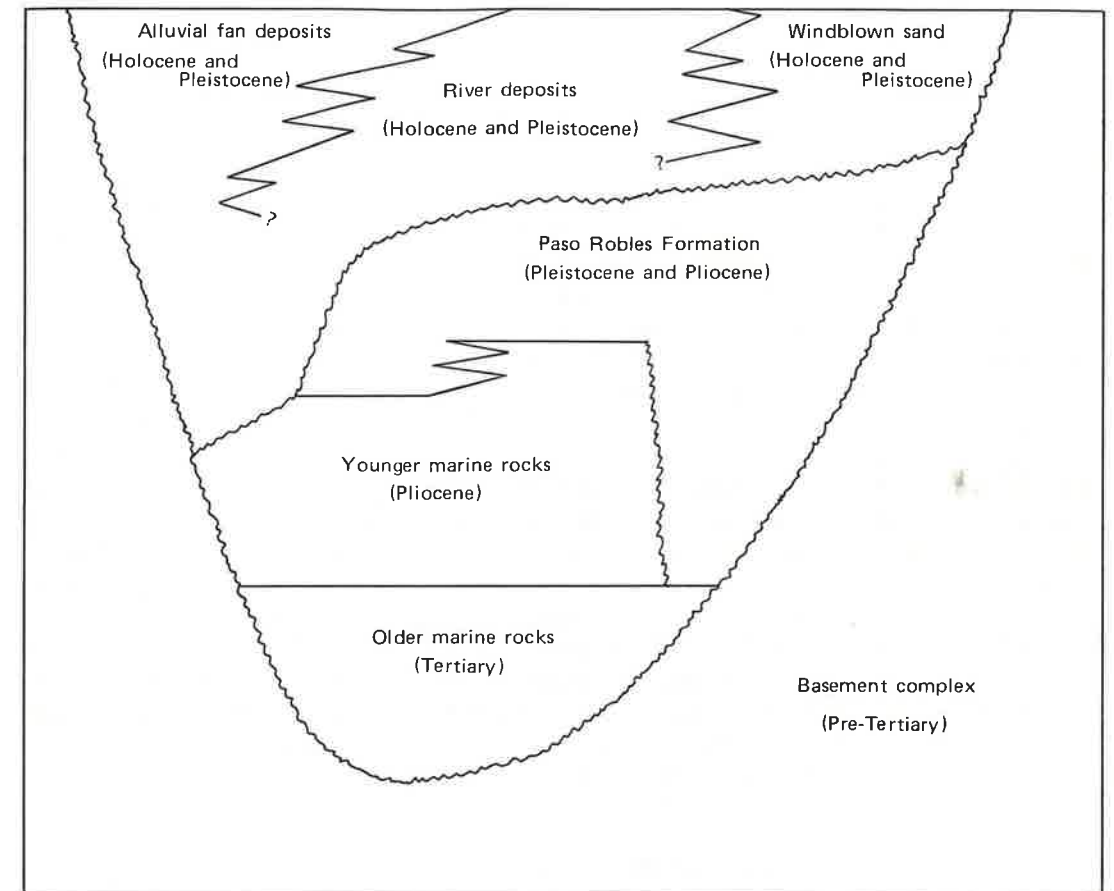
The consolidated, virtually non-water-bearing rocks exposed in the study area have been grouped into two main units. From oldest to youngest they consist of crystalline rocks, which form the basement complex of the area, and a complicated series of indurated marine deposits, which are designated as the older marine rocks.

Basement complex.--The basement complex, of pre-Tertiary age (Compton, 1966), is composed of igneous and metamorphic rocks. It is extensively exposed in the Sierra de Salinas and the Gabilan Range. The basement complex is also exposed in isolated outcrops in the uplands southeast of the Gabilan Range. It is deeply weathered locally, and where weathered and saturated it supplies minor quantities of water to wells, commonly sufficient only for domestic and stock uses.

Older marine rocks.--The older marine rocks that are exposed in the Salinas Valley rest unconformably on the basement complex and locally are folded and faulted. These rocks crop out west of the Salinas River in the southeastern part of the study area, near Salinas, and offshore beneath Monterey Bay. The older marine rocks include in ascending order the Reliz Canyon, Berry, Vaqueros, Tierra Redonda, and Monterey Formations (Durham, 1974). Within the study area, the Monterey Formation, of Miocene age (Bramlette, 1946) and stratigraphically at the top of the sequence, represents the bulk of the older marine rocks. The Monterey Formation is chiefly shaly to massive mudstone, but it contains some sandstone beds near its base that range in thickness from 1 inch to several feet and commonly are grouped into sandstone units several tens of feet thick. Locally these sandstone units yield water to wells in sufficient quantity for individual homes. The mudstone facies of the Monterey Formation yield virtually no water.

TABLE 2. - Geologic units of the Salinas Valley

Geologic unit	Geologic age	Maximum thickness (ft)	General lithologic character	Water-bearing properties
Unconsolidated deposits	Windblown sand	200	Unconsolidated to semiconsolidated, well-sorted, fine to medium sand.	Generally above the water table.
	River deposits	300	Loose, moderately to well-sorted gravel; coarse to fine sand; silt; and clay.	Wells yield 500 to 4,000 gal/min.
	Alluvial fan deposits	500	Unconsolidated to semiconsolidated, poorly sorted gravel, sand, silt, grading into coarse gravel near fan heads.	Locally wells yield as much as 1,000 gal/min. Yields on east side of valley, near Salinas, are considerably less.
Semi-consolidated deposits	Paso Robles Formation	2,000	Deposits consisting of unconsolidated to consolidated gravel, sand, and silt.	Wells yield as much as 4,000 gal/min.
	Younger marine rocks	1,200	Marine sandstone, conglomerate, and mudstone.	In southern part of study area, well yields are small. In northern part, in upper units, wells yield moderate quantities.
Consolidated rocks	Older marine rocks	10,000	Marine mudstone with some sandstone near base.	Sandstone units yield water sufficient for individual homes. Mudstone facies yield virtually no water.
	Basement complex	--	Igneous and metamorphic rocks.	Locally wells yield small quantities from fractures or weathered zone.



EXPLANATION

- CONFORMITY
- ~ UNCONFORMITY
- ⚡ LATERAL GRADATION OR INTERTONGUING

FIGURE 6.--Generalized stratigraphic relations in the Salinas Valley.



## Semiconsolidated Rocks

Younger marine rocks.--The semiconsolidated rocks consist of marine beds that conformably overlie the Monterey Formation at most places in the study area and unconformably overlie the basement complex where the Monterey Formation is locally absent. In the southeastern part of the study area these deposits are represented by the Pancho Rico Formation. This formation crops out extensively northeast of the Salinas River and in scattered belts and patches southwest of the river. In the northwestern part of the study area the stratigraphic equivalent of the Pancho Rico Formation is the Purisima Formation. The Purisima Formation is not exposed in the study area but is found in the subsurface.

The Pancho Rico Formation, of Pliocene age (Durham and Addicott, 1964), is chiefly and characteristically sandstone, but the formation also contains conglomerate and mudstone. The gross lithologic aspect of the Pancho Rico Formation differs considerably from place to place. On the northeast side of the Salinas River the Pancho Rico Formation is mainly very fine- and fine-grained sandstone and interbedded mudstone. The sandstone is well sorted, massive, friable, and deeply weathered. The mudstone is porous and easily broken. On the northwest side of the Salinas River the Pancho Rico Formation is mostly moderately friable, fine-grained sandstone. Wells in the formation generally yield water in quantities sufficient for domestic and stock uses.

The Purisima Formation, of Pliocene age (Hickey, 1968), consists mostly of poorly indurated sand, silt, and clay. It has three members of slightly differing lithologic characteristics (Hickey, 1968). The lower member consists of poorly indurated sand beds interbedded with clay and shale. The middle member consists of intercalated beds of poorly indurated sand, silt, and clay with some gravel. The sand is admixed with silt. The upper member is made up largely of a sequence of poorly indurated, thin sand beds with interbeds of silt and clay. The water-bearing properties of the Purisima Formation are largely unknown, but the upper and (or) middle members probably would yield 100 gal/min to a well.

## Unconsolidated Deposits

The unconsolidated deposits in the study area compose the principal aquifers of the Salinas Valley ground-water basin. The deposits include the Paso Robles Formation of Pliocene and Pleistocene age (Fairbanks, 1898) and the alluvium of Pleistocene and Holocene age (Durham, 1974). The alluvium includes alluvial fan deposits, river deposits, and windblown sand. Most ground water stored in the basin is in the Paso Robles Formation, but the principal water-producing beds are in the alluvium.

Paso Robles Formation.--The Paso Robles Formation is nonmarine and largely of fluviatile origin (Durham, 1974). It represents the beginning of nonmarine deposition following the last withdrawal of the Tertiary sea from the study area. In the southeastern part of the study area the Paso Robles Formation conformably overlies the Pancho Rico Formation. In the northwestern part it unconformably overlies the Purisima Formation at most places, unconformably overlies the Monterey Formation where the Purisima Formation is absent, and unconformably overlies the basement complex where the Monterey and Purisima Formations are both absent.

The Paso Robles Formation underlies most of Salinas Valley, but exposures of the formation are limited. It crops out in patches on ridgetops northeast of the Salinas River near King City, in the hills southwest of the river between Greenfield and King City, and in the hills southwest of Salinas. The thickness of the formation is variable, mainly because the upper part has been removed by erosion (Durham, 1974). About 500 ft remains near King City, 1,500 ft near Greenfield, 1,200 ft near Spreckels, and 1,000 ft near Salinas.

The Paso Robles includes beds that were deposited over a wide area under various conditions and during a long period that included one or more episodes of tectonic activity (Durham, 1974). The formation includes lithologic facies representing alluvial fan, flood-plain, and lacustrine depositional environments (Greene, 1970). In the southeastern part of the study area the formation is mostly sandstone and conglomerate with some mudstone and limestone. The sandstone ranges from fine to coarse grained and is generally poorly sorted, massive or poorly bedded, and friable. The conglomerate generally consists of pebbles or small cobbles and is locally friable and moderately porous. In the northwestern part of the study area the Paso Robles consists of unconsolidated to poorly indurated sand, silt, and clay (Greene, 1970). These sediments occur in alternating beds of generally coarse and fine materials. In the upper part of the formation individual beds range in thickness from 20 to 60 ft.

The Paso Robles Formation yields moderate to large quantities of water to wells. In the northwestern part of the study area, the upper 200 ft of the formation contains the 400-foot aquifer. Near Salinas the yield of wells perforated exclusively in this aquifer ranges generally from 300 to 4,000 gal/min and probably averages 1,200 gal/min. The specific capacity of wells averages about 30 (gal/min)/ft of drawdown, which indicates that the upper part of the Paso Robles Formation is moderately permeable. Few wells penetrate much below the 400-foot aquifer, but determination of the hydraulic conductivity of side-hole cores from a test hole (Thorup, 1976) indicates that the material near the base of the Paso Robles Formation may be only about half as permeable as material near its top.

Well yields from the Paso Robles Formation are generally higher in the southeastern part of the study area. Deep wells here penetrate more of the formation and commonly yield 4,000 gal/min. The average specific capacity of these wells is about 60 (gal/min)/ft, twice that of wells completed in only the upper part of the formation in the northwestern part of the study area. The hydraulic conductivity of the Paso Robles Formation seems to vary from top to bottom, but within a given layer it is probably nearly the same throughout the valley.

Alluvial fan deposits.--Alluvial fan deposits are prominent physiographic forms in the Salinas Valley, as well as characteristic lithologic units. These deposits are exposed in belts of generally coalesced fans along both sides of the valley. The alluvial fan deposits comprise about half the geographic extent of the alluvium and have a maximum saturated thickness of about 500 ft. Where exposed, the alluvial fan deposits commonly are composed of poorly sorted gravel, sand, silt, and clay, which were derived from the nearby mountains or hills. Near the heads of the fans the deposits commonly contain cobbles in a matrix of sand, silt, and some clay. Downslope the degree of sorting improves, and the range in grain size decreases.

Lithologic contrasts occur between the alluvial fan deposits on the separate sides of Salinas Valley. Along the northeast side of the valley the Gabilan Range is mostly granite and supplies granitic material to the adjacent fans. The fragments weather rapidly, and the pores in the poorly sorted materials are plugged with clay minerals. Along the southwest side of the valley the Sierra de Salinas is mostly schist. The adjacent alluvial fans are composed of rock fragments that do not weather quickly, and the deposits are relatively porous.

Corresponding to the lithologic contrasts are permeability contrasts between the alluvial fan deposits on the separate sides of Salinas Valley. The permeability of deposits on the southwest side of the valley is generally greater than the permeability of deposits on the northeast side. The average specific capacity of wells on the alluvial fan of the Arroyo Seco, which is the largest fan on the southwest side of the valley, is about 100 (gal/min)/ft of drawdown. The average specific capacity of wells on the alluvial fan of Gabilan Creek, the largest fan on the east side of the valley, is about 20 (gal/min)/ft of drawdown.

River deposits.--The alluvium contains a medial complex of river deposits, which bilaterally interfingers with the alluvial fan deposits and unconformably overlies the Paso Robles Formation. The thickness of the river deposits is difficult to estimate in most parts of the valley because these deposits are difficult to distinguish from the Paso Robles Formation in well logs, but they probably range in thickness from 100 to 300 ft along the axis of the valley.

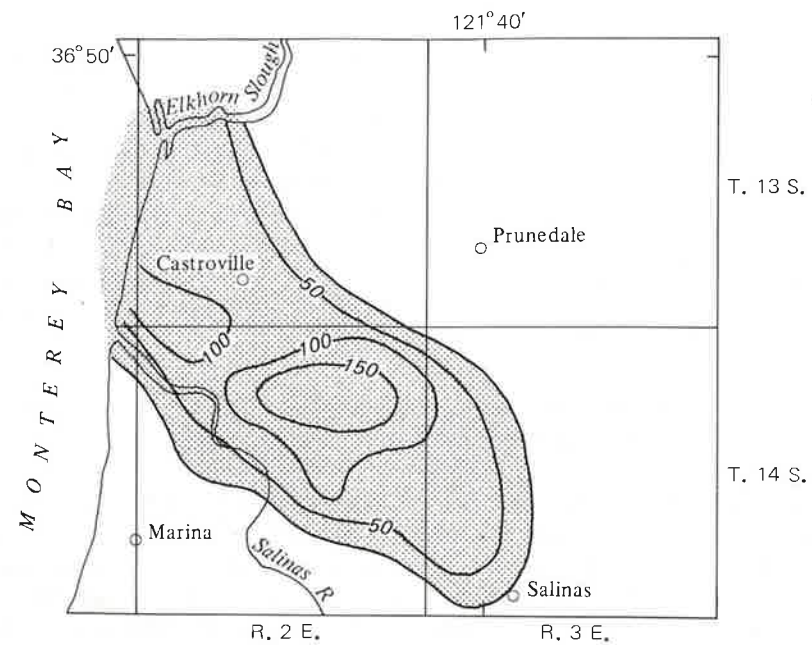
The river deposits have been distributed by the Salinas River and its tributaries. The Salinas River has repeatedly eroded and alluviated its channels in response to cyclical glacio-eustatic sea level changes (Tinsley, 1975). During some of the periods of sea level rise, the rate of rise exceeded the rate at which the river could realluviate its valley, and parts of the northern Salinas Valley were submerged. Shallow marine to brackish-water estuarine environments prevailed during much of the deposition of the materials that compose the 180-foot aquifer (Tinsley, 1975). Estuarine deposits extend from Monterey Bay to about Gonzales. Southeast of Gonzales the river deposits are of continental origin.

The river deposits consist of gravel, sand, silt, and clay. In the areas of estuarine deposition massive clay units locally make up the bulk of the aquifer. A continuous, virtually impermeable clay body underlies much of the area between Monterey Bay and Salinas (fig. 8). The top of the clay is at the land surface in some places, while in other places it is as much as 100 ft below the land surface. The thickness is variable and, in general, decreases toward the margins of the body. The maximum thickness is about 150 ft. Between Salinas and Gonzales the clay body is discontinuous. Under the clay is the 180-foot aquifer. This aquifer consists of a complex zone of interconnected gravel, sand, sandy clay, and clay beds.

Southeast of Gonzales, in the area of nonestuarine deposition, sand and silt make up the bulk of the river deposits. Large-scale depositional structures are not generally identifiable from well records for this area.

Well yields from the river deposits range from 500 to 4,000 gal/min and tend to increase southward. The median specific capacity of wells perforated exclusively in the river deposits is about 70 (gal/min)/ft of drawdown in the northwestern part of the study area and about 100 (gal/min)/ft of drawdown in the southeastern part of the study area.

Windblown sand.--Windblown sand occurs in extensive areas south of the Salinas River between Salinas and Monterey Bay and north of the river between Salinas and Castroville. It also is in patches in the lowlands between King City and San Ardo. Windblown sand generally overlies the alluvial fan and river deposits, but it locally underlies these deposits. The windblown sand in the northwestern part of the study area is as much as 200 ft in thickness and is saturated in part. The windblown sand in the southeastern part of the study area is above the regional water table and does not contain usable water. Nevertheless, in both localities rainfall penetration into the windblown sand provides locally important recharge to the ground-water basin.



EXPLANATION


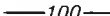
-  CONFINING UNIT
-  —100— LINE OF EQUAL THICKNESS OF CONFINING UNIT—Interval 50 feet

FIGURE 8.--Distribution and thickness of the confining unit overlying the 180-foot aquifer.

Configuration of the Ground-Water Basin

Base of the Ground-Water Basin

Figure 9 shows the altitude of the base of the ground-water basin. The altitude along the axis of the basin ranges from about 100 ft above sea level near San Ardo to about 2,200 ft below sea level near Greenfield. Figure 9 was constructed from various types of data defining the base of the unconsolidated deposits. For the area between San Ardo and Greenfield, the altitude of the base of the ground-water basin was estimated from electric logs for oil wells. For the area between Greenfield and Monterey Bay the altitude was estimated from gravity data (Bishop and Chapman, 1967) and from a few electric logs. Offshore, beneath Monterey Bay, the altitude was estimated by Greene (1970) from seismic data.

The configuration of the base of the ground-water basin is closely related to the structure of underlying rocks. In the southeastern part of the study area, between San Ardo and Greenfield, the ground-water basin, which has a lenticular transverse cross section, occupies the axis of a broad synclinal flexure in the basement complex. The younger marine deposits outcrop along both the eastern and western limits of the ground-water basin and bilaterally dip under the aquifer system toward the axis of the flexure, which plunges toward the northwest. At San Ardo the axial base altitude of the aquifer system is about 100 ft, which corresponds to a saturated thickness of the ground-water basin, at this point, of 300 ft. At King City the axial base altitude is about -800 ft, and the saturated thickness is 1,100 ft. At Greenfield the axial base altitude is about -1,300 ft, and the saturated thickness is 1,500 ft.

Northwest of Greenfield the flexural structure degenerates into a fault-controlled structure. The basement complex has topographically high areas in the Sierra de Salinas and in the Gabilan Range that are separated by a cuneate depression formed by faulting and tilting (Greene and others, 1973). The mountain blocks are separated by the King City fault at the southwest margin of Salinas Valley, and both have been tilted with their west edges down. The King City fault (fig. 9) is a major structural feature that extends from near King City to at least several miles offshore beneath Monterey Bay. The vertical separation along the fault decreases to the northwest, toward Monterey Bay, where it may die out. Beneath the alluvial fans southwest of Chualar, gravity data (Fairborn, 1963) suggest about 8,000 ft of separation in the basement complex, whereas southwest of Salinas, at the northwest end of the Sierra de Salinas, gravity data (Sieck, 1964) indicate between 3,000 and 4,000 ft of separation.

The wedge of alluvium that partly fills the structural depression between the Sierra de Salinas and the Gabilan Range is thickest along the southwest side of the valley. The altitude of the base of the ground-water basin adjacent to the King City fault near Greenfield is about -2,000 ft. South of Salinas the altitude of the base is about -1,600 ft. The saturated thickness in the ground-water basin is 2,200 ft near Greenfield, whereas it is 1,600 ft south of Salinas.

The geographic limits of the ground-water basin (fig. 2) are well defined in some parts of the study area and less well defined in other parts. In the southeastern part of the study area, between San Ardo and Greenfield, the southwestern limit is defined by the contact of the alluvium with either the Pancho Rico Formation or the Monterey Formation. The northeastern limit is assumed to be the contact of the alluvium with the Pancho Rico Formation. But ground water does occur in the Pancho Rico Formation east of this location and may interact with ground water in the alluvium.

In the central part of the study area, between Greenfield and Salinas, the geographic limits of the ground-water basin are well defined. The southwestern limit of the ground-water basin is the outcrop of metamorphic rocks of the Sierra de Salinas. On the opposite side of the valley, the limit of the ground-water basin is the outcrop of igneous rocks of the Gabilan Range.

In the northern part of the study area, between Salinas and Monterey Bay, the limits of the ground-water basin are arbitrarily defined. The southern limit coincides with the presumed trace of the King City fault. Vertical displacement seems to have occurred on the fault, with the north side dropped down (Martin, 1964). If the offshore correlations are correct (Greene, 1970), the vertical separation of the Monterey Formation may be as much as 800 ft where the fault crosses the shoreline. This has brought the virtually non-water-bearing sediments of the Monterey Formation on the south side of the fault into juxtaposition with the more permeable material of the Paso Robles Formation on the north side of the fault. The upper part of the alluvium, however, may be more or less continuous across the fault.

The northern limit of the ground-water basin between Salinas and Monterey Bay coincides with a buried clay-filled gorge that extends inland near Elkhorn Slough (fig. 2) in an easterly direction from the present head of the offshore submarine Monterey Canyon (Starke and Howard, 1968). The gorge apparently was formed terrestrially as part of the present Monterey Canyon at a time in the past when sea level was lower. With the rise of sea level, the gorge became filled with tidal muds. These muds now act as a partial barrier to the movement of ground water between Salinas Valley and the Pajaro River valley to the north.

The ground-water basin extends about 6 mi offshore into Monterey Bay (Greene, 1970). The southern limit of the submarine extension of the ground-water basin coincides with the offshore trace of the King City fault. The western limit is the contact between the Paso Robles Formation and the Monterey Formation. The northern limit coincides with a major unnamed fault in the south wall of the Monterey Canyon.

### Outline of the Models

The hydrologic system of Salinas Valley is influenced by important interactions between a surface-water subsystem and a ground-water subsystem. Correspondingly, interacting models of the major components of these subsystems have been developed. These models include a small-stream model, river model, two-dimensional ground-water model, and three-dimensional ground-water model. A schematic diagram showing the interconnections among these models is shown in figure 10.

The small-stream model simulates ground-water recharge from the channels of tributaries to the Salinas River. Where these tributaries cross the ground-water basin, infiltration from their channels recharges the ground-water system. Inputs to the model are streamflow at the edge of the ground-water basin and selected physical characteristics of the channels. Outputs from the model are ground-water recharge and the residual surface-water discharge into the Salinas River.

The river model simulates infiltration from the Salinas River. Input to the model is discharge in the river at Bradley (fig. 1) and tributary inflow to the river. Additional inputs are physical characteristics of the river channel and regional ground-water level near the channel. Output from the model is infiltration from (or percolation to) and discharge in the Salinas River.

The two-dimensional ground-water model simulates hydraulic head in the ground-water basin. The area covered by the two-dimensional model extends from the shoreline of Monterey Bay to San Ardo. Inputs to the model are the geographic extent of the ground-water basin, the depth-averaged water-bearing properties of the ground-water basin, such as transmissivity and storage coefficient, and ground-water recharge and pumpage. Output from the model is the depth-averaged hydraulic head at specified locations and times.

The three-dimensional ground-water model also simulates hydraulic head in the ground-water basin. The area covered by the model, however, is somewhat limited and extends from offshore beneath Monterey Bay to near Gonzales. Inputs to the model are the geographic extent and thickness of the ground-water basin, point water-bearing properties of the ground-water basin (on a macroscopic scale), such as horizontal and vertical hydraulic conductivity, specific storage, and ground-water recharge and pumpage. Output from the model is the hydraulic head at specified locations, depths, and times.

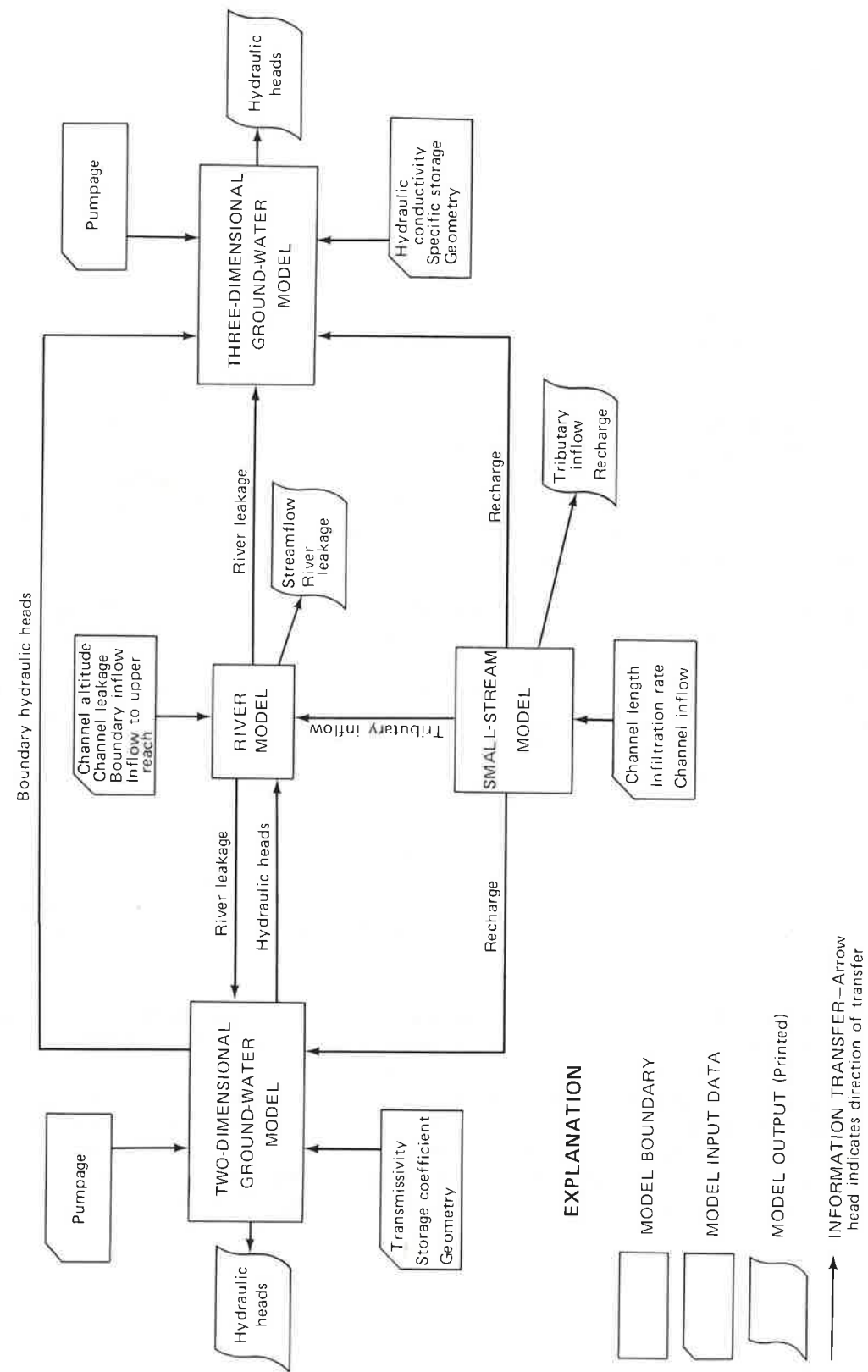


FIGURE 10.--Schematic diagram showing the data input to and output from the models used in the study and the interconnections between the models.

Information is passed between the models. The small-stream model passes tributary flow to the river model and ground-water recharge to the two-dimensional and three-dimensional ground-water models. The river model passes ground-water recharge or discharge to the two-dimensional and three-dimensional ground-water models. The two-dimensional ground-water model passes hydraulic heads to the river model. The two-dimensional ground-water model also passes hydraulic heads to the three-dimensional ground-water model. These hydraulic heads are used to produce the boundary conditions of the three-dimensional ground-water model near Gonzales.

Model Calibration

Each of the models employs a fixed set of mathematical expressions, which are adapted to the Salinas Valley by selecting the proper set of numerical values for certain critical parameters (table 3) within the mathematical expressions. Values for the parameters are selected by a calibration process that requires field data concerning the stresses on the ground-water basin and its corresponding response. Initial values of the model parameters are assigned by analysis of field data and on the basis of prior experience with the model. The response of the model to the input of a mathematical representation of the stresses on the ground-water basin is then compared to the observed response of the prototype and adjustments are made to the parameter values to better reproduce the observed response. Adjustment is continued, by repeated trials, until the response of the model represents the prototype to an acceptable degree.

SMALL-STREAM MODEL

Development of the Model

The Salinas Valley ground-water basin is recharged in part by infiltration of streamflow from the channels of tributaries to the Salinas River. These tributaries drain the highland areas contiguous to the ground-water basin. For the most part, this streamflow is ephemeral. During storm periods, streamflow debouches along the valley perimeter and moves down the alluvial fans that border the valley. As streams flow down the alluvial fans most of the water infiltrates the permeable surficial deposits. On the average, little streamflow reaches the Salinas River. The infiltrate is partly evaporated from the wetted channel bed and partly transpired by riparian vegetation. The remainder percolates through the alluvial deposits until it reaches the water table.

TABLE 3. - Model parameters and their application in the models

Model	Parameter identifier	Application	References Equation	Page	Calibration period
Small-stream	a, b	Flow-width coefficients	5	30	1960-75
	$\bar{f}$	Average infiltration rate	4	29	1944-45
River	$a_w, b_w$	Flow-width coefficients	12	50	1969-75
	$a_d, b_d$	Flow-depth coefficients	10	50	1969-75
	$C_L$	Channel-bed leakage coefficient	9	49	Dec. 1968-Nov. 1971
Two-dimensional ground-water	$T_{xx}, T_{yy}$	Transmissivity	16	62	1970
	S	Storage coefficient	16	62	Dec. 1968-Nov. 1971
Three-dimensional ground-water	$K_{xx}, K_{yy}$	Horizontal hydraulic conductivity	24	99	1970
	$K_{zz}$	Vertical hydraulic conductivity	24	99	1970
	$S_s$	Specific storage	24	99	Dec. 1968-Nov. 1971

The vertical distance between the channel bed and the ground-water table is generally at least several hundred feet at the top of the alluvial fans, and the infiltration from stream channels is an unsaturated-flow phenomenon. The infiltration rate is controlled mostly by the soil-moisture gradient at the channel bed and is independent of the ground-water level beneath the channel. The infiltration rate is highest during the initial absorption of moisture following wetting of the channel. As the infiltrate penetrates below the channel, the infiltration rate rapidly declines. The infiltration rate eventually approaches a steady-state value that is dependent on the vertical hydraulic conductivity of the alluvial fan deposits underlying the channel and the depth of flow in the channel.

Development of the Governing Equation

The infiltration rate is a complex function of location and time, but with a few simplifying assumptions a tractable model of the infiltration-percolation process can be developed. Let the infiltration rate be designated symbolically by  $f$ , where  $f$  is a function of location along the channel, location in a cross section, and time. Then the infiltration at a cross section  $q_i$  is given by

$$q_i = \int_0^{w_i} f dy \tag{1}$$

where  $w_i$  is the width of flow. The infiltration from a reach  $Q_i$  is given by

$$Q_i = \int_0^L q_i dx \tag{2}$$

where  $L$  is the length of the channel reach. By substituting equation 1 into equation 2, the relation

$$Q_i = \int_0^L \int_0^{w_i} f dy dx \tag{3}$$

is obtained. If average infiltration rate in the reach is  $\bar{f}$  at some instant, then the infiltration from the reach is

$$Q_i = \bar{f} \bar{w} L \tag{4}$$

where  $\bar{w}$  is the average width of flow in the reach.

At this point simplifying assumptions can be introduced. The first assumption is that evapotranspiration withdrawals are small compared to infiltration and can be neglected. The second is that the average infiltration rate is a constant. The third assumption is that the average width of flow can be represented by a power function of the form

$$w_i = aQ^b \quad (5)$$

where  $Q$  is the discharge at the upstream end of the reach and  $a$  and  $b$  are numerical coefficients. Then, the governing equation describing infiltration is

$$Q_i = \bar{f} a Q^b L \quad (6)$$

The reason for the first two assumptions is that the model would be intractable without those assumptions. The justification for the first assumption is that the average infiltration rate is probably much larger than the average evapotranspiration withdrawal rate. Although at specific instances withdrawal from a reach may be greater than infiltration, the total infiltration over a long period of time is probably at least an order of magnitude larger than the total withdrawal for the same period. The justification for the second assumption is that, on the basis of generalized infiltration data (Smith, 1972), the infiltration rate probably closely approaches the steady-state rate during the initial part of a streamflow event.

The justification for the third assumption is that channels with beds of similar erodible material tend to have similarly proportioned channel geometry (Leopold and others, 1964). The description of natural channels based upon measurements of selected hydraulic and channel parameters has led to the formation of empirical relations describing the average behavior of a wide variety of rivers. Field studies suggest that in many rivers the increase in width with discharge may be generally described by simple power function of the discharge (Leopold and Maddock, 1953; Wolman, 1955; Leopold and Miller, 1956; and Wolman and Brush, 1961).

#### Use of the Governing Equation in the Model

To apply the equation describing infiltration from a channel reach, the channel is divided into one or more reaches. Starting with the most upstream reach, the infiltration for the reach for a specified discharge is computed by substituting the discharge value into equation 6 along with appropriate values for the quantities  $\bar{f}$ ,  $a$ , and  $b$ . If the computed infiltration rate is greater than or equal to the surface-water inflow rate to the reach, all inflow infiltrates within the reach and the infiltration rate is set equal to the inflow rate. If the computed infiltration rate is less than the surface-water inflow rate, surface-water outflow occurs from the reach. The outflow rate is equal to the inflow rate minus the infiltration rate. The outflow from this reach becomes the inflow to the next downstream reach, and the procedure is repeated until the outflow rate from a reach is zero or the procedure has been applied to all reaches. The outflow from the most downstream reach is the surface-water inflow to the Salinas River from the tributary.

The time period to be simulated is divided into one or more time steps. The above procedure is repeated for each reach and for each time step. The discharges and infiltration rates used in or obtained from the procedure are the averages for the time step.

Two factors need to be considered in the application of the model. The first is the reach length, and the second is the time step. The relation between flow width and discharge (eq. 5) is applied with the discharge at the upstream end of the reach. Reach lengths should be short enough that for the dominant discharges the infiltration does not cause significant reduction of discharge within a reach. With reference to the time-step factor, the model was developed with the tacit assumption of a steady-state condition. Time steps should be long enough that the transient effects of a flood wave moving through the reach do not significantly affect the average discharge during the time step. Reach lengths of about 5,000 ft and time steps of 1 day were used in the model.

#### Model Calibration

Values for the coefficients of the power function relating flow width to discharge (eq. 5) and for the constant infiltration rate (eq. 4) were estimated from streamflow data. Measurements of flow width and discharge are plotted logarithmically in figure 11. On a logarithmic graph a power curve is a straight line. The line representing the average relation between the data is also shown in figure 11. The coefficient  $a$  is the log-intercept of the line, and the coefficient  $b$  is the slope of the line. The relation represented by the line is

$$\bar{w} = 5.5Q^{0.44} \quad (7)$$

Discharge records of Arroyo Seco near Soledad (fig. 1), together with observations of surface-water inflow to the Salinas River from the Arroyo Seco, provide data for estimating the constant-infiltration rate. Special observations of discharge at the lower end of the Arroyo Seco channel were made during the period December 1944-April 1945 (California Department of Public Works, Division of Water Resources, 1946). These observations indicate that with a discharge of 250 ft<sup>3</sup>/s at the gaging station, which is located at the top of the alluvial fan, flow in the Arroyo Seco just reaches the Salinas River, that is, all the discharge of 250 ft<sup>3</sup>/s has infiltrated and the flow in the Arroyo Seco is near zero at its confluence with the river. This relation holds for a wide range of antecedent flow sequences in the channel and also holds for the rising and falling limbs of the discharge hydrograph.

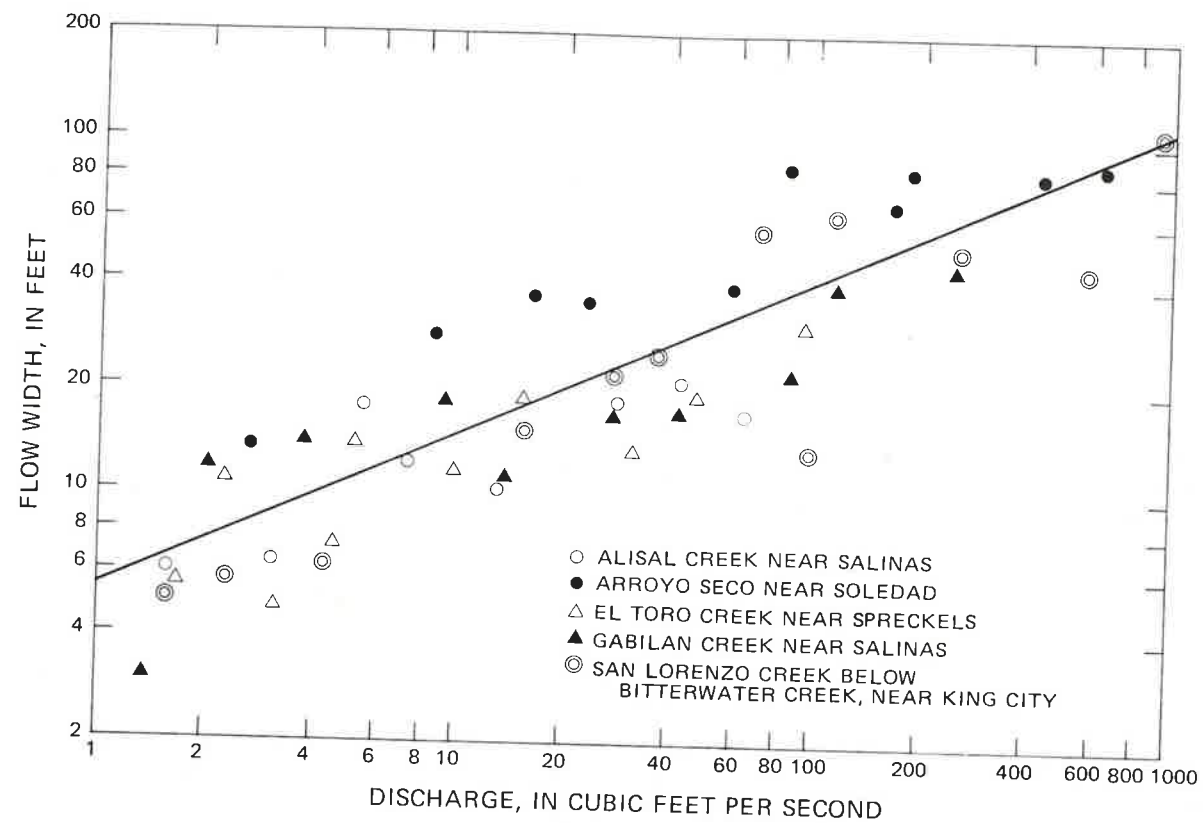


FIGURE 11.--Relation between flow width and discharge for selected small streams in the Salinas River drainage basin.

The infiltration rate constant in equation 4 was estimated using an upstream discharge of 250 ft<sup>3</sup>/s in the model and then adjusting the infiltration rate constant until the model simulated incipient flow in the channel at the Salinas River. The infiltration rate constant derived from this procedure equaled 5 ft/d. This value was used for all small-stream channels in Salinas Valley. The Arroyo Seco accounts for most of the ground-water recharge from small streams, and the extrapolation of the infiltration-rate constant for the Arroyo Seco to other small streams should not cause serious error in the computation of the cumulative ground-water recharge from all the small streams. Unfortunately, the limited field data available for calibration of the small-stream model preclude a quantitative assessment of the predictive accuracy of the model, even for the Arroyo Seco.

## Application of Model to Estimate the Mean Ground-Water Recharge Rate

### Integration of Flow-Duration Curve

The small-stream model was designed so that hydrographs of surface-water inflow could be routed through the model to produce hydrographs of surface-water outflow and infiltration. The flow-duration curve for a drainage basin is in a sense a hydrograph for the drainage basin, with discharge events reordered in time on a dimensionless time scale. The flow-duration curve has the important characteristic that the integration of the area under the curve yields the mean annual discharge for the drainage basin. If the flow-duration curve is routed through the model exactly as any other hydrograph would be, appropriate integrations yield the mean annual surface-water outflow and mean annual ground-water recharge.

Figure 12 shows a hypothetical flow-duration curve. Corresponding to each discharge on the flow-duration curve is the infiltration rate for a channel reach (eq. 6), which is also shown in figure 12. The infiltration rate is the potential infiltration rate, in that surface-water inflow to the reach may not be able to satisfy the computed infiltration rate. The integral of the diagonally cross-hatched area in figure 12 equals the mean annual ground-water recharge rate from the channel reach. The integral of the shaded area in figure 12 equals the mean annual surface-water outflow. Within the area representing surface-water outflow, the difference between the ordinates of the flow-duration curve and the infiltration curve is the ordinate of the flow-duration curve of surface-water outflow from the reach (or inflow to the next reach).

### Regionalized Flow-Duration Curve

To apply the above approach to the small streams, the flow-duration curve of surface-water inflow to the channel must be available. Flow-duration curves are available for three tributaries of the Salinas River in the study area (Jorgensen and others, 1971). The gaging stations for these tributaries are San Lorenzo Creek near King City, Arroyo Seco near Soledad, and El Toro Creek near Spreckels. Dimensionless flow-duration curves for these stations are shown in figure 13. Dimensionless flow-duration curves for three additional stations, which are tributaries of the Salinas River but outside the study area, are also shown in figure 13. The drainage area and average discharge at the six stations are listed in table 4.



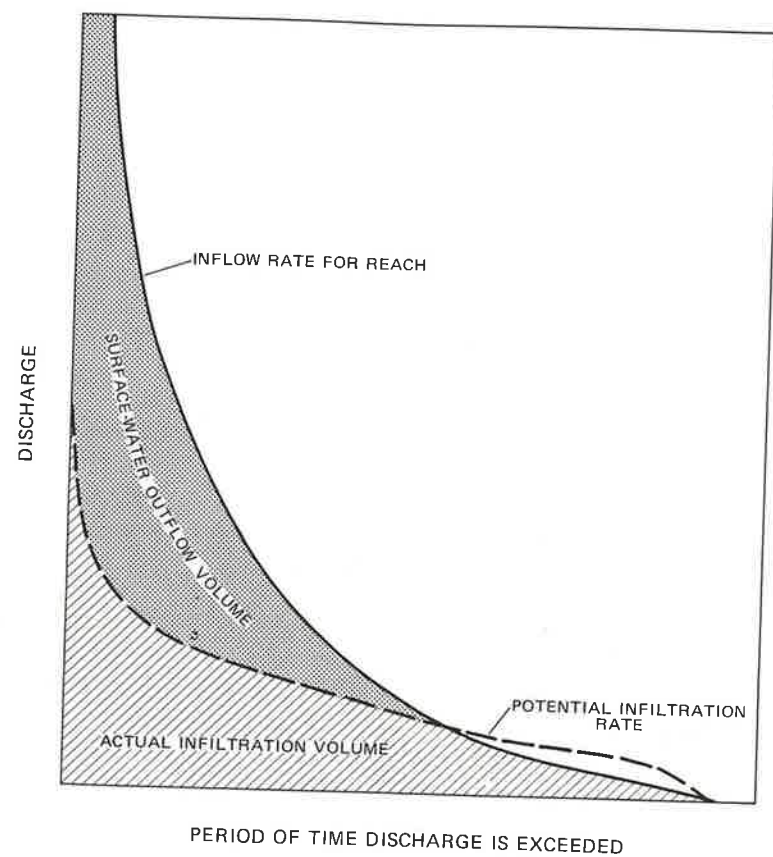


FIGURE 12.--Hypothetical flow-duration and potential-infiltration curves.

A dimensionless flow-duration curve applicable to the ungaged tributaries in the study area was developed by averaging the curves shown in figure 13. Unequal and subjective weighting was given to the curves in the development of the regionalized flow-duration curve. Greatest weight was given to the stations considered to be most representative of the ungaged basins. The regionalized flow-duration curve is shown in figure 14. To establish the flow-duration curve for a particular ungaged tributary, the ordinates of the regionalized dimensionless curve are multiplied by the estimated mean discharge for the tributary.

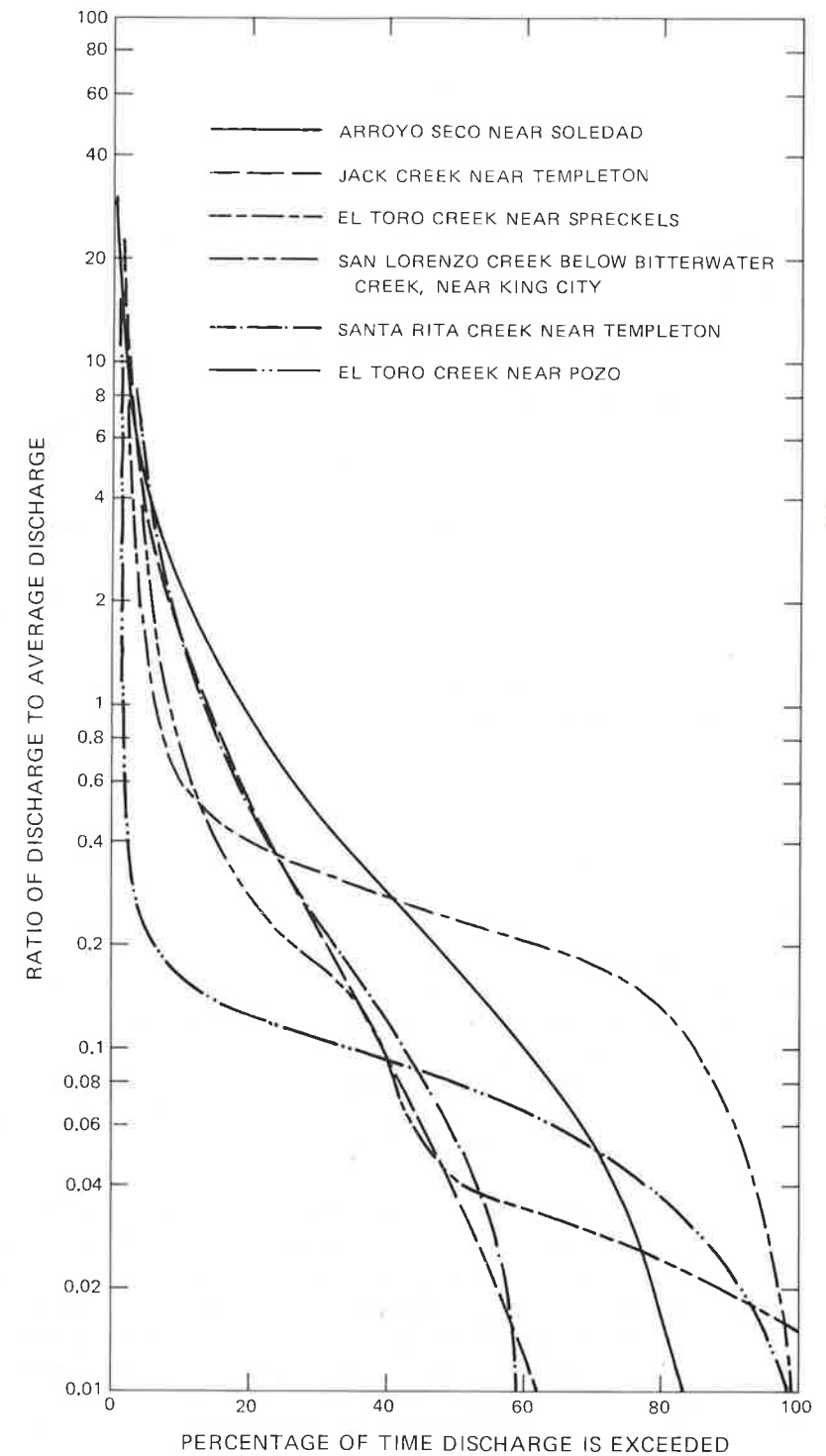


FIGURE 13.--Dimensionless flow-duration curves for selected stream-gaging stations in the Salinas River drainage basin.

TABLE 4. - Stream-gaging stations used in the development of regionalized flow-duration curve

Station name <sup>1</sup>	Station No.	Drainage area (mi <sup>2</sup> )	Period of record (water year <sup>2</sup> )	Average discharge (ft <sup>3</sup> /s)
Arroyo Seco near Soledad	11152000	244	1902-68	159
Jack Creek near Templeton	11147000	25.3	1950-68	13.1
El Toro Creek near Spreckels	11152540	31.9	1962-68	.381
San Lorenzo Creek below Bitterwater Creek, near King City	11151300	233	1959-68	6.36
Santa Rita Creek near Templeton	11147070	18.2	1962-68	13.4
Toro Creek near Pozo	11144000	9.61	1962-68	.248

<sup>1</sup>Locations given in figure 1.

<sup>2</sup>The water year is the 12-month period ending September 30 and is designated by the calendar year in which it ends.

#### Mean Discharge from Ungaged Tributaries

The mean discharge in the ungaged tributaries was estimated from a mean annual precipitation-runoff relation. Precipitation data for the relation were provided by a map showing the geographic variation of mean annual precipitation in the study area (fig. 15). Runoff data for the development of the relation were obtained from discharge records for the three gaging stations in the study area that were used to develop the regionalized flow-duration curve.

Figure 16 shows the mean annual precipitation-runoff relation for the Salinas Valley. The procedure used to develop the relation is described in detail by Rantz (1974). Briefly, the procedure was first to develop decile precipitation values for each of the gaged drainage basins. The precipitation-runoff relation was then established by trial-and-error procedures in which a first-trial relation was obtained by plotting mean annual basinwide runoff against mean annual basinwide precipitation. Runoff values for the trial relation were then obtained from the decile precipitation values for each basin to compute mean annual runoff. For each basin the computed runoff was compared to the measured runoff (which was adjusted for the 73-year base period, 1902-74), and adjustments were made to the precipitation-runoff relation until the relation produced acceptable agreement between the computed and measured runoff for each basin. The maximum deviation between computed and measured runoff was about 8 percent (fig. 17).

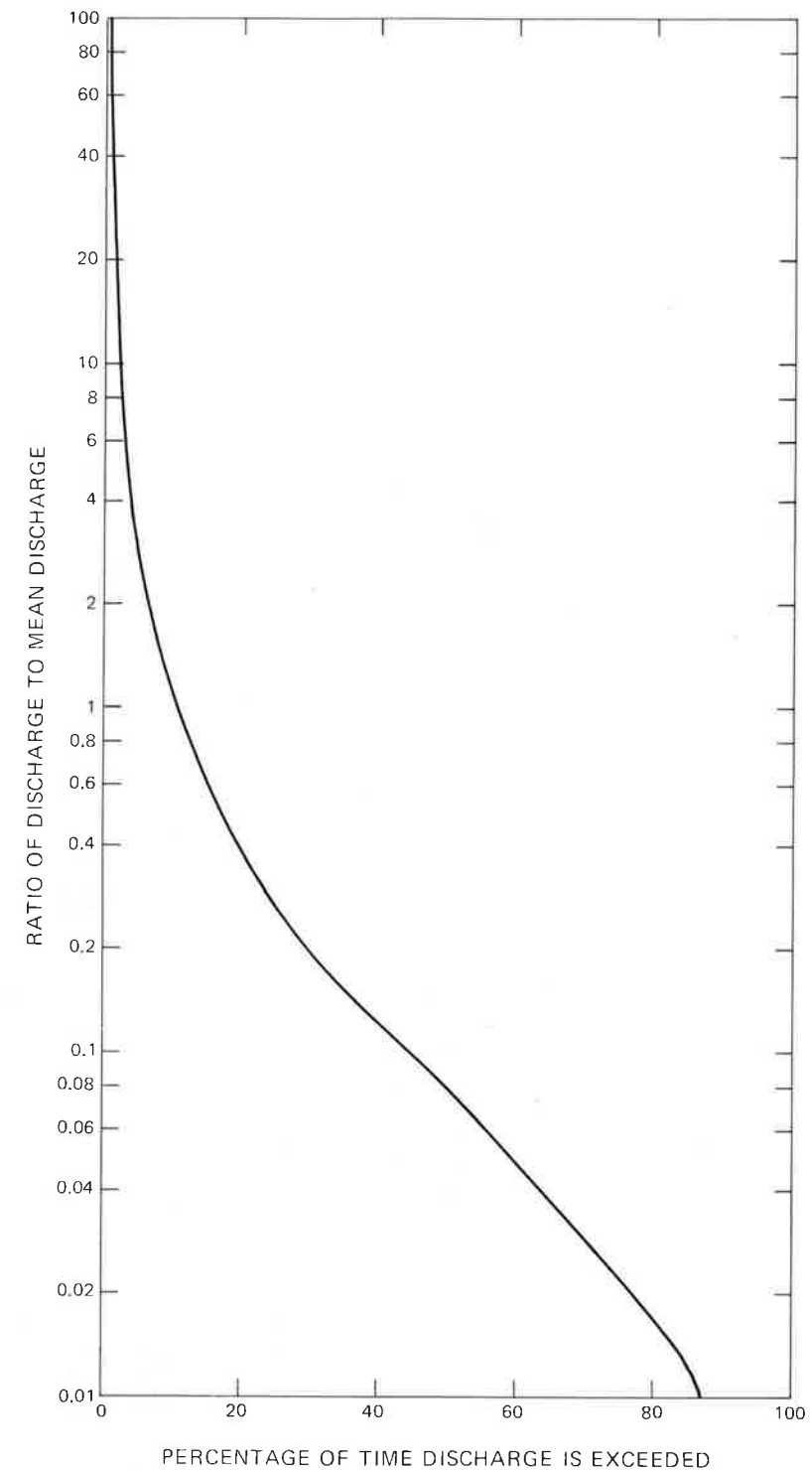


FIGURE 14.--Regionalized flow-duration curve used for ungaged tributaries to the Salinas River.

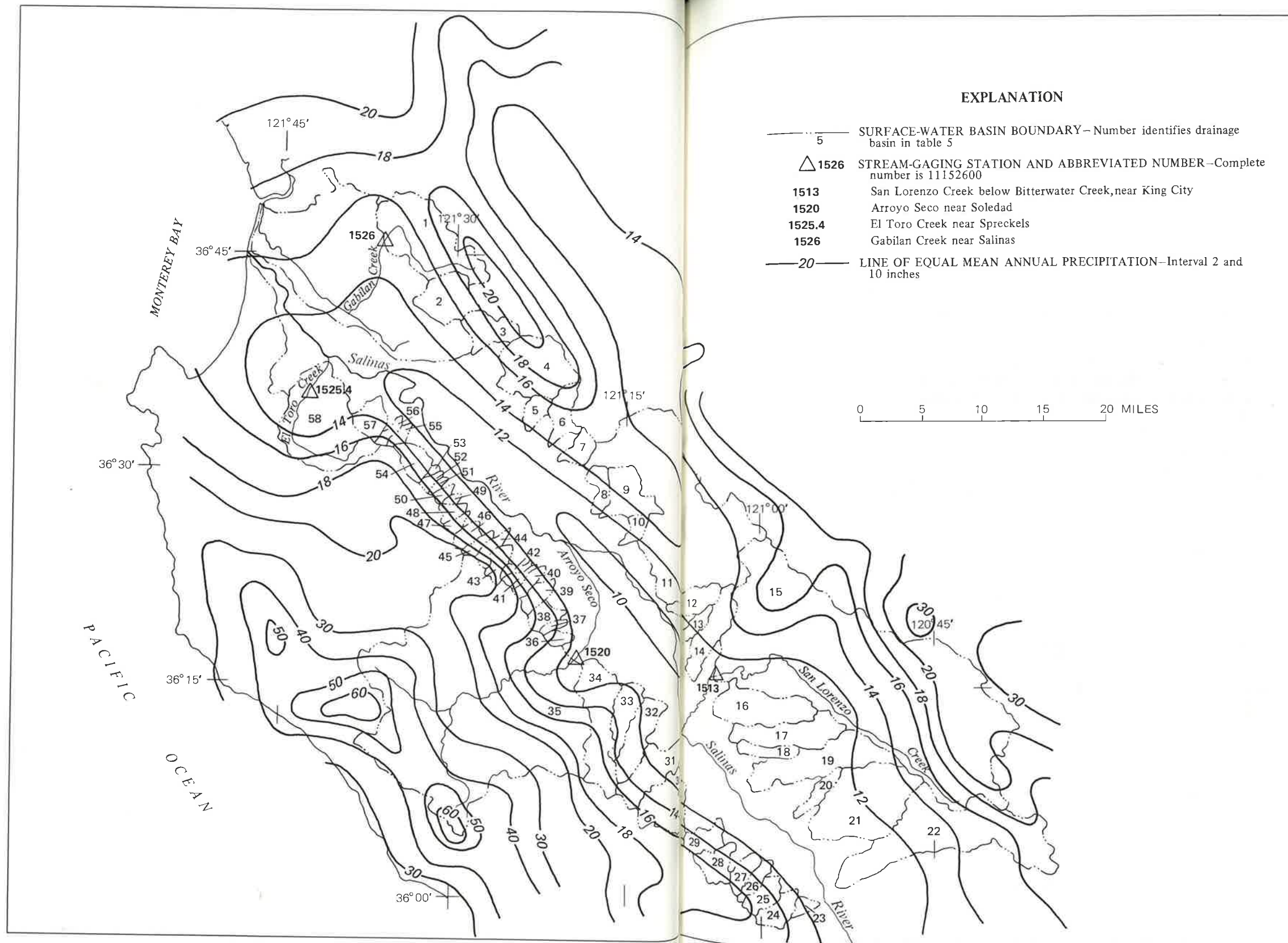


FIGURE 15.--Mean annual precipitation in the Salinas Valley. Precipitation data from Rantz (1969).

FIGURE 15.--Continued

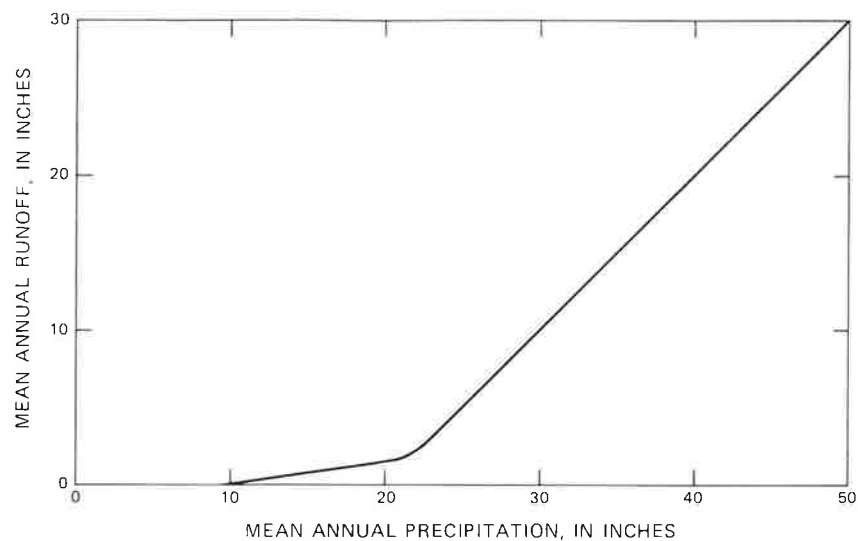


FIGURE 16.--Relation between mean annual precipitation and mean annual runoff.

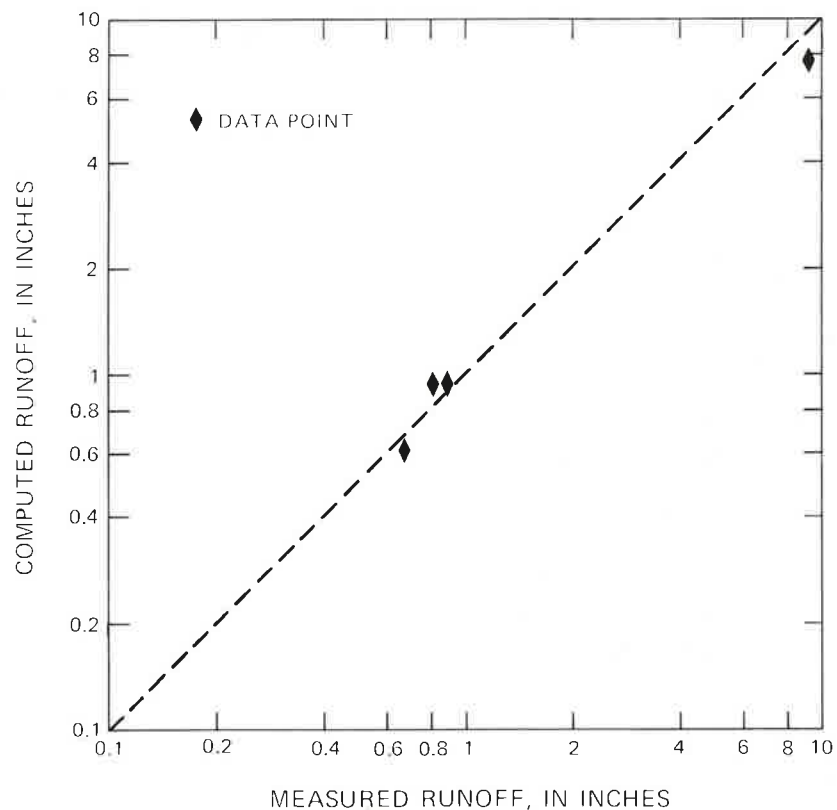


FIGURE 17.--Comparison of runoff computed by the precipitation-runoff relation and measured runoff.

The precipitation-runoff relation was used to develop a map showing mean annual runoff (fig. 18). For each line of equal precipitation on the precipitation map (fig. 15) there is a corresponding line of equal runoff on the runoff map (fig. 18). The precipitation-runoff relation gives the correspondence between the lines on the two maps. The average discharge from each of the ungaged basins was developed (table 5) by first estimating the mean annual basinwide runoff for each basin from the runoff map and then converting the runoff, in inches, to discharge, in cubic feet per second, based on the drainage area.

#### Mean Ground-Water Recharge

The final step in the use of the small-stream model to estimate the mean annual ground-water recharge from tributaries to the Salinas River was to combine the previously developed components of the estimate. The estimates of average discharge were combined with the regionalized flow-duration curve to obtain flow-duration curves for the ungaged tributaries. The tributary channels were divided into as many as 10 reaches, and the flow-duration curves were routed through the small-stream model to obtain, for each tributary, estimates of the mean ground-water recharge rate and the mean surface-water outflow rate to the Salinas River. These estimates are listed in table 5.

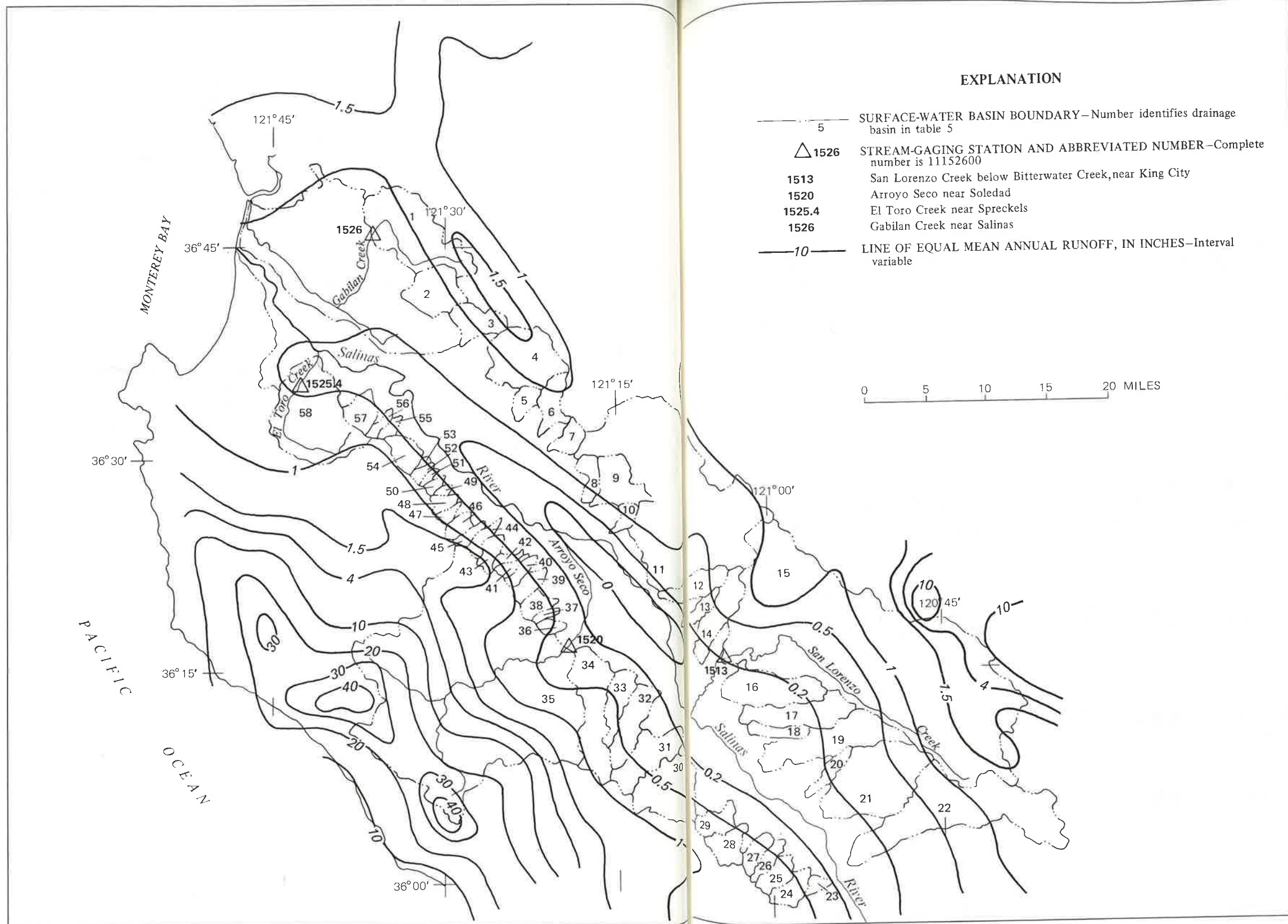


FIGURE 18.--Mean annual runoff in the Salinas Valley.

FIGURE 18.--Continued

TABLE 5. - Mean ground-water recharge rate and surface-water outflow rate to the Salinas River from small streams

Drainage basin No. (figs. 15 and 18)	Drainage area (mi <sup>2</sup> )	Mean runoff (in/yr)	Mean runoff (ft <sup>3</sup> /s)	Channel length (ft)	Reaches used in model	Mean ground-water recharge rate (ft <sup>3</sup> /s)	Outflow rate to the Salinas River (ft <sup>3</sup> /s)
1	36.7	0.90	2.43	34,000	8	2.32	0.110
2	14.1	.90	.934	40,000	1	.934	0
3	9.49	1.20	.838	30,000	1	.838	0
4	23.8	1.20	2.10	26,000	6	1.94	.158
5	4.37	.75	.241	34,000	1	.241	0
6	7.59	.80	.447	35,000	1	.447	0
7	4.99	.65	.239	33,000	1	.239	0
8	4.89	.60	.216	17,000	1	.216	0
9	13.0	.60	.574	15,000	1	.566	.008
10	3.28	.50	.121	3,000	1	.101	.020
11	142	.61	6.38	2,000	1	1.16	5.22
12	12.2	.40	.359	3,000	1	.229	.130
13	5.69	.35	.147	6,000	1	.143	.004
14	15.0	.50	.552	20,000	1	.552	0
15	233	.81	13.9	45,000	9	10.9	2.97
16	18.7	.15	.206	19,000	1	.206	0
17	18.1	.20	.266	13,000	1	.266	0
18	5.69	.15	.063	12,000	1	.063	0
19	28.7	.30	.634	6,000	1	.481	.153
20	5.15	.20	.076	7,000	1	.076	0
21	41.8	.40	1.23	4,000	1	.640	.590
22	59.3	.70	3.06	5,000	1	1.36	1.70
23	2.50	.35	.064	4,000	1	.063	.001
24	6.71	.50	.247	12,000	1	.247	0
25	6.78	.60	.299	16,000	1	.299	0

TABLE 5. - Mean ground-water recharge rate and surface-water outflow rate to the Salinas River from small streams - Continued

Drainage basin No. (figs. 15 and 18)	Drainage area (mi <sup>2</sup> )	Mean runoff (in/yr)	Mean runoff (ft <sup>3</sup> /s)	Channel length (ft)	Reaches used in model	Mean ground-water recharge rate (ft <sup>3</sup> /s)	Outflow rate to the Salinas River (ft <sup>3</sup> /s)
26	3.90	0.50	0.144	16,000	1	0.144	0
27	4.99	.60	.220	14,000	1	.220	0
28	8.67	.70	.447	14,000	1	.442	.005
29	7.59	.60	.335	12,000	1	.332	.003
30	27.5	.50	1.01	18,000	4	.948	.062
31	15.0	.35	.386	8,000	1	.357	.029
32	13.1	.40	.386	7,000	1	.344	.042
33	9.36	.40	.276	18,000	1	.276	0
34	25.0	.75	1.38	5,000	1	.775	.605
35	244	9.08	157	56,000	1	101	55.9
36	2.18	.50	.080	40,000	1	.080	0
37	1.56	.60	.069	32,000	1	.069	0
38	4.37	.70	.225	28,000	1	.225	0
39	4.32	.60	.191	14,000	1	.191	0
40	2.65	.50	.098	14,000	1	.098	0
41	2.18	.70	.112	12,000	1	.112	0
42	1.72	.60	.076	12,000	1	.076	0
43	3.90	1.00	.287	10,000	1	.283	.004
44	3.43	.80	.202	7,000	1	.195	.007
45	2.03	.90	.134	6,000	1	.131	.003

TABLE 5. - Mean ground-water recharge rate and surface-water outflow rate to the Salinas River from small streams - Continued

Drainage basin No. (figs. 15 and 18)	Drainage area (mi <sup>2</sup> )	Mean runoff (in/yr)	Mean runoff (ft <sup>3</sup> /s)	Channel length (ft)	Reaches used in model	Mean ground-water recharge rate (ft <sup>3</sup> /s)	Outflow rate to the Salinas River (ft <sup>3</sup> /s)
46	3.43	0.90	0.227	10,000	1	0.225	0.002
47	1.87	.80	.110	10,000	1	.110	0
48	2.65	.80	.156	10,000	1	.156	0
49	.94	.70	.048	8,000	1	.048	0
50	1.56	.70	.080	4,000	1	.077	.003
51	1.09	.70	.056	6,000	1	.056	0
52	1.56	.70	.080	6,000	1	.080	0
53	.78	.50	.029	6,000	1	.029	0
54	5.93	.70	.306	8,000	1	.291	.015
55	1.87	.60	.083	4,000	1	.079	.004
56	1.89	.60	.083	4,000	1	.080	.003
57	6.86	.70	.353	11,000	1	.347	.006
58	43.1	.67	2.13	3,000	1	.786	1.34
Total	1,184	--	202	--	--	133	69

Application of Model to Estimate the Monthly Mean Tributary Inflow Rate

While estimates of the long-term ground-water recharge suffice for input to the ground-water models estimates of monthly mean tributary inflow to the Salinas River are needed for input to the river model (fig. 10). The small-stream model was used to estimate this inflow by routing through the model estimated daily mean discharges for each of the tributaries to the Salinas River. The resulting estimates of daily mean tributary inflow to the Salinas River were aggregated to establish estimates of the monthly mean tributary inflow.

For the gaged drainage basins, the measured daily mean discharge was used as input to the small-stream model. For the ungaged drainage basin estimates of daily mean discharge were developed from the relation

$$q = q_{SL} \frac{\bar{Q}}{\bar{Q}_{SL}} \quad (8)$$

where q is the daily mean discharge from the ungaged basin, q<sub>SL</sub> is the daily mean discharge for San Lorenzo Creek below Bitterwater Creek near King City, Q̄ is the mean discharge from the ungaged basin (table 5), and Q̄<sub>SL</sub> is the mean discharge for San Lorenzo Creek below Bitterwater Creek.

San Lorenzo Creek was chosen for use in equation 8 because this stream was assumed to be more characteristic of the ungaged tributaries than the other gaged tributaries in the study area. The relation itself was chosen because it is simple and because it has the desirable property that the estimated mean discharge of the ungaged tributary is preserved. The relation also conforms to the previously adopted assumption that the flow regimen of the ungaged tributaries can be represented by a regionalized flow-duration curve.

Table 6 gives the results of routing the measured daily mean discharge for the gaged drainage basins and the estimated daily mean discharge for the ungaged drainage basins through the small-stream model. The mean tributary inflow for December 1968 through November 1971, which was the calibration period used for the river model and the ground-water models (table 3), was 135 ft<sup>3</sup>/s. Tributary inflow does not occur, however, for most of this period, and the months not listed in table 6 are months for which it was estimated that tributary inflow to the Salinas River did not occur.

TABLE 6. - Monthly mean tributary inflow rate to the Salinas River, in cubic feet per second<sup>1</sup>

Year	Month	Tributary to Salinas River between Bradley and Soledad			Tributary to Salinas River between Soledad and Monterey Bay		
		Tributaries, excluding San Lorenzo Creek	San Lorenzo Creek	Total	Tributaries, excluding Arroyo Seco	Arroyo Seco	Total
1968	Dec.	0	0	0	0	1	1
1969	Jan.	355	250	605	156	1,380	1,530
	Feb.	307	192	499	124	978	1,100
	Mar.	69	15	84	17	347	364
	Apr.	23	2	25	5	21	26
1970	Dec.	0	0	0	0	6	6
	Jan.	6	0	6	1	219	220
	Mar.	20	2	22	4	179	183
	Nov.	5	0	5	1	90	91
Mean discharge (December 1, 1968, through November 30, 1971)		22	13	35	9	91	100

<sup>1</sup>Table lists only months with non-zero tributary inflow.

RIVER MODEL

Development of the Model

The most important source of ground-water recharge to the Salinas Valley ground-water basin is percolation from the channel of the Salinas River. The river is hydraulically connected with the ground-water basin, and exchanges of water occur between the two systems. Percolation to or from the river occurs mostly in the reach from San Ardo to Spreckels. Downstream from Spreckels the riverbed consists of or is underlain by fine-grained materials that, for the most part, prevent significant percolation.

Ground-water levels near the river are generally within a few feet of the riverbed. Figure 19 shows the ground-water profile along the river. The solid line in figure 19 represents computed ground-water levels at their seasonal highest level, and the dashed line represents computed water levels at their seasonal lowest level for the 1971 water year. Along the upper reach of the river, both ground-water profiles are, for the most part, within 5 ft of the river thalweg. In the lower reach, however, where the river is underlain by fine-grained material, the depth below the river thalweg to ground water in places exceeds 20 ft.

Development of the Governing Equation

Muskat (1937, p. 350) gave an approximate relation for the seepage discharge from canals and ditches that merge with a shallow water table. By this relation the seepage discharge is approximately linear for small head differentials between the river stage and water table (fig. 20). For larger head differentials, the seepage discharge is nonlinearly related to the head differential. The incremental increase in the seepage discharge with incremental increase in the head differential decreases with increasing head differential. For large head differentials the seepage rate becomes constant and is independent of the ground-water level.

In the river model, the seepage discharge from a channel reach was assumed to be proportional to the head differential between the river stage and ground-water level at the midpoint of the reach and proportional to the flow width of the river. Symbolically, the seepage rate,  $Q_R$ , is given by

$$Q_R = C_R (h_R - h) W_R L \quad (9)$$

where  $C_R$  is a constant of proportionality,  $h_R$  is the river stage,  $h$  is the ground-water level,  $W_R$  is the flow width, and  $L$  is the reach length.



The river stage and flow width were expressed as power functions of the upstream discharge in the reach. The river stage depends on the channel-bed altitude and on the depth of flow in the channel. The depth of flow,  $D$ , was represented by the relation

$$D = a_d Q^{b_d} \quad (10)$$

and the river stage was represented by the relation

$$h_R = H_R + a_d Q^{b_d} \quad (11)$$

where  $H_R$  is the channel-bed altitude,  $Q$  is the river discharge, and  $a_d$  and  $b_d$  are numerical coefficients. The flow width was represented by the relation

$$W_R = a_w Q^{b_w} \quad (12)$$

where  $a_w$  and  $b_w$  are numerical coefficients. The substitution of equations 11 and 12 into equation 9 yields the governing equation for the river model. This equation is

$$Q_R = C_R (H_R + a_d Q^{b_d} - h) a_w Q^{b_w} L. \quad (13)$$

#### Use of the Governing Equation in the Model

To apply the governing equation for seepage, the river is divided into a number of reaches. The equation of continuity for a reach is

$$Q_{in} + Q_{trib} - Q_R = Q_{out} \quad (14)$$

where  $Q_{in}$  is the river inflow to the reach,  $Q_{trib}$  is the surface-water inflow contribution of tributaries to Salinas River,  $Q_R$  is the seepage rate, and  $Q_{out}$  is the river outflow from the reach. If the value of  $Q_{out}$  computed from equation 14 is negative, the river and tributary inflow to the reach cannot satisfy the potential seepage rate computed from equation 13. In this instance  $Q_{out}$  is zero, and  $Q_R$  is computed from

$$Q_R = Q_{in} + Q_{trib}. \quad (15)$$

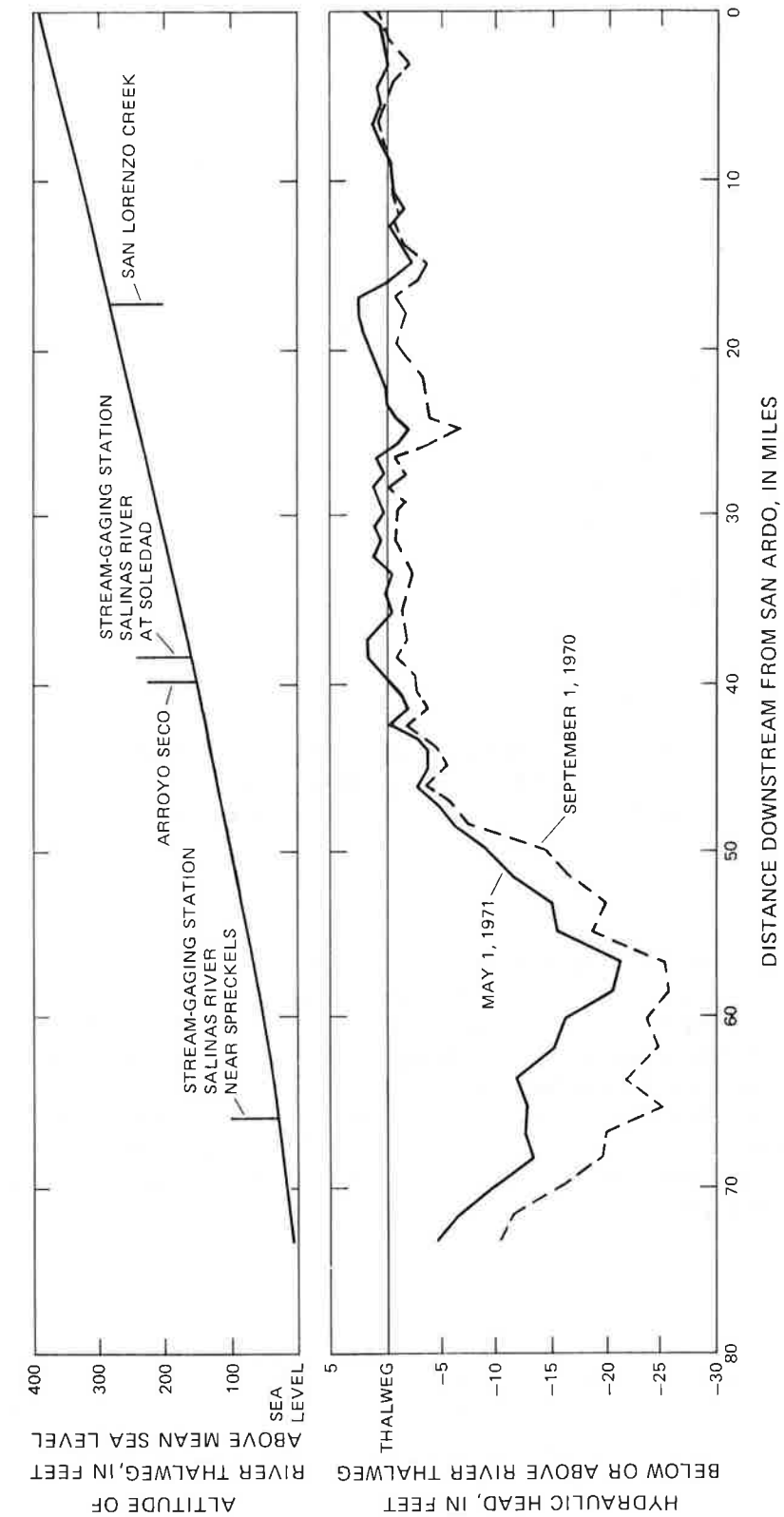


FIGURE 19.--Ground-water profiles computed by the two-dimensional ground-water model and thalweg profile along the Salinas River.

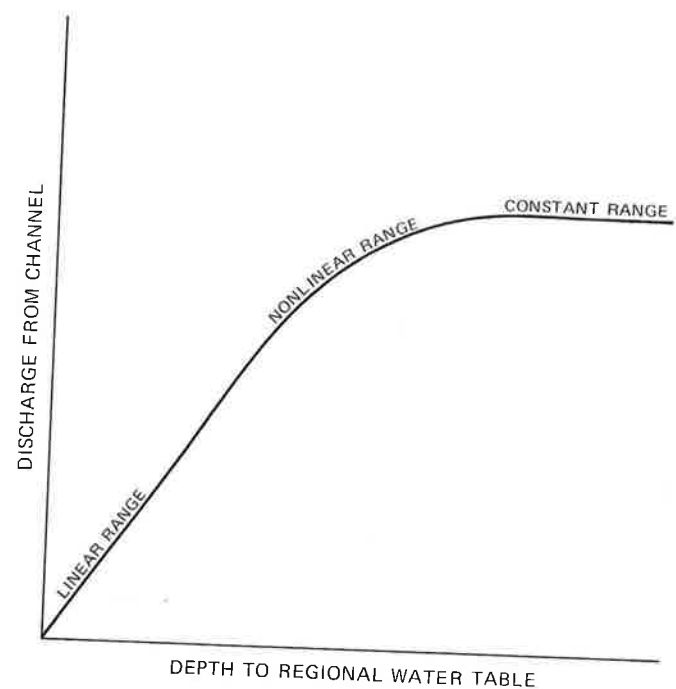


FIGURE 20.--Generalized relation between seepage discharge from a stream channel and depth to the regional water table.

Starting at the most upstream reach and proceeding in the downstream direction, the seepage and the river outflow are computed for each reach. The procedure is then repeated for each time step. Similar to considerations for the small-stream model, reach lengths should be short enough that the average river stage and flow width can be computed from the power functions. In addition, the time step should be long enough that the assumption of steady-state flow in the river is valid. With respect to these criteria, the river was divided into 65 reaches with an average length of 6,000 ft, and time steps of 1 month were used.

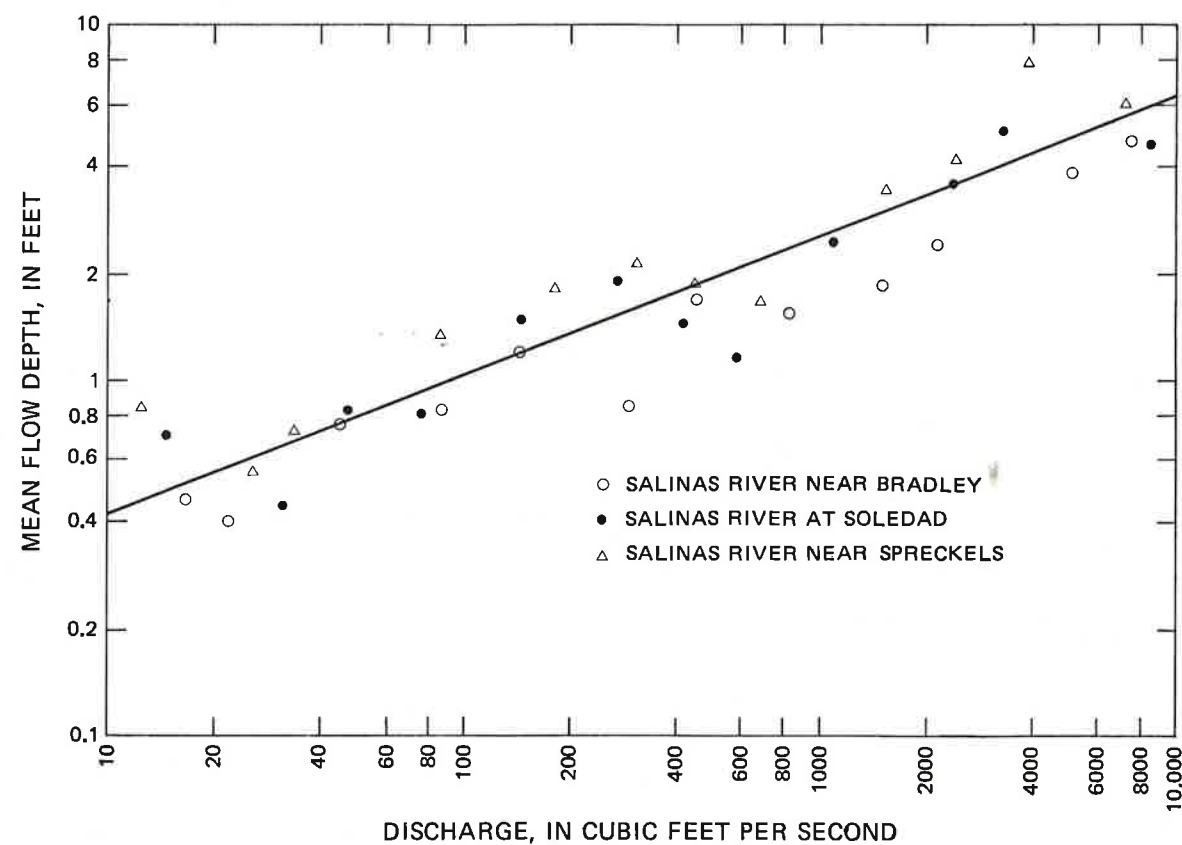


FIGURE 21.--Relation between mean flow depth and discharge for the Salinas River.

#### Model Calibration

Measured values of discharge, width, and depth for the Salinas River were used to estimate values for the numerical coefficients of the power functions (eqs. 10 and 12). Measurements of mean depth and discharge are plotted logarithmically in figure 21. The line representing the average relation between the data has  $a_d$  equal to 0.17 and  $b_d$  equal to 0.39.

Measurements of flow width and discharge are plotted logarithmically in figure 22. The line representing the average relation between the data has  $a_w$  equal to 10 and  $b_w$  equal to 0.44.

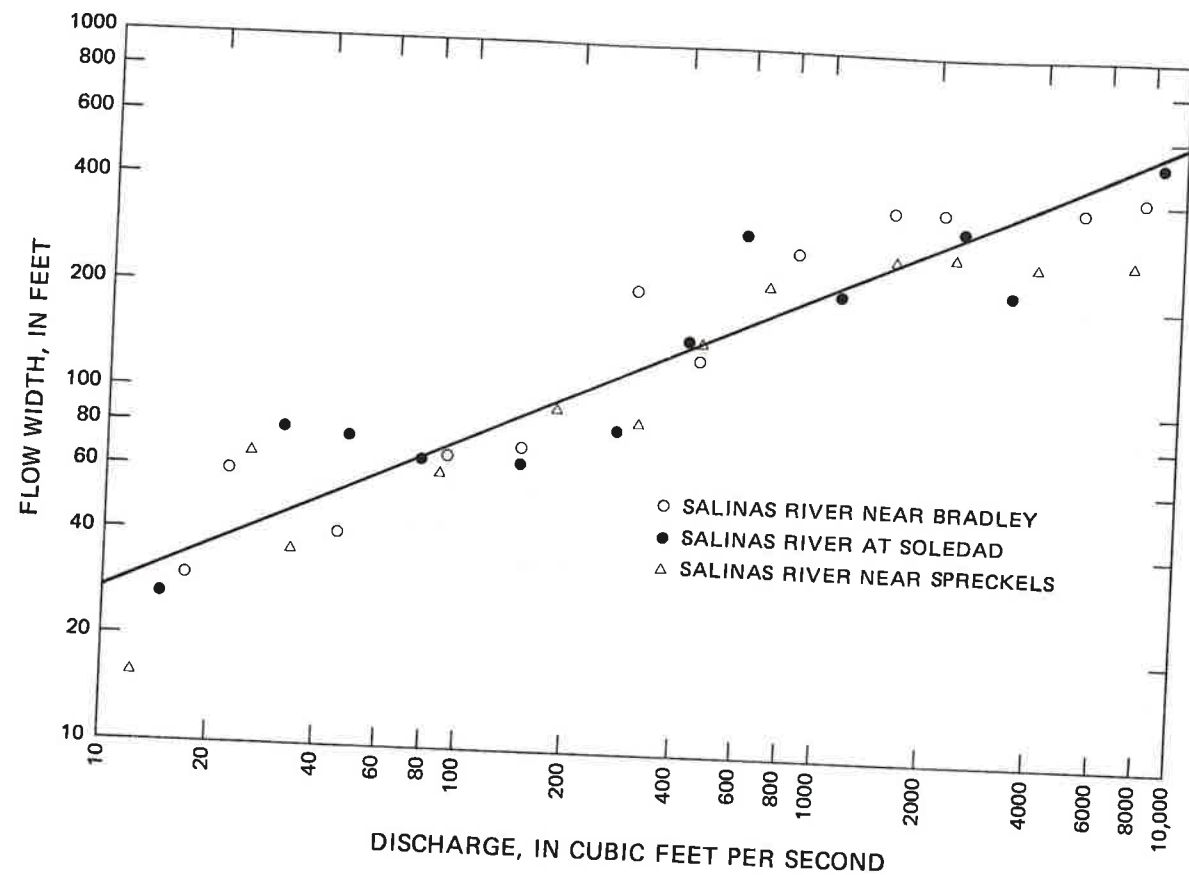


FIGURE 22.--Relation between flow width and discharge for the Salinas River

The constant of proportionality in the seepage equation (eq. 9) depends in part on the vertical permeability of the channel bed and on the ability of ground water to move laterally in the immediate vicinity of the river. Clearly, the value of this constant may vary along the river. The estimated value of the constant decreases in the downstream direction. The value was  $2.7 \times 10^{-6}$  per second at San Ardo and  $5.4 \times 10^{-7}$  per second at Spreckels. These values were selected through the joint calibration of the river model and the two-dimensional ground-water model so that the models simulated the observed head differentials between the river and the ground-water basin.

Although the parameters of the river model (table 3) were not adjusted during the calibration procedure with the objective of improving the simulation of streamflow, the comparison of measured and computed streamflow for the Salinas River provides a check on the overall performance of the river model. In table 7, measured and computed annual mean discharge for the Salinas River at Soledad and the Salinas River near Spreckels are compared. For the 3-year calibration period, December 1968-December 1971, the model overestimated the cumulative discharge for the Salinas River at Soledad by about 4 percent and underestimated the discharge for the Salinas River near Spreckels by about 0.1 percent. The deviation of computed discharge from measured discharge for individual years, however, is in general larger than the cumulative deviation for the 3-year period. For example, for 1971 the model overestimated the discharge for the Salinas River at Soledad by about 60 percent.

In fact, the departure of the model from the prototype increases as even smaller time intervals are examined. Figure 23 shows the monthly mean discharge for the Salinas River near Bradley, which is the principal input to the river model. Figures 24 and 25 show the corresponding monthly mean discharge for the Salinas River at Soledad and the Salinas River near Spreckels, respectively. For specific months the model underestimates discharge by as much as 100 percent and overestimates discharge by as much as 8,000 percent.

The largest errors, however, tend to be associated with the low measured discharges for the Salinas River near Spreckels, which is apparent from figure 26. This figure shows a scattergram of measured and computed monthly mean discharge for the Salinas River at Soledad and near Spreckels. The standard deviation of log residuals for the river at Soledad is 0.24 log units or -42 to +72 percent, while the standard deviation of log residuals for the Salinas River near Spreckels is 0.90 log units or -57 to +690 percent. Clearly, the monthly mean discharge for the river near Spreckels is more poorly simulated by the model than the monthly mean discharge for the river at Soledad.

Admittedly these disparities between model and prototype are large. The compared streamflows, however, are the residual streamflows after water has been removed from the river by percolation to ground water. For low river discharge at Bradley, the percolation rate is a substantial part of this river discharge, and large errors in the simulation of river discharge at Spreckels do not necessarily mean a large error in the simulation of ground-water recharge from the river. Correspondingly, the monthly mean percolation rate is, in general, better simulated by the model than the monthly mean river discharge. In fact, for the 3-year calibration period, the standard deviation of log residuals for percolation from the Salinas River between Bradley and Spreckels was 0.25 log units, or -44 to +78 percent, which is much smaller than the same measure of the simulation of discharge for the Salinas River near Spreckels.

TABLE 7. - Comparison of measured and computed annual mean discharge for the Salinas River at Soledad and the Salinas River near Spreckels  
[Discharge, in cubic feet per second]

Year	Stream-gaging station					
	Salinas River at Soledad			Salinas River near Spreckels		
	Measured	Computed	Difference	Measured	Computed	Difference
1969	2,073	2,004	69	2,144	2,115	29
1970	169	248	-79	172	166	6
1971	133	207	-74	46	79	-33
Average	792	820	-28	788	787	1

The model seems to simulate percolation with about equal reliability for both high and low streamflow, while the model better simulates streamflow for high streamflow than for low streamflow. Table 8, which gives the mass balance for the Salinas River between Bradley and Spreckels (tables 9 and 10 give the mass balance for the Salinas River between Bradley and Soledad and between Soledad and Spreckels, respectively), lists for each year of the calibration period the annual mean seepage rate based on measured discharge for the Salinas River near Spreckels and on computed discharge. The difference between the seepage rates based on the two river discharges ranges from 4 to 15 percent, while the differences between the measured and computed river discharges ranged from 1 to 72 percent (table 7).

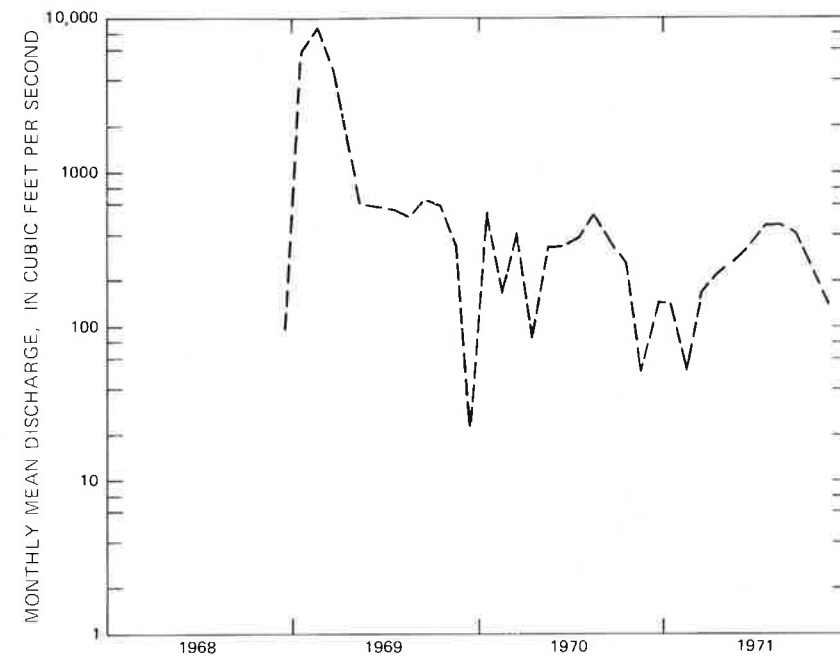


FIGURE 23.--Monthly mean measured discharge for the Salinas River near Bradely.

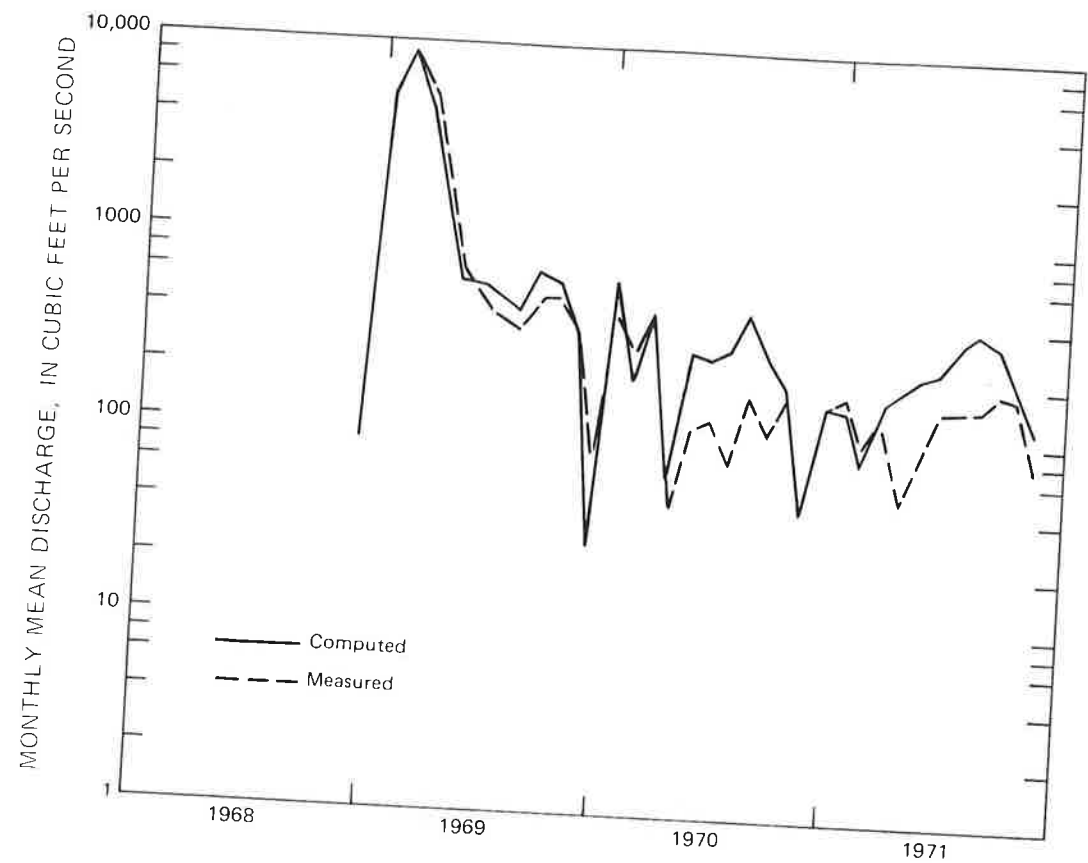


FIGURE 24.--Comparison of monthly mean discharge computed by the river model and monthly mean measured discharge for the Salinas River at Soledad.

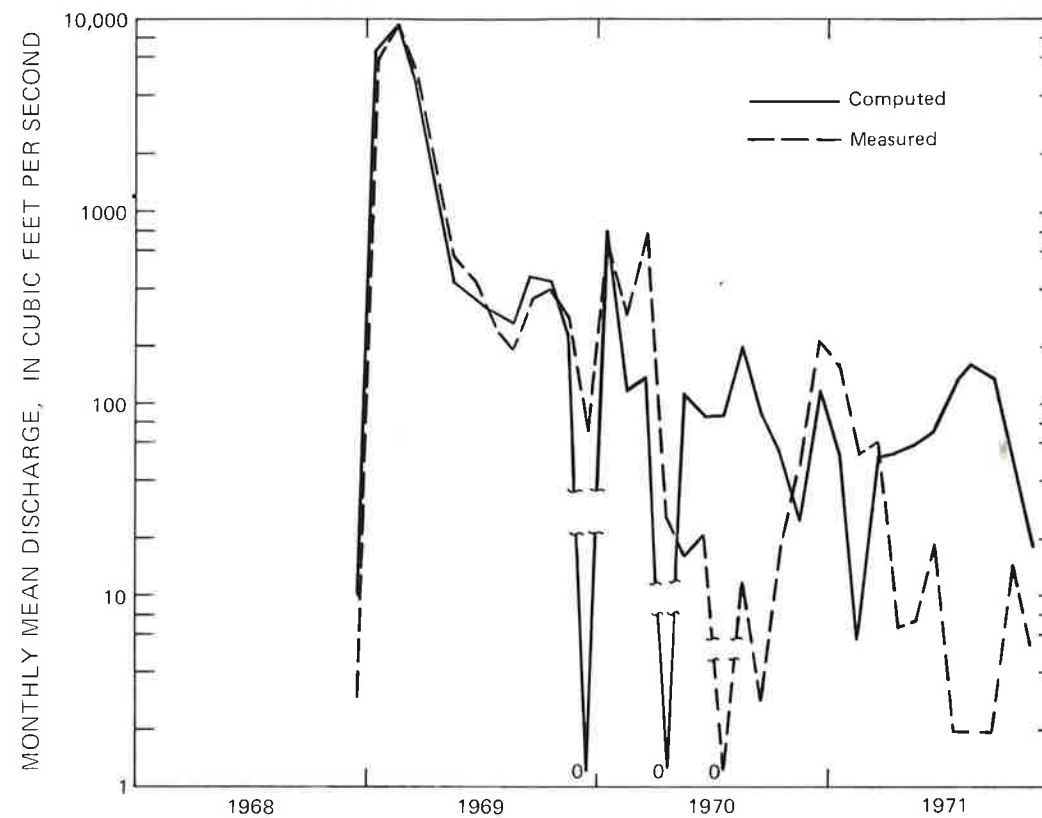


FIGURE 25.--Comparison of monthly mean discharge computed by the river model and monthly mean measured discharge for the Salinas River near Spreckels.

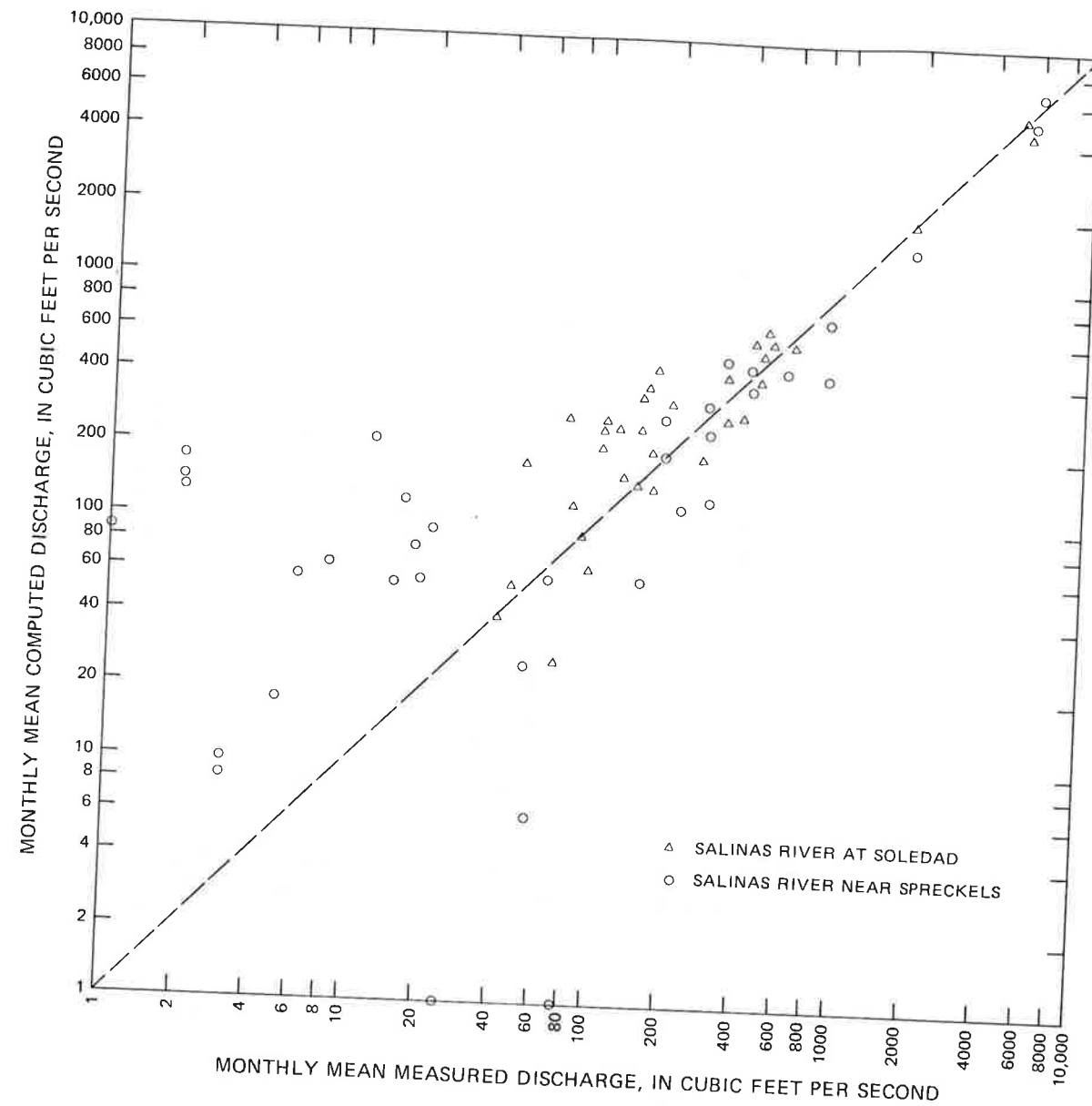


FIGURE 26.--Scattergram of monthly mean discharge computed by the river model and monthly mean measured discharge for the Salinas River at Soledad and near Spreckels.

TABLE 8. - Mass balance for the Salinas River between Bradley and Spreckels  
[Annual mean discharges, in cubic feet per second]

Year	River inflow rate	Tributary inflow rate	River outflow rate		Seepage rate		
			Measured	Computed	Measured	Computed	Difference
1969	1,904	353	2,144	2,115	113	142	-29
1970	298	44	172	166	170	176	-6
1971	262	9	46	79	225	192	33
Average	821	135	187	787	169	170	-2

TABLE 9. - Mass balance for the Salinas River between Bradley and Soledad  
[Annual mean discharges, in cubic feet per second]

Year	River inflow rate	Tributary inflow rate	River outflow rate		Seepage rate		
			Measured	Computed	Measured	Computed	Difference
1969	1,904	101	2,073	2,004	<sup>1</sup> -68	1	-69
1970	298	3	169	248	132	53	79
1971	262	2	133	207	131	57	74
Average	821	35	792	820	65	37	28

<sup>1</sup>A negative percolation rate indicates that the river gained water from ground water.

TABLE 10. - Mass balance for the Salinas River between Soledad and Spreckels

[Annual mean discharges, in cubic feet per second]

Year	River inflow rate		Tributary inflow rate	River outflow rate		Seepage rate		
	Measured	Computed		Measured	Computed	Measured	Computed	Difference
1969	2,073	2,004	252	2,144	2,115	181	141	40
1970	169	248	41	172	166	38	123	-85
1971	133	207	7	46	79	94	135	-41
Average	792	820	100	788	787	104	133	-29

## TWO-DIMENSIONAL GROUND-WATER MODEL

### Description of the Model

The two-dimensional model of the Salinas Valley ground-water basin treats the prototype as a single-aquifer system. The modeling of the ground-water basin is accomplished by substituting a simplified conceptual model for the prototype. Some of the more important simplifying assumptions that relate directly to the mathematical model are (1) that ground-water movement is strictly horizontal (hence the hydraulic head is invariant with depth), (2) that the hydraulic gradient is equal to the slope of the free surface and is invariant with depth, (3) that the physical parameters of the system do not change with the state of the system, (4) that the ground-water basin is isotropic, and (5) that changes in ground-water storage occur instantaneously with changes in hydraulic head. Although these assumptions may appear paradoxical, in many ground-water problems solutions based on these assumptions compare favorably with those of more rigorous methods.

The equation that describes ground-water flow for the above assumptions is (Bear, 1972, p. 215)

$$\frac{\partial}{\partial x} \left( T_{xx} \frac{\partial h}{\partial x} \right) + \frac{\partial}{\partial y} \left( T_{yy} \frac{\partial h}{\partial y} \right) - S \frac{\partial h}{\partial t} - W = 0 \quad (16)$$

where  $T_{xx}$  and  $T_{yy}$  are the principal components of the transmissivity tensor (the coordinate axes are assumed to be aligned with the principal directions),  $h$  is the hydraulic head,  $S$  is the storage coefficient, and  $W$  is the discharge of a source or sink. The source-sink function was used to introduce well discharge, irrigation return, recharge from small streams, and recharge from the Salinas River. In the model these quantities are treated as point sources and sinks (Pinder and Frind, 1972).

Approximate solutions to the ground-water-flow equation were obtained using the Galerkin finite-element method. Pinder and Frind (1972) gave a mathematical description of this method. Briefly, it involves subdividing the ground-water basin into elements having quadrilateral shape and assuming that the solution to the differential equation can be written as a linear combination of relatively simple trial functions. Associated with the trial functions are adjustable coefficients, which the Galerkin computational scheme adjusts in order to give some best approximation to equation 16. The computer program used to approximate the solution to the ground-water-flow equation is a Galerkin finite-element program developed by G. F. Pinder (written commun., 1975). The program employs isoparametric quadrilateral elements.

Figure 27 shows the element configuration used for the analyses of the Salinas Valley ground-water basin. The geometrical relations in the ground-water basin are specified in the model through the configuration of elements. The water-bearing properties of the prototype are specified in the model by assigning parameter values to the elements. These values represent the prototype transmissivity and storage coefficient. The model uses the above specifications to compute hydraulic heads that mathematically satisfy the ground-water-flow equation for the sources and sinks applied, for the boundary conditions imposed, for the initial conditions specified, and for the system parameters specified.

### Source and Sink Discharge

The two-dimensional ground-water model was calibrated on the 3-year period December 1968-November 1971. Source and sink discharges for input to the model were estimated for this period. The source and sink discharges include agricultural and municipal pumpage, recharge from irrigation-return water, discharge from riparian vegetation, recharge from small streams, recharge from precipitation, and recharge from the Salinas River.

### Agricultural and Municipal Pumpage

Estimates of ground-water pumpage for the model calibration period (table 3) were developed for input to the two-dimensional ground-water model. Agricultural pumpage was estimated from records of metered electrical power consumption and from estimates of the local average unit power consumption per unit volume of water pumped. Data used were obtained through the cooperation of the Pacific Gas and Electric Co. Table 11 lists the estimated total agricultural pumpage for the Salinas Valley ground-water basin for agricultural years 1969-71. (The agricultural year is the 12-month period beginning April 1 and is designated by the year in which it begins.) Figure 27 shows the estimated geographic distribution of pumpage for agricultural year 1970. For input to the model, pumpage for 1969 and 1970 was similarly distributed.

The ground-water model uses 1-month time steps, and the monthly pumpage for input to the model was obtained by multiplying the seasonal pumpage (table 11) by a monthly distribution factor. The monthly distribution of pumpage is shown in figure 28. This distribution is based on the average monthly distribution of seasonal electrical power consumption for the Salinas Valley.

Municipal pumpage was estimated by multiplying the population by an annual per capita demand factor of 0.25 acre-ft. Population data were obtained from the U.S. Bureau of the Census (1971). The per capita demand factor was estimated by analysis of population and metered pumpage data from a limited number of communities in Santa Barbara, San Luis Obispo, and Monterey Counties (Muir, 1973). Table 12 lists the municipal pumpage from the Salinas Valley ground-water basin for 1970. Similar pumpages were used for the other years. Figure 29 shows the estimated geographic distribution of municipal pumpage. For input to the model, municipal pumpage was assumed to be evenly distributed throughout the year.

#### Ground-Water Recharge from Irrigation-Return Water

When land is being irrigated, water in excess of the moisture requirement of the crop is applied to control the salt level in the root zone. Thus, only part of the applied water is consumed by the crop. The residual penetrates past the root zone and may percolate to the water table. In the Salinas Valley about 30 percent of applied irrigation water returns to ground water (California Water Resources Board, 1955) and is an important source of ground-water recharge.

TABLE 11. - Agricultural pumpage for agricultural years 1969-71

Agricultural year <sup>1</sup>	Pumpage (acre-ft)
1969	387,000
1970	460,000
1971	450,000

<sup>1</sup>The agricultural year is the 12-month period beginning April 1 and is designated by the year in which it begins.

TABLE 12. - Municipal pumpage for 1970

Community	Population <sup>1</sup>	Pumpage (acre-ft/yr)
Castroville	3,200	800
Gonzales	2,600	650
Greenfield	2,600	650
King City	3,700	920
Marina	8,300	2,080
Salinas	58,900	14,720
San Ardo	500	120
Soledad	6,800	1,700
Total <sup>2</sup>	87,000	22,000

<sup>1</sup>Population based on 1970 census (U.S. Bureau of the Census, 1971).

<sup>2</sup>Rounded to nearest 1,000.



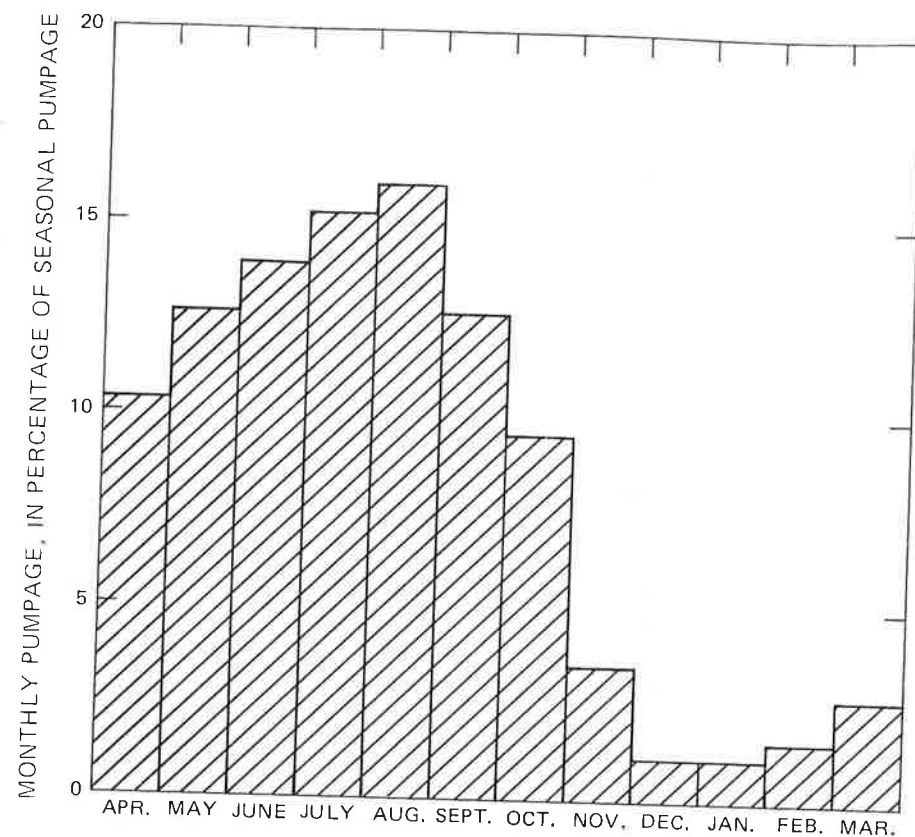


FIGURE 28.--Monthly distribution of agricultural pumpage that was used in the two-dimensional ground-water model.

Direct precipitation supplies some water for crops. Most precipitation occurs, however, during nongrowing periods, and a large part of this precipitation is consumed nonbeneficially. The remainder is carried over as soil moisture and is, in part, consumed beneficially during the cultural periods.

The California Department of Public Works, Division of Water Resources (1946) estimated the consumptive use of water by irrigated crops in the Salinas Valley for the irrigation practices and cropping patterns existing in 1944 (table 13). Part of the water estimated to be consumed by crops is supplied by applied irrigation water and part is supplied by direct precipitation, or

$$C_T = C_A + C_P \quad (17)$$

where  $C_T$  is the total consumptive use,  $C_A$  is the consumptive use of irrigation water, and  $C_P$  is the consumptive use of precipitation.

TABLE 13. - Disposition of applied irrigation water and precipitation for 1944

Ground-water area	Irrigated land <sup>1</sup> (acres)	Applied irrigation water <sup>1</sup> (acre-ft)	Precipitation (acre-ft)	Consumptive use <sup>1</sup> (acre-ft)	Water-use efficiency (percent)	Ground-water recharge (acre-ft)
Pressure	50,000	104,000	55,000	85,000	54	74,000
East Side	15,000	33,000	16,000	28,000	57	21,000
Forebay	39,000	124,000	39,000	82,000	50	81,000
Upper Valley	22,000	87,000	18,000	47,000	45	58,000
Total	126,000	348,000	128,000	242,000	--	234,000
Average	--	--	--	--	51	--

<sup>1</sup>Data from California Department of Public Works, Division of Water Resources (1946).

The part of applied irrigation water that is consumed is expressed by the irrigation efficiency. Irrigation efficiency is the ratio of consumptive use of applied irrigation water to the total amount of water applied. The consumptive use that is supplied by irrigation water, then, is given by the relation

$$C_A = E_A A \quad (18)$$

where  $E_A$  is the irrigation efficiency and  $A$  is the applied irrigation water.

The part of precipitation that is consumed is expressed by the effective precipitation. Effective precipitation is that part of direct precipitation that is consumptively used and does not run off or percolate to ground water. Effective precipitation is identical with  $C_P$  in equation 17 and is given by the relation

$$C_P = E_P P \quad (19)$$

where  $E_P$  is a coefficient and  $P$  is the precipitation that infiltrates the soil. The quantity  $P$  is the total precipitation less the precipitation that runs off.

By making the appropriate substitutions into equation 17 and by assuming that  $E_A$  equals  $E_P$ , the resulting relation for irrigation efficiency (or the effective precipitation coefficient) is

$$E_A = \frac{C_T}{A+P} \quad (20)$$

Table 13 lists the irrigation efficiency for the various ground-water areas of the Salinas Valley ground-water basin. Efficiencies range from 45 to 57 percent and generally decrease southward in the valley, probably because of the occurrence of heavier soils in the northern part of the study area. The overall efficiency for the valley is 51 percent. This value was increased to 70 percent during the calibration of the two-dimensional ground-water model and the river model in order to better reproduce the annual mean measured discharge for the Salinas River. The higher value for the calibration period (December 1969-November 1971) may in fact represent an actual change in irrigation efficiency since 1944.

In the ground-water model, ground-water recharge from precipitation on cultivated areas was not treated explicitly. Instead, the total ground-water recharge was assumed to equal 45 percent of ground-water pumpage, which is approximately equivalent to an irrigation efficiency (or effective precipitation coefficient) of 70 percent.

In most parts of the ground-water basin, ground-water recharge was assumed to occur at the location of ground-water pumpage. In the Pressure Area, however, the confining member above the 180-foot aquifer (fig. 8) probably prevents ground-water recharge. In this area, ground-water recharge by water pumped from beneath the confining member was assumed to occur along the perimeter of the confining member.

#### Ground-Water Discharge from Riparian Vegetation

Native phreatophytes grow along the banks and in the channel of the Salinas River. Phreatophytes are plants that depend for their water supply upon ground water that lies within reach of their roots (Meinzer, 1927; and Robinson, 1958). The phreatophytes along the Salinas River cover about 12,000 acres (Gene L. Gerdes, California Department of Fish and Game, written commun., 1977) and discharge about 25,000 acre-ft of water into the atmosphere annually.

The phreatophytes include both woody and shrub species. The woody species cover about 6,000 acres. They include mostly cottonwoods (*Populus fremontii* and *P. trichocarpa*) and willows (*Salix*) but also include sycamore (*Plantanus racemose*), saltcedar (*Tamarix*), and other species. The woody species occur mostly in the southeastern part of the study area (table 14). The shrub species of phreatophytes also cover about 6,000 acres. They include tule (*Scirpus olneyi*), blackberry (*Rubus vitifolius*), mule fat (*Baccharis vemiea*), grant reed (*Arundo donax*), and other species (Gene L. Gerdes, California Department of Fish and Game, written commun., 1977), but no particular species is dominant. The shrub species are more or less evenly distributed along the Salinas River (table 14).

The amount of water used by phreatophytes depends not only on climatic factors, but also on plant species, thickness of the foliage canopy, density of cover, and depth to the water table (Robinson, 1958; Gatewood and others, 1950; Blaney and Criddle, 1962; and Blaney, 1954). The consumptive use of water by woody and shrub species of phreatophytes was estimated by the Blaney-Criddle method (Blaney and Criddle, 1962). The general method expresses the relation between consumptive use of water, average air temperature, and daylight hours in a given area. The effects of unevaluated factors, such as depth to water and density of growth, are contained in an empirical coefficient.

The Blaney-Criddle method is based on the assumption that with ample moisture available, evapotranspiration is affected primarily by air temperature, duration of daylight, and plant species. For a complete description of the method, the reader is referred to Blaney and Criddle (1962). In brief, the Blaney-Criddle equation for evapotranspiration is

$$Q = \left( K \frac{T_p}{100} - P \right) A \quad (21)$$

where  $Q$  is evapotranspiration of ground water during the growing period,  $K$  is an empirical consumptive-use coefficient that is primarily dependent on the plant species and depth to water table,  $p$  is the monthly percentage of total daytime hours in the year (Rantz, 1968, gave such a table of daylight hours),  $T$  is the mean monthly temperature,  $P$  is the effective precipitation, and  $A$  is the area covered by vegetation.

Based on the application of equation 21 to the study area, the annual use of ground water by phreatophytes along the Salinas River is about 25,000 acre-ft. The distribution of vegetated area along the river is given in table 14. Also given in table 14 and shown in figure 30 is the distribution of discharge from the phreatophytes.

TABLE 14. - Areal distribution of and mean consumptive use of ground water by riparian vegetation along the Salinas River

River reach (fig. 30)	Distribution of vegetation (acres)			Total	Consumptive use of ground water <sup>1</sup> (acre-ft/yr)			Total
	Woody species	Shrub species	Total		$zK = 1.1$		Shrub species	
					Woody species	Shrub species		
1	90	1,380	1,470	240	1,970	1,970	2,210	
2	1,340	980	2,320	3,550	1,400	1,400	4,950	
3	760	360	1,120	2,020	510	510	2,530	
4	640	160	800	1,700	230	230	1,930	
5	1,020	730	1,750	2,700	1,040	1,040	3,740	
6	990	400	1,390	2,620	570	570	3,190	
7	860	860	1,720	2,280	1,230	1,230	3,510	
8	290	540	830	770	770	770	1,540	
9 (mouth of river)	370	350	720	980	980	500	1,480	
Total <sup>3</sup>	6,300	5,800	12,100	16,900	8,200	8,200	25,100	

<sup>1</sup>Effective precipitation was assumed to equal 0.9 ft/yr.

<sup>2</sup>Consumptive-use coefficients were based on data given by Rantz (1968).

<sup>3</sup>Rounded to nearest 100 acres or acre-ft/yr.

Ground-Water Recharge from Small Streams

Ground-water recharge computed by the small-stream model (table 5) was used as input to the two-dimensional ground-water model. Figure 31 shows the geographic distribution of recharge from the small streams. For input to the ground-water model, the recharge was assumed to be evenly distributed in time. The justification for this assumption is that, because the water table is at least several hundred feet below the land surface in most of the recharge areas, percolation to the water table of streamflow infiltration probably is delayed several months and perhaps as much as a year. Piper and others (1939) have shown that on the east side of the San Joaquin Valley the effect of infiltration from a single storm usually could not be detected where the water table was more than 30 ft below the land surface. Successive increments of recharge moving downward to the water table were attenuated and largely merged before reaching it, and the recharge to the ground-water basin took place throughout much of the year. Corresponding conditions probably prevail in the Salinas Valley. Further, the successive yearly increments of streamflow infiltration, at least in years of normal streamflow, probably merge to such an extent that the rate of accretion of water on the water table is nearly constant throughout the year and from year to year.

Ground-Water Recharge from Precipitation

In most of the nonirrigated areas of the Salinas Valley, direct precipitation does not contribute significantly to ground-water recharge (California Department of Public Works, Division of Water Resources, 1946) because most precipitation is consumed by the native vegetation. Blaney, Taylor, and Young (1930) measured the evapotranspiration of native vegetation on experimental plots in the Santa Ana River valley, which is climatically similar to much of the Salinas Valley. They found that deep penetration of precipitation below the root zone may be expected on grass and weed plots after 10 to 12 inches of seasonal precipitation. Over most of the southeastern part of the Salinas Valley, mean annual precipitation is less than 12 inches (fig. 15), and little ground-water recharge from deep penetration of precipitation would be expected.

In the northwestern part of the Salinas Valley, however, mean annual precipitation in nonirrigated areas generally exceeds 14 inches. In addition, these areas are, for the most part, underlain by permeable surficial deposits of windblown sand, and significant deep penetration of precipitation probably occurs, principally near Marina and near Prunedale. On the basis of the frequency distribution of seasonal precipitation, the mean annual ground-water recharge near Marina is about 1,000 acre-ft and near Prunedale is about 5,000 acre-ft. Figure 31 shows the geographical distribution of ground-water recharge near these localities. For input to the ground-water model this recharge was assumed to be evenly distributed in time. The justification for this assumption follows the justification for using uniform recharge from small streams, which was discussed in a previous section.

#### Ground-Water Recharge from the Salinas River

The river model was used to compute ground-water recharge from the Salinas River. Direct interactions occur between the Salinas River and the ground-water basin and, correspondingly, between the river model and the two-dimensional ground-water model. Consequently, these models are included in a single computer program so that the interactions can be evaluated for each time step of the ground-water model. Because recharge from the river is nonlinearly related to the hydraulic head in the ground-water basin, at each time step of the ground-water model iterations are executed between the ground-water model and river model until the mass balance for the river (eqs. 14 and 15) is satisfied.

#### Boundary Conditions

The equation of ground-water flow (eq. 16) has an infinite number of solutions. The question naturally arises as to how one may choose, among the infinity of solutions, those applying to any particular problem. Without any detailed analysis, differences in the solutions are related, in part, to differences in the boundaries defining the ground-water basin and to the conditions that are imposed at these boundaries. The boundary conditions used on the two-dimensional ground-water model are of two types: Specification of hydraulic head on the boundary and specification of discharge across the boundary.

#### Specified-Head Boundaries

The boundary of the ground-water basin at Monterey Bay was represented in the model by the specification of hydraulic heads. The hydraulic head in the ground-water basin along this boundary was assumed to equal the mean sea level in Monterey Bay. Because time steps of 1 month are used in the model, diurnal tidal variations in sea level were not considered in the specification of hydraulic head on the boundary.

#### Specified-Discharge Boundaries

No-flow boundary.--Boundaries with specified discharge are used in other parts of the model. The discharge is specified to be zero (an impermeable boundary) along the southwest side of the ground-water basin from Monterey Bay to San Ardo and along the east side from Monterey Bay to King City. Minor quantities of water may enter the ground-water basin as underflow through the alluvial deposits that typically underlie the stream channels debouching from the highlands adjacent to the ground-water basin. Tongues of alluvium generally extend along the stream channels far up into their canyons. This source of underflow was ignored, however, in the ground-water model. As mentioned earlier, evapotranspiration processes were ignored in the development of the small-stream model. The omission of evapotranspiration tends to increase the estimated ground-water recharge from the small streams, which tends to cancel the effects of omitting underflow locally.

Constant-discharge boundary.--Non-zero values of discharge were specified for the boundary segment on the northeast side of the ground-water basin from near King City to San Ardo and for the boundary segment that transverses the Salinas River at San Ardo.

The deep soil mantle that has formed on the Pancho Rico Formation, where it crops out northeast of the Salinas River, is moderately permeable and well drained (U.S. Soil Conservation Service, 1975). Part of the precipitation that falls on the soil penetrates past the root zone of the sparse vegetation that covers the outcrop area and percolates downward until it enters the ground-water system within the Pancho Rico Formation. The Pancho Rico Formation directly overlies the basement complex. The buried surface of the basement complex slopes toward the Salinas River, and ground water in the Pancho Rico Formation moves southwestward over the basement complex until it eventually enters the Salinas Valley ground-water basin.

Based on the geographic variability of mean annual precipitation on outcrops of the Pancho Rico Formation, on the year-to-year variability of seasonal precipitation, and on the extent of the contributing area, the mean annual discharge across the boundary segment on the east side of the ground-water basin between King City and San Ardo is about 20,000 acre-ft. The configuration of the potentiometric surface in the Pancho Rico Formation is unknown, and consequently the distribution of the discharge along the boundary is also unknown. If, however, the configuration of the potentiometric surface is similar to the configuration of the buried basement-complex surface, the discharge is probably more or less uniformly distributed along the boundary. This assumption was used in the ground-water model.

Discharge into the ground-water basin also occurs along the boundary segment that crosses the Salinas River at San Ardo. The alluvium at that location is about 3 mi wide and as much as 300 ft thick. Based on hydraulic-head gradient, average transmissivity, and width, the mean annual underflow at San Ardo is about 1,000 acre-ft.

#### Initial Conditions

When a steady-state (or time-invariant) simulation is performed with the ground-water model, the preassigned values of hydraulic head or discharge at all points on the model boundary suffice to determine the hydraulic-head distribution in the interior of the region that is defined by the boundaries for given source and sink discharge and given system parameters. When a transient-state (or time-variant) simulation is performed, the hydraulic-head distribution depends on the initial conditions (or initial hydraulic heads) that are specified.

To generate initial conditions for the two-dimensional ground-water model, a combination of steady-state and transient-state simulations was used. The Salinas Valley ground-water basin has been in a quasi-steady-state condition since about 1965. Considering periods of several years, the water level in the ground-water basin has remained virtually unchanged with time. Cyclical variations in water level of as much as 80 ft occur seasonally, but water levels observed on the same date each year tend to be similar.

The procedure for generating initial conditions for the two-dimensional ground-water model was as follows: First, steady-state water levels were computed for the steady annual mean pumping and recharge rates. Second, transient-state water levels were computed for a 1-year cycle of transient pumpage and recharge using the steady-state water levels as initial conditions. The computed water levels representing the end of the 1-year cycle were used as initial conditions for the calibration period.

#### System Parameters

The system parameters are the transmissivity and storage coefficient of the ground-water basin. One important source of uncertainty in the model is the unavoidable lack of definitive measurements of the system parameters. The aggregate character of the transmissivity and storage coefficient make laboratory measurements of little use. Current methods of field testing, such as aquifer tests, are of limited use in providing values that can be used directly or can be extrapolated to the large-scale phenomena simulated by the model. As a result, model calibration was the principal method for estimating the system parameters for the two-dimensional ground-water model.

#### Transmissivity

Development of an approach to model calibration.--Limited aquifer-test data are available for the Salinas Valley ground-water basin (Monterey County Flood Control and Water Conservation District, 1967; and McClelland, 1963). These data, in conjunction with specific-capacity data (California Department of Public Works, Division of Water Resources, 1946), were used to develop initial estimates of transmissivity for the ground-water basin. To improve the initial estimates of this parameter, the model was calibrated by iteratively adjusting the transmissivity values until the model reproduced historical conditions to an acceptable degree.

Because of insufficient field data, a unique distribution of transmissivity for the ground-water basin, in a mathematical sense, cannot be obtained from the calibration procedure. It is apparent that additional field data would tend to reduce the variation between possible distributions for the unknown transmissivity that would satisfy equally well the equation of ground-water flow. If we accept some reasonable assumptions regarding the general nature of the distribution of transmissivity, however, the available data provide a basis for obtaining a quantitative estimate of the transmissivity distribution that is hydrologically reasonable.

The assumptions were designed to reduce unexplained geographic variability of transmissivity by explaining the variability, to the extent possible, through indirect data sources. The local transmissivity is a function of the local thickness of materials in the ground-water basin and of the thicknesses and permeabilities of individual lithologic units that occupy the ground-water basin. Estimates were made of the total thickness of materials in the ground-water basin, and indirectly, of the thicknesses of individual lithologic units. The unexplained geographic variability in the transmissivity, then, was assumed to be entirely the result of geographic variability in the permeability of individual lithologic units.

To further reduce the unexplained geographic variability in transmissivity, the various lithologic units that are encountered in a vertical column were categorized as either fine-grained units or coarse-grained units. The fine-grained units, which represented, for the most part, the clay beds of various thicknesses that occur in the ground-water basin, were assumed to have geographically constant permeability. The coarse-grained deposits were assumed to have relative variability in permeability with depth. Unknown was the geographic variability in the permeability of the coarse-grained units. The general problem of estimating the geographic variability in transmissivity was thus reduced to the problem of estimating the geographic variability in the permeability of the coarse-grained units. The calibration procedure was used to estimate this permeability.

Equivalent hydraulic conductivity.--Within the framework of the approach described in the preceding paragraphs, the mechanics of implementing the approach were as follows. The lithologic units encountered in a vertical column through the ground-water basin consist of alternating fine-grained and coarse-grained units. The thickness of individual beds is generally small compared to the total thickness of materials in the ground-water basin, and the distribution of different lithologies is more or less uniform throughout the column. Then, in a small interval of the column the part of the interval occupied by fine-grained units is designated  $P$ , which is constant throughout the column. The average combined hydraulic conductivity of the coarse-grained and fine-grained units within the interval is given by (Bear, 1972, p. 152)

$$\bar{K} = K_c (1-P) + K_f P \quad (22)$$

where  $\bar{K}$  is the average hydraulic conductivity of the interval,  $K_c$  is the hydraulic conductivity of a coarse-grained unit, and  $K_f$  is the hydraulic conductivity of a fine-grained unit. The basis for the relation is that, given equivalent hydraulic gradients, the horizontal discharge across the interval is the same for both the averaged and binary systems.

Spatial relations.--Laboratory analysis of side-hole cores from a test hole in the northern part of the study area (Thorup, 1976) suggests that the hydraulic conductivity of coarse-grained units decreases with depth. Figure 32 shows the relation between hydraulic conductivity and depth. At a depth of about 1,200 ft, the hydraulic conductivity is about one-half the hydraulic conductivity at the water table.

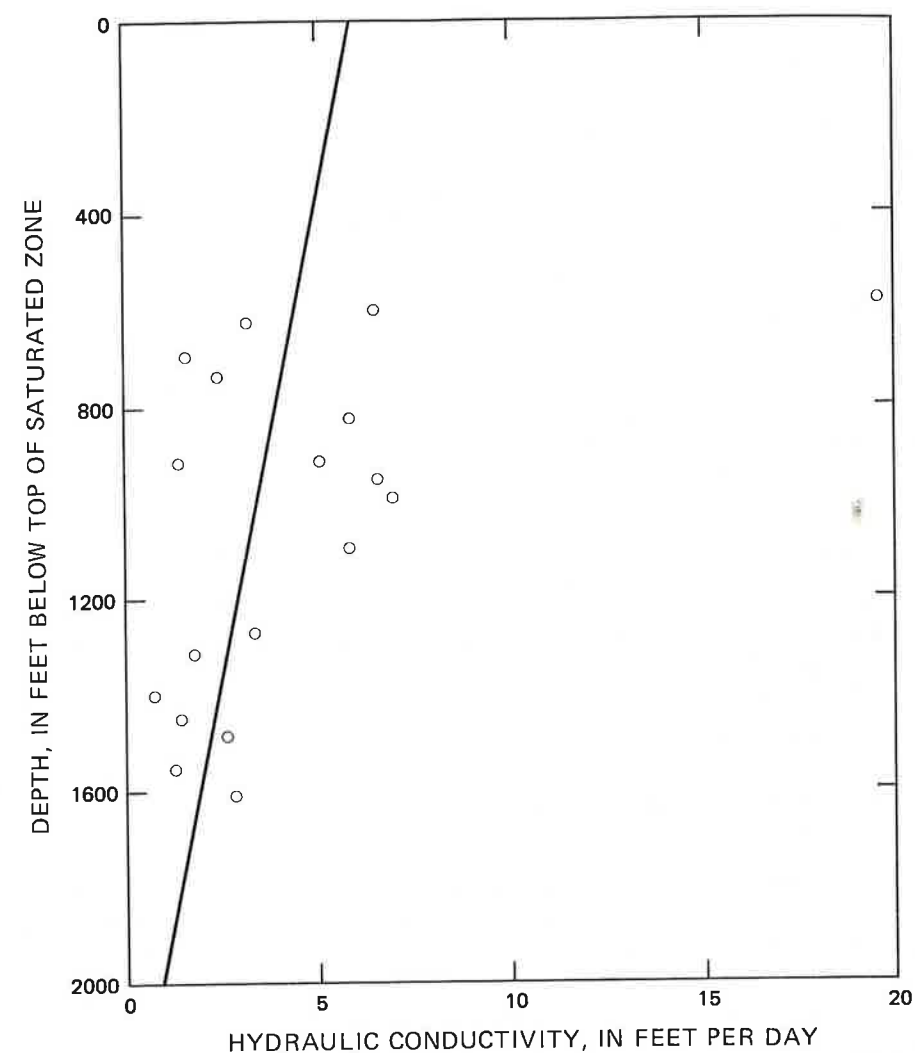


FIGURE 32.--Relation between hydraulic conductivity of coarse-grained lithologies and depth below the water table. Plotted data are from Thorup (1976).

The transmissivity for the ground-water basin, then, is given by the integration of equation 22 over the saturated thickness. Symbolically,

$$T_{xx} = \int_0^b (K_c (1-P) - K_f P) dz \quad (23)$$

where  $b$  is the saturated thickness for the ground-water basin and the relative variation of  $K_c$  with depth follows the relation shown in figure 32.

The quantities P and b were estimated directly from field data. The cumulative proportion of fine-grained units in a vertical column through the ground-water basin (P), expressed as a percentage of the local thickness for the ground-water basin, is shown in figure 33. These data were generated from lithologic logs for wells. A great deal of variability is exhibited between nearby wells, partly as a result of subjective interpretations by different drillers. To smooth the data, the percentage indicated in figure 33 for a particular location represents the average of data from all wells within a radius of about 1 mi.

The altitude of the base of the ground-water basin is shown in figure 9. The thickness of saturated materials in the ground-water basin (b) was estimated by subtracting the base altitude from the water-level altitude for autumn 1970, which is shown in figure 2.

The hydraulic conductivity of fine-grained units ( $K_f$ ) is only a small fraction of the hydraulic conductivity of the coarse-grained deposits and, as a consequence, its exact value has a negligible influence on the transmissivity computed from equation 23. A value of 0.2 ft/d<sup>1</sup> was used. This value was derived from the calibration of the three-dimensional ground-water model, and its basis will be discussed later.

Calibration results.--The hydraulic conductivity of the coarse-grained units ( $K_c$ ) was estimated from the calibration procedure. A steady-state simulation was used in this procedure. Pumpage and autumn water-level measurements for 1970 were used in this simulation. This particular year was chosen because pumpage and recharge during 1970 were representative of longer term conditions. Autumn water-level measurements were used because these measurements approximately represent the steady-state response of the ground-water basin to pumpage and recharge.

Ground-water levels in the ground-water basin were generated by the model using initial estimates of hydraulic conductivity. These model-generated water levels deviated locally as much as 50 ft from the measured water levels. The objective of the calibration procedure was to iteratively reduce the local deviations to a reasonable level by adjusting the hydraulic conductivity within a range of physically plausible values. During the early iterations, gross adjustments were made to the hydraulic conductivity of large areas. Finer adjustments were made to the hydraulic conductivity over smaller areas during later iterations of the calibration procedure. The net effect of these adjustments was to reduce the initial hydraulic conductivity by about 20 percent below the initial estimates (fig. 34). The adjusted hydraulic conductivity of the coarse-grained units range from 19 to 170 ft/d, and are shown in figure 35.

<sup>1</sup>In this report, hydraulic conductivity is expressed in cubic feet per day per square foot, which is reduced to feet per day (ft/d).

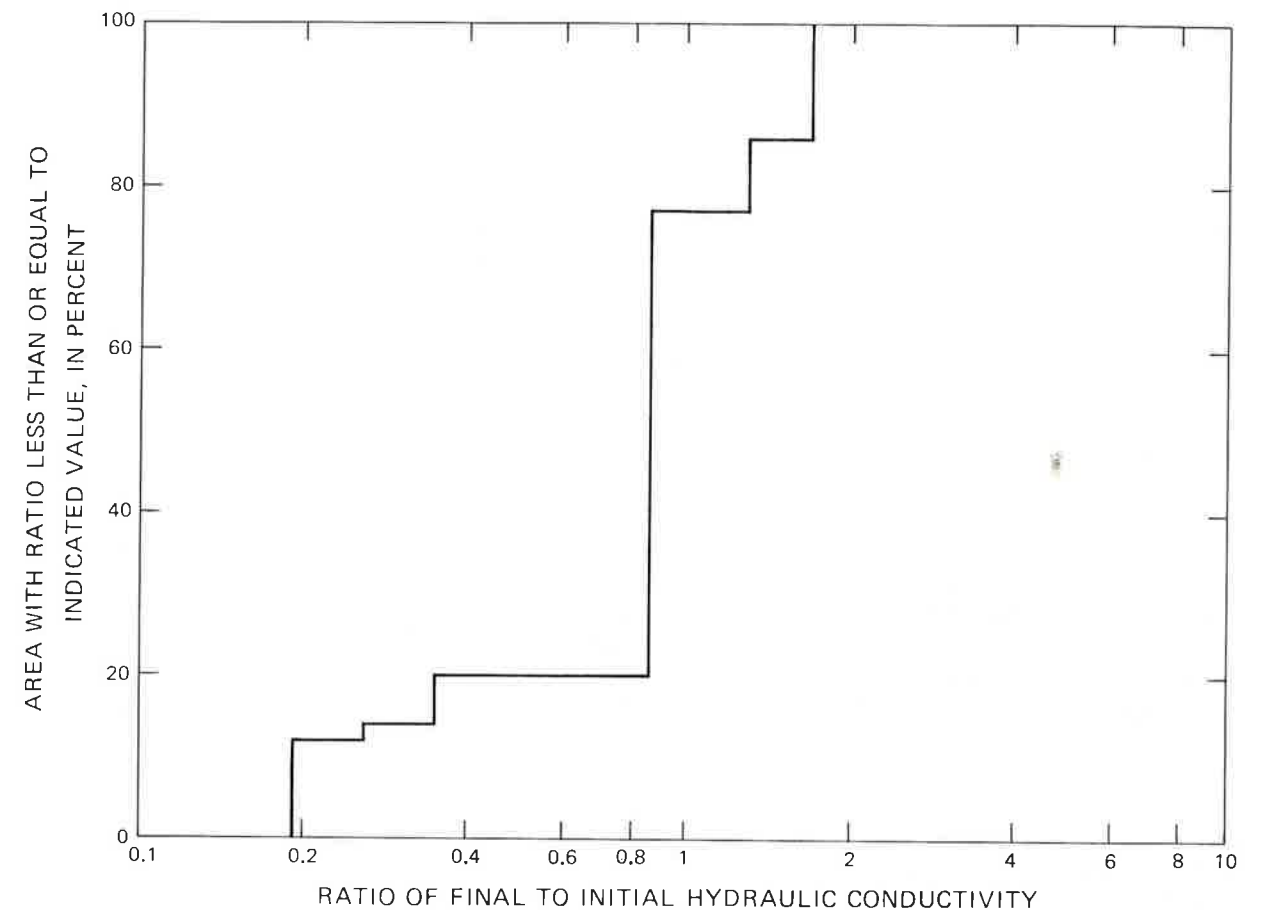


FIGURE 34.--Cumulative distribution of the deviation of the final hydraulic-conductivity estimates from the initial estimates that were used in the two-dimensional ground-water model.

Figure 36 shows the distribution of steady-state water levels in the ground-water basin that was computed by the two-dimensional ground-water model using the hydraulic conductivity shown in figure 34. The shape of the computed solution compares well with the potentiometric map of the prototype water levels, which is also shown in figure 36. The cumulative distribution of the deviation of model-generated water levels from prototype water levels is shown for each ground-water area in figure 37. The median deviations for the areas range from 3 to 6 ft, and the maximum deviations range from 15 to 42 ft. The largest deviations occur in areas where sparse field data introduce considerable uncertainty into the shape of the prototype potentiometric surface.

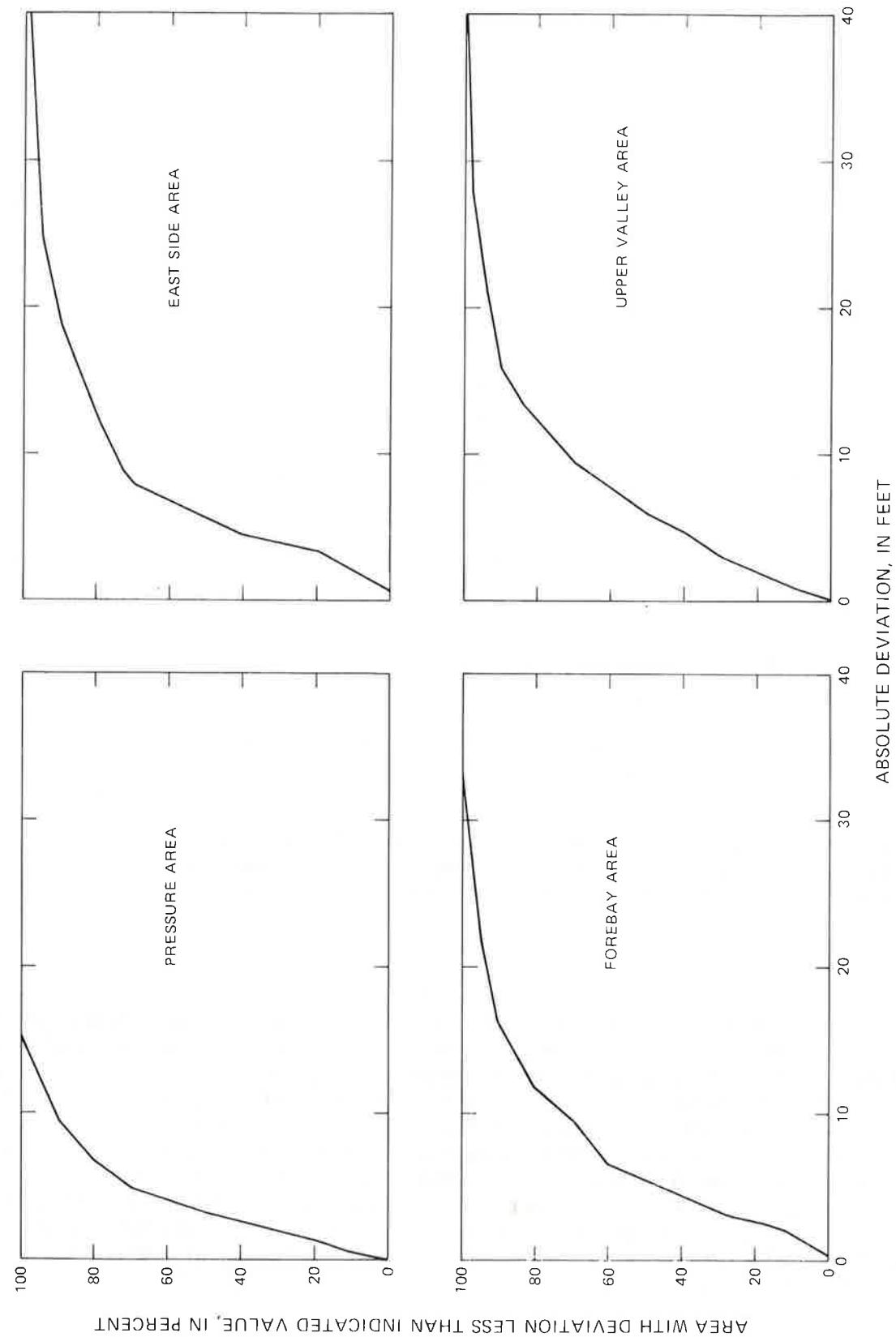


FIGURE 37.--Cumulative distribution, for each of the ground-water areas, of the deviation of steady-state water level generated by the two-dimensional ground-water model from measured water level for autumn 1970.

### Storage Coefficient

A transient-state simulation was used to calibrate storage coefficient values. The calibration procedure was started by making initial estimates of storage coefficient using lithologic logs for wells, geologic data, and laboratory tests of material from other ground-water basins (Johnson, 1966). The transmissivity estimates obtained from the steady-state simulation were used in the transient-state simulation. The values for this parameter were invariant during the calibration of storage coefficient; hence, the objective of this calibration was to fit the water level that was computed using the model to the seasonal variations of measured water levels (for the period December 1968-November 1971) by adjusting the storage coefficient.

Figure 38 shows the final estimates of storage coefficient for the two-dimensional ground-water model of the Salinas Valley ground-water basin. Storage-coefficient values range from 0.00085 to 0.15 and tend to increase southward. The value representing the lower bounds of the range occurs in the Pressure Area beneath the principal confining member for the 180-foot aquifer (fig. 8). This value agrees well with the rule of thumb that the ratio of the storage coefficient of a confined aquifer to the aquifer thickness is about  $10^{-6}$  per foot (Lohman, 1972). Storage-coefficient values that represent semiconfined conditions occur in other parts of the Pressure Area and in parts of the East Side Area.

Storage coefficient values that represent unconfined conditions occur in the Upper Valley and Forebay Areas and in parts of the Pressure and East Side Areas. These storage-coefficient values, which generally correspond to expected specific yields of material such as silt, sand, or clay (Johnson, 1966), are lower than initially estimated. (The deviation of the final storage-coefficient estimates from the initial estimates is shown in figure 39.) This disparity can be explained, in part, by the fact that the storage coefficient of an unconfined aquifer depends on the ability of water to drain from desaturated parts of the aquifer following lowering of the water table. The occurrence of even minor clay lenses may sufficiently restrict vertical drainage so that the storage coefficient is reduced below the value expected for the coarse-grained lithologies that are interbedded with the clay lenses.

The disparity between initial and final estimates of storage coefficient may also be explained on the basis of the cyclical changes in water level. Although the drainage rate from desaturated material is relatively rapid immediately following desaturation, as much as 1 year may be required for the drainage rate to approach zero (Piper, 1933). In the Salinas Valley the period between cyclical desaturation and resaturation is usually less than 1 year. For horizons near the least decline of water level, this period is only momentary. Consequently, cyclical variations of water level may be too rapid to allow maximum drainage, and the effective storage coefficient is smaller than if time were available for more complete drainage.



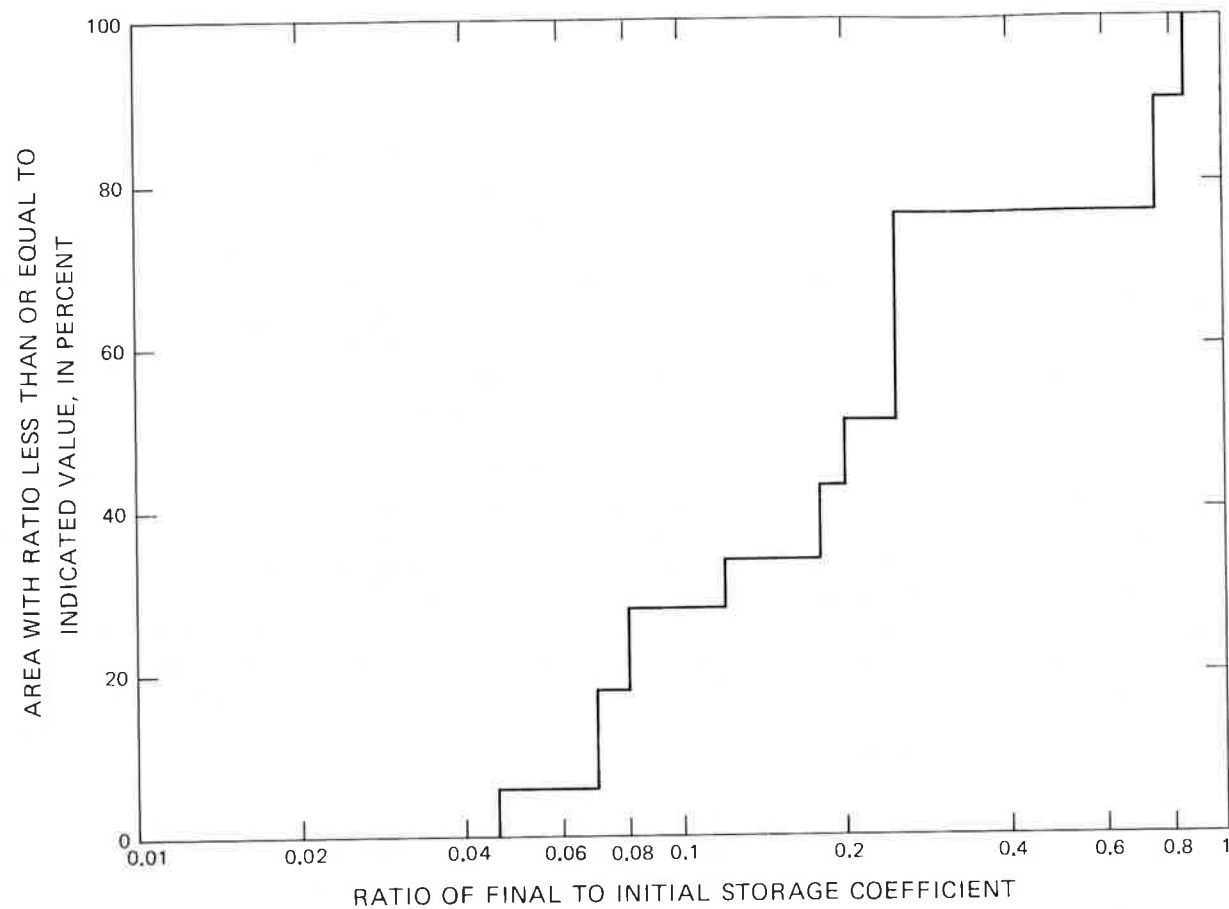


FIGURE 39.--Cumulative distribution of the deviation of the final storage coefficient estimates that were used in the two-dimensional ground-water model from the initial estimates.

To obtain estimates of storage coefficient, the model-generated water level was fitted to hydrographs of measured water levels for 59 wells in the Salinas Valley. These wells were generally evenly distributed among the four areas of the ground-water basin. Comparisons of model-generated water level and measured water level are shown in figures 40 through 43 for two wells in each of the areas.

The critical comparison between hydrographs of model-generated water levels and measured water levels was the difference between the corresponding amplitudes on the two hydrographs. Figure 44 shows, for each ground-water area, the cumulative distribution of the deviation of the amplitude of the model-generated water levels from the amplitude of the measured water levels. The median deviation for individual areas ranges from 3 to 10 ft. The maximum deviation ranges from 18 to 45 ft.

Figure 45 shows water levels in the ground-water basin that were computed by the model for the end of the calibration period. As in the case of the steady-state model-generated water levels (fig. 36), the shape of the computed solution compares well with the potentiometric map of prototype water levels, which is also shown in figure 45. The cumulative distribution of the deviation of model-generated water levels from prototype water levels is shown in figure 46. For individual ground-water areas, the median deviation ranges from 4 to 7 ft, and the maximum deviation ranges from 22 to 40 ft.

#### Model Verification

Data from the 3-year period December 1968-November 1971 were used in the calibration procedure to estimate the transmissivity and storage coefficient for the two-dimensional ground-water model. To test the behavior of the model for longer simulation periods, the estimates of transmissivity and storage coefficient were verified using the 26-year period December 1944-November 1970. Model verification involved simulating water levels for some period not used in model calibration and comparing the simulated water levels to measured water level. The system parameter values derived from model calibration are used in the model for the verification.

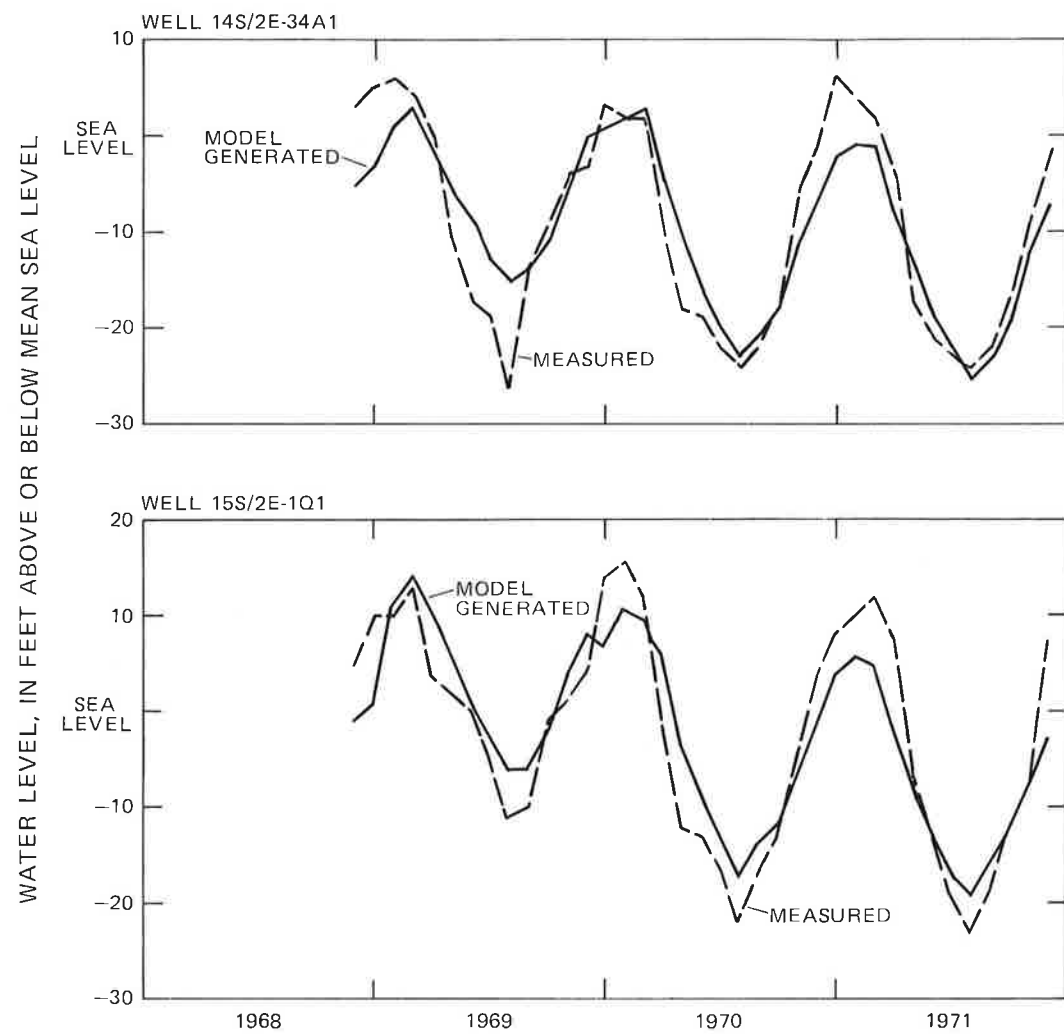


FIGURE 40.--Comparison of water level generated by the two-dimensional ground-water model and measured water level for wells 14S/2E-34A1 and 15S/2E-1Q1 in the Pressure Area.

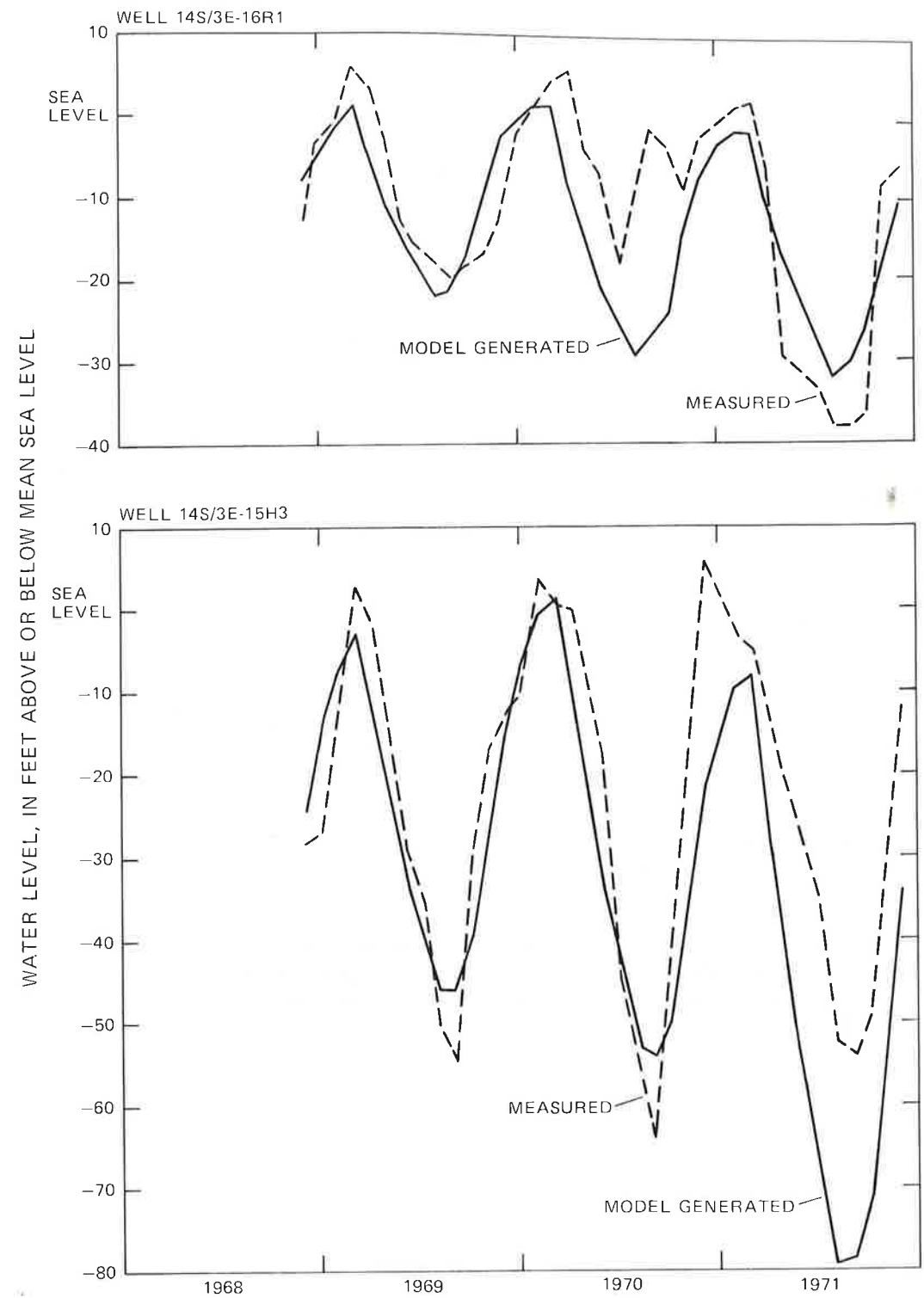


FIGURE 41.--Comparison of water level generated by the two-dimensional ground-water model and measured water level for wells 14S/3E-15H3 and 14S/3E-16R1 in the East Side Area.

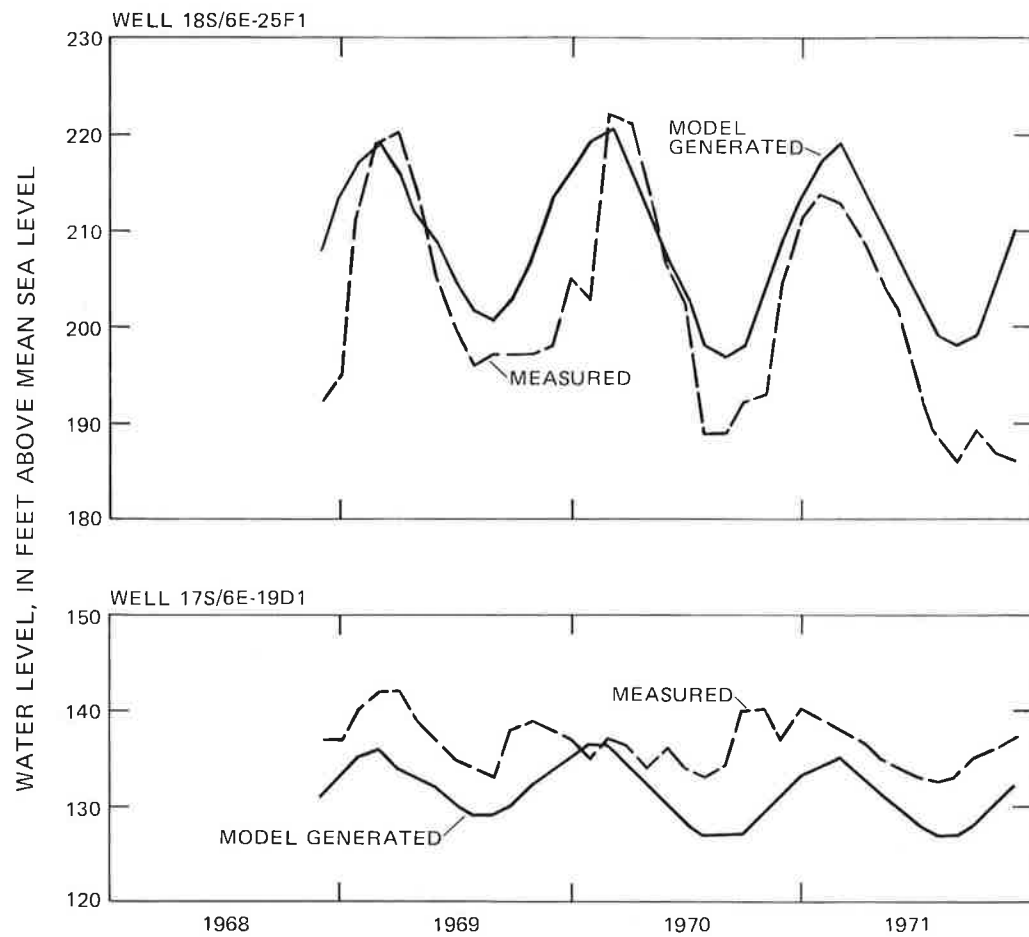


FIGURE 42.--Comparison of water level generated by the two-dimensional ground-water model and measured water level for wells 17S/6E-19D1 and 18S/6E-25F1 in the Forebay Area.

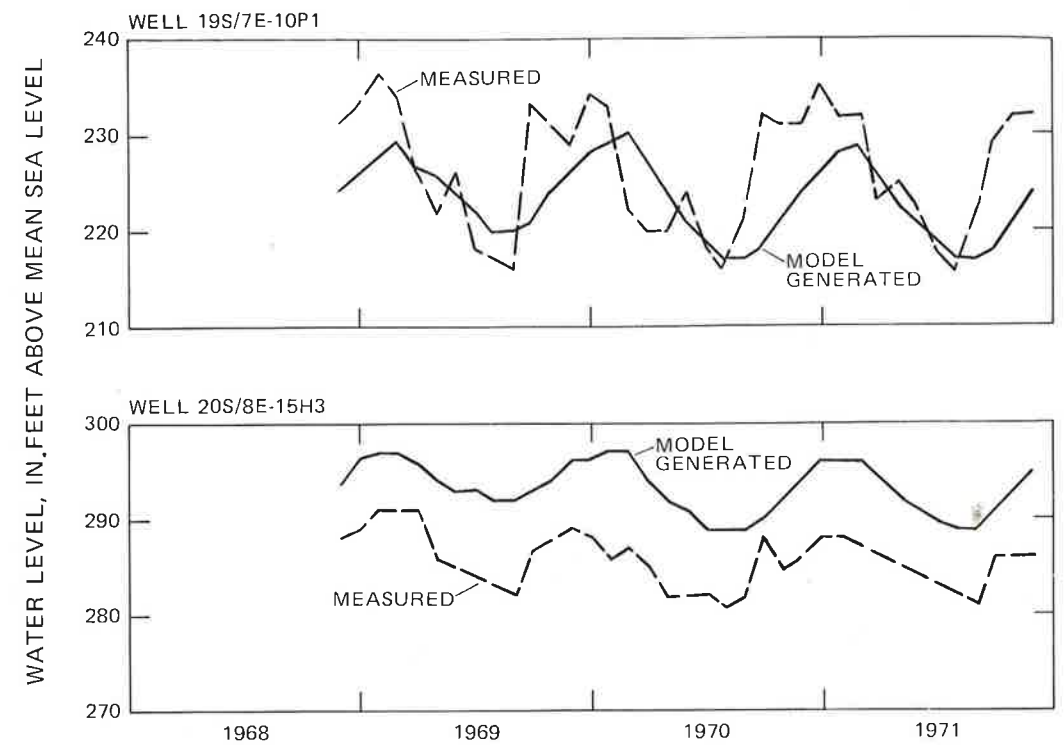


FIGURE 43.--Comparison of water level generated by the two-dimensional ground-water model and measured water level for wells 19S/7E-10P1 and 20S/8E-15H3 in the Upper Valley Area.

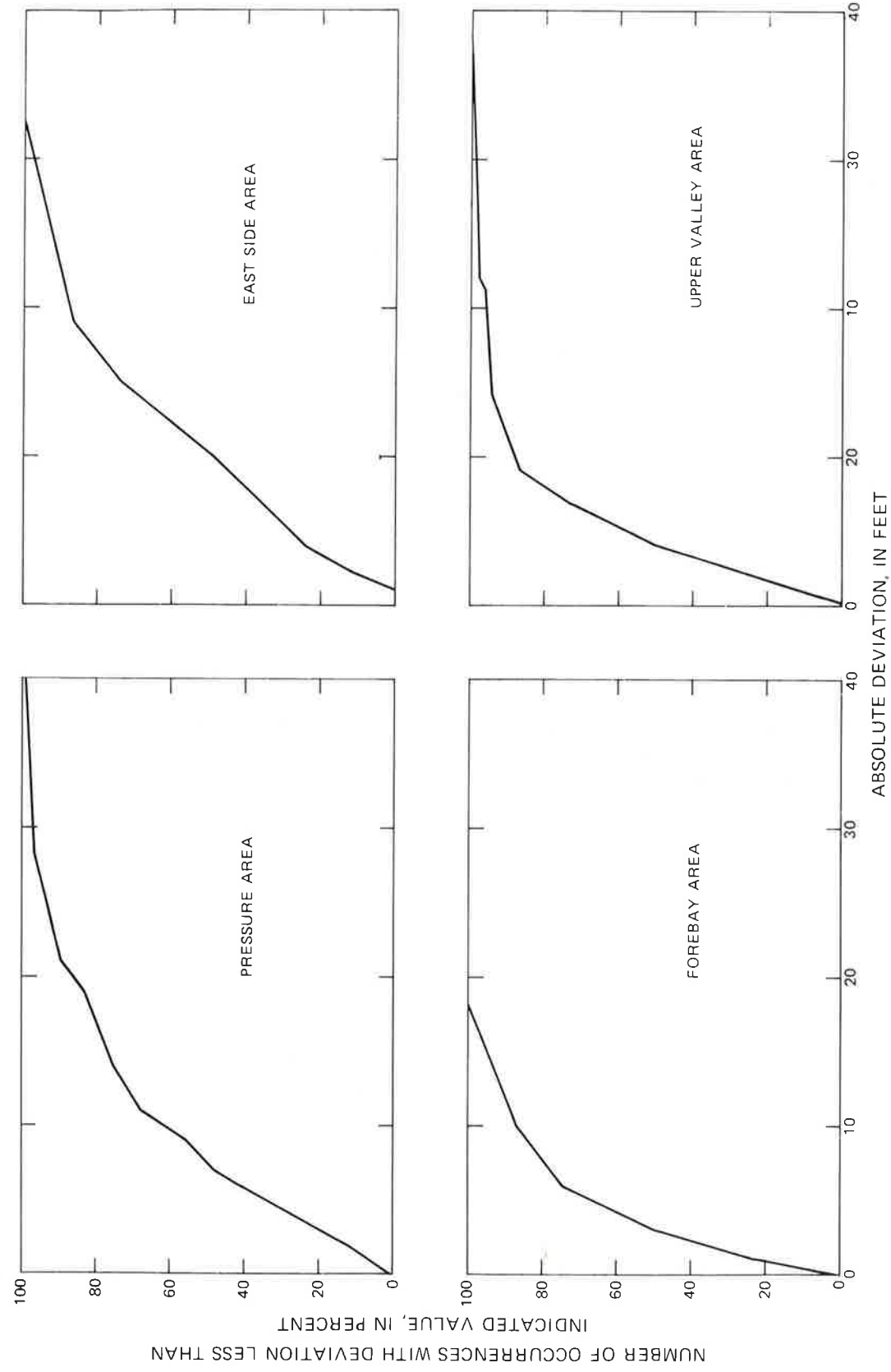


FIGURE 44.--Cumulative distribution, for each of the ground-water areas, of the deviation of the amplitude of seasonal fluctuations of water level generated by the two-dimensional ground-water model from the amplitude of measured water level.

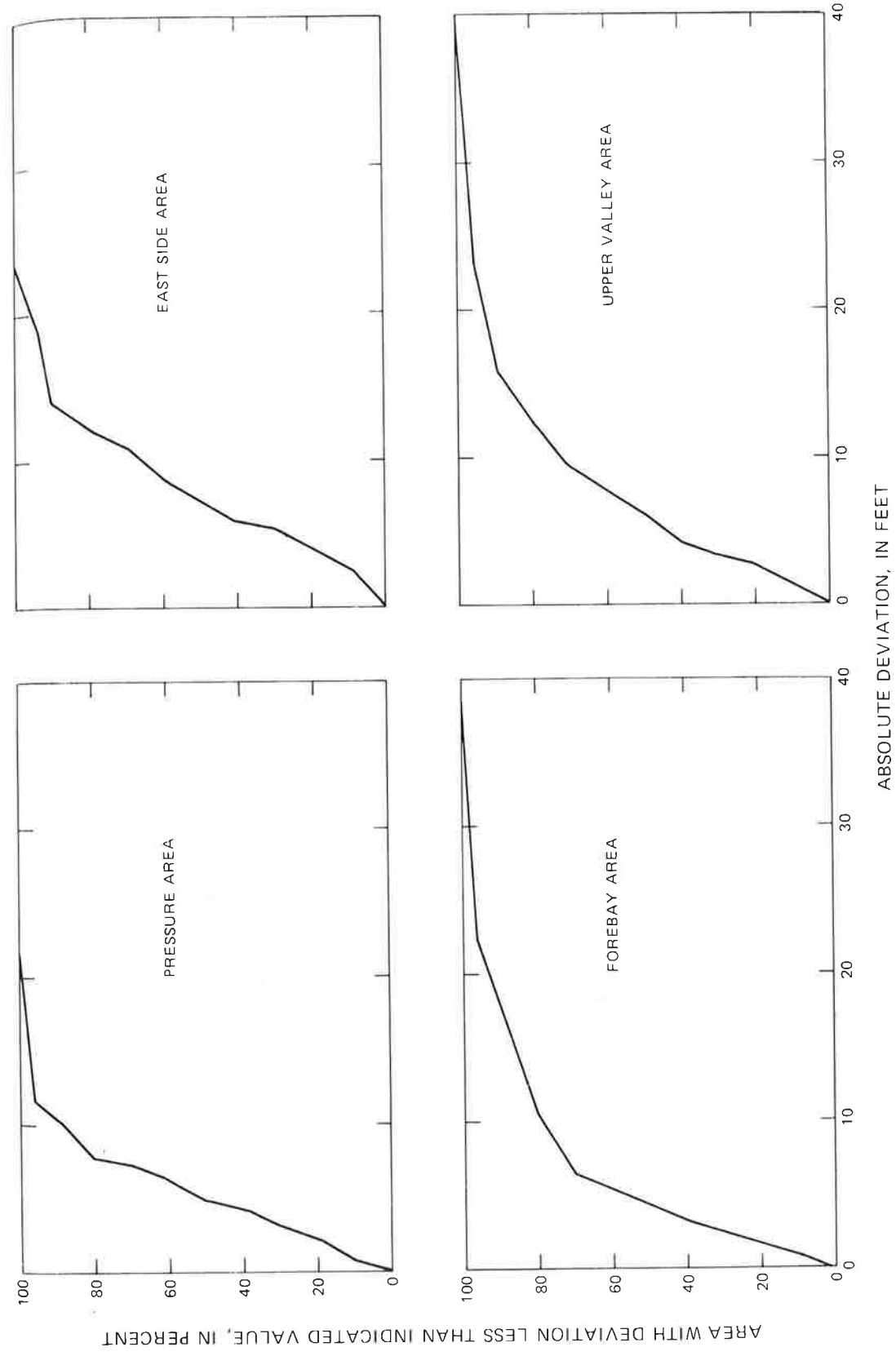


FIGURE 46.--Cumulative distribution, for each of the ground-water areas, of the deviation of transient-state water level generated by the two-dimensional ground-water model from measured water level for autumn 1971.

## Source and Sink Discharge Used for Model Verification

Agricultural and municipal pumpage.--Irrigation with ground water in the Salinas Valley began about 1900. Hamlin (1904) reported that in 1902 about 7,500 acres were being irrigated with ground water. (Additional acreage at that time was irrigated from surface-water diversions, particularly along the Salinas River between Gonzales and King City.) By 1944 the irrigated area had increased to 125,000 acres (California Department of Public Works, Division of Water Resources, 1946). In 1970, 180,000 acres were irrigated with ground water.

As the irrigated acreage in Salinas Valley increased, the annual quantity of ground water pumped also increased. Based on the extrapolation of unit application of pumped water for 1944 (California Department of Public Works, Division of Water Resources, 1946), ground-water pumpage in 1902 was 20,000 acre-ft. On the basis of crop surveys and estimates of the consumption of water by various crops, the Department of Water Resources estimated that pumpage in 1944 was 350,000 acre-ft. Electrical-power records for 1970 indicate that pumpage for that year was 460,000 acre-ft. Figure 47 shows the annual agricultural pumpage for 1945 through 1970 that was used for the verification of the two-dimensional ground-water model.

The geographic distribution of agricultural pumpage has changed over the years. In 1900 the pumpage was concentrated in the northern part of Salinas Valley. By 1944, agricultural pumpage was distributed fairly evenly throughout the valley. The principal change in the distribution of pumpage between 1944 and 1970 was the increased density of the distribution. That is, the irrigated acreage in 1944 was interspersed with nonirrigated land, but by 1970 much of this interspersed land came under irrigation. Thus, considering an area that in 1944 contained both irrigated and nonirrigated land, the pumpage in 1970 from that area tended to be greater than in 1944.

The preceding paragraph gave a qualitative description of changes in the geographic distribution of agricultural pumpage. For the development of data for input to the model, however, a quantitative description was needed. The geographic distribution of pumpage for 1970 was developed for the calibration of the two-dimensional ground-water model (fig. 27). In addition, land-use maps are available for 1944 (California Department of Public Works, Division of Water Resources, 1950) from which the geographic distribution of pumpage for 1944 was estimated. To fill in the remaining years, the distribution for 1944 was assumed to apply for 1945 through 1955, and the distribution for 1970 was assumed to apply for 1956 through 1970.

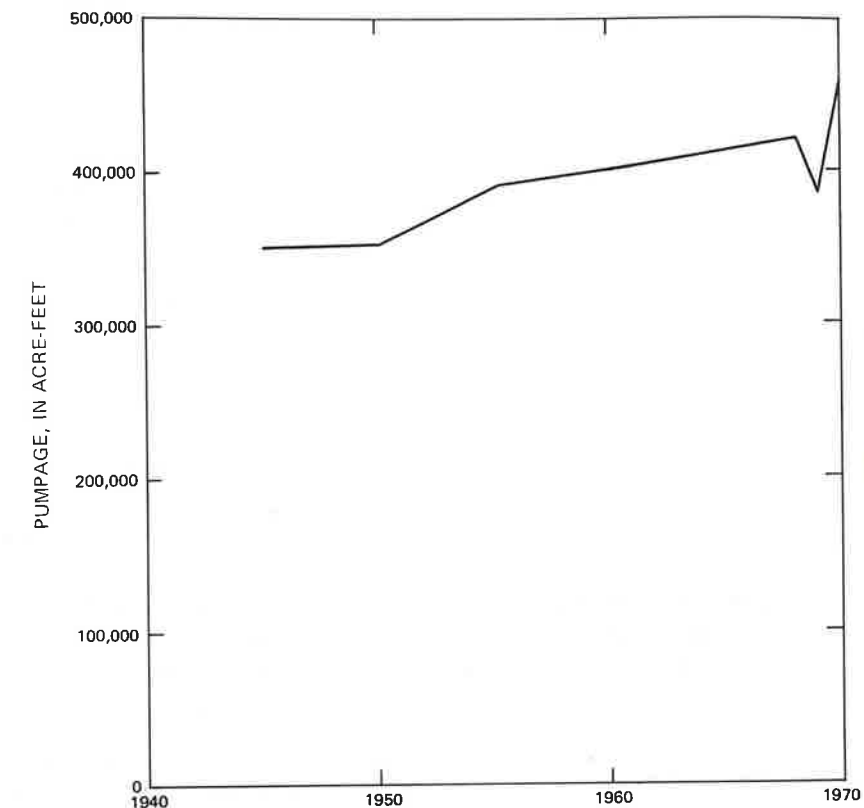


FIGURE 47.--Annual agricultural pumpage for 1945 through 1970 that was used for the verification of the two-dimensional ground-water model.

Municipal pumpage increased during the period selected for model verification. Changes in municipal pumpage during this period probably paralleled changes in population. The municipal pumpage for 1970 was 22,000 acre-ft (table 12). Based on the assumption that municipal pumpage is proportional to population, municipal pumpage was 5,000 acre-ft in 1940. Figure 48 shows the annual municipal pumpage that was used for the verification of the two-dimensional ground-water model. Figure 29 shows the geographic distribution of municipal pumpage for 1970. The geographic distribution of pumpage throughout the verification period was assumed to be proportional to the distribution for 1970.

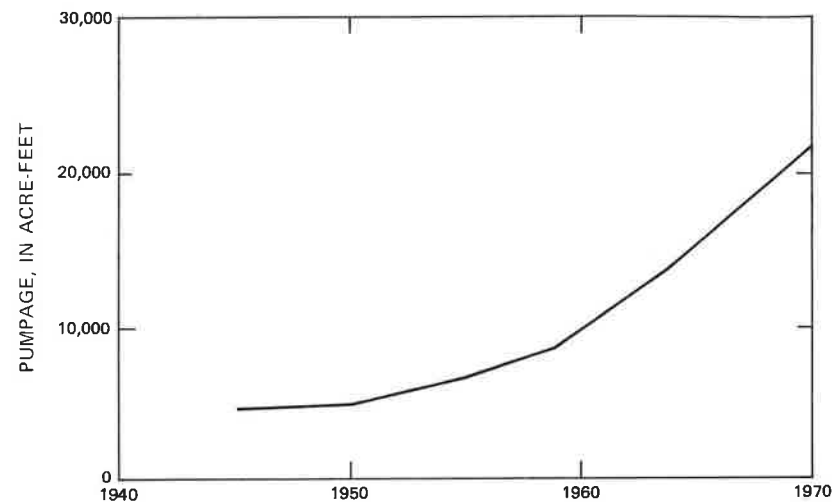


FIGURE 48.--Annual municipal pumpage for 1945 through 1970 that was used for the verification of the two-dimensional ground-water model.

Natural ground-water recharge and discharge.--Natural ground-water recharge refers to recharge from small streams, precipitation, and the Salinas River. Natural ground-water discharge refers to the consumptive use of ground water by the riparian vegetation that grows along the Salinas River. The mean annual ground-water recharge from small streams and precipitation that was used for model calibration (fig. 31) was also used for model verification. Additionally, the mean annual natural discharge of ground water that was used in model calibration (fig. 30) was used in model verification.

Ground-water recharge from the Salinas River was computed by the river model. For model verification, monthly time steps were used in the ground-water and river models, and monthly mean discharge for the Salinas River near Bradley was used as input to the river model. The stream-gaging station near Bradley was established in September 1948, and for October 1948 through December 1970 the measured discharge for this station was used as input to the river model. For times prior to October 1948, monthly mean discharge was estimated, based on correlation with annual mean discharge for Arroyo Seco near Soledad and with the average seasonal distribution of discharge for the Salinas River near Bradley.

## Boundary and Initial Conditions

The boundary conditions used for the calibration of the two-dimensional ground-water model were also used for model verification. The initial conditions, however, were different. Initial hydraulic heads for the verification period were based on measured water levels for autumn 1944 (California Department of Public Works, Division of Water Resources, 1946).

## Verification Results

Water levels.--Comparisons of model-generated water levels and measured autumn water levels are shown in figure 49 for 1945 through 1970. The general trend of model-generated water levels follows the general trend of measured water level. In some instances, the details of the year-to-year changes in autumn water levels also are preserved in the model-generated water level.

The largest disparity between model and prototype occurred in the East Side Area. As indicated by figure 49, model-generated water level declined much more rapidly than measured water level. The more rapid decline of model-generated water level may have been caused by either the incorrect specification of storage coefficient for the model or the incorrect estimation of pumpage. With respect to the first possible cause, the model was calibrated for storage coefficient on the seasonal variation of measured water level. The resulting storage-coefficient values may be lower than if more long-term variations of measured water levels had been used for the calibration. (Except for the East Side Area, significant long-term water-level changes have not occurred, which precluded the use of long-term water-level changes for the model calibration.) Hence, for long-term simulations, the model may predict more rapid model-generated water-level declines (or rises) than may actually occur in the prototype.

Lack of precision in the pumpage estimates for the East Side Area may be a cause of the disparity between model and prototype. Pumpage for 1944 was based on land-use surveys and on estimates of the consumptive use of water by various crops (California Department of Public Works, Division of Water Resources, 1946), and considerable error may exist in the estimated pumpage from the East Side Area. Therefore, rapid decline of model-generated water level in the East Side Area may be caused by the overestimation of pumpage.

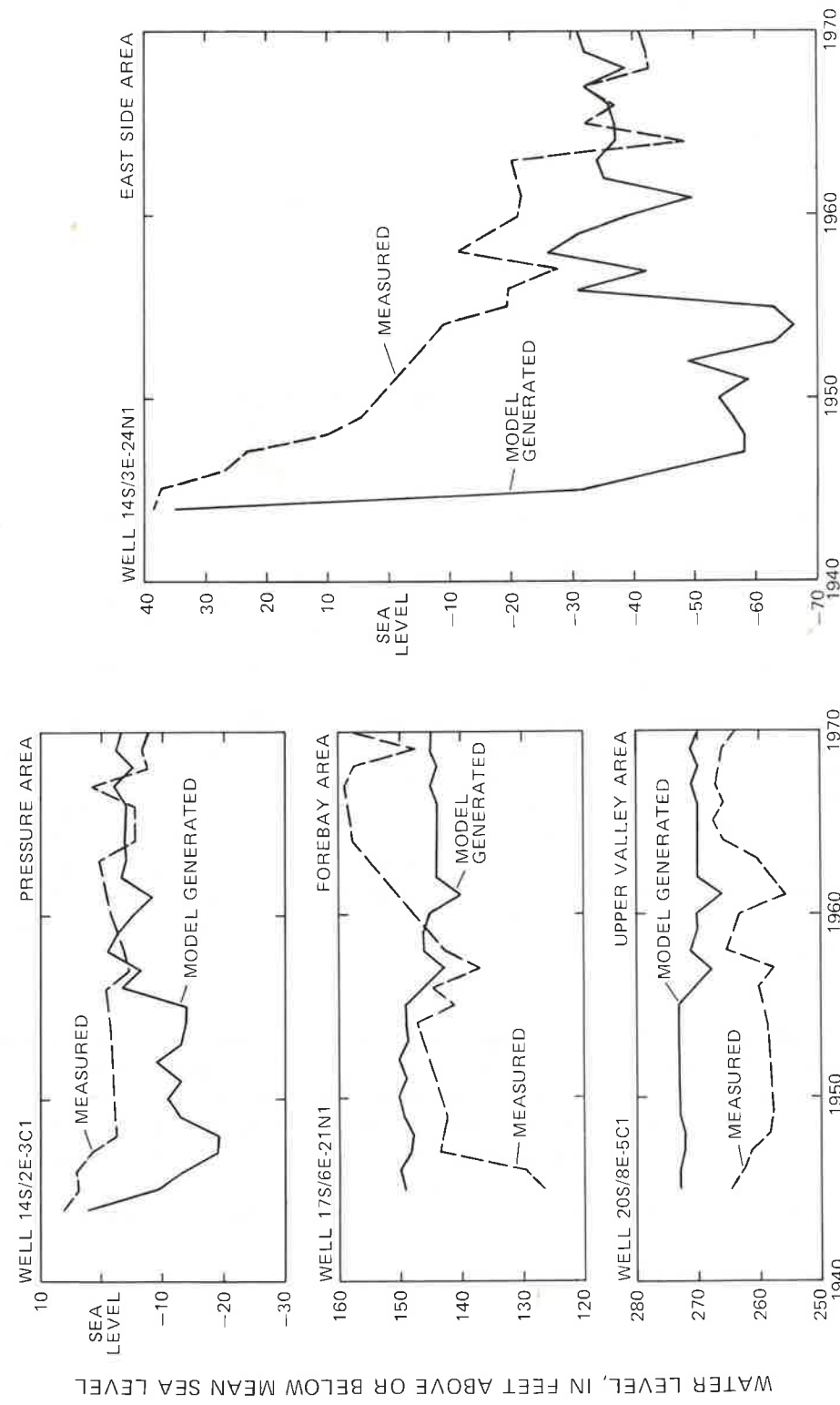


FIGURE 49.--Comparison of water level generated by the two-dimensional ground-water model and measured autumn water level for 1945 through 1970 for wells 14S/2E-3C1, 14S/3E-24N1, 17S/6E-21N1, and 20S/8E-5C1. Measured water levels are from California Department of Water Resources, Division of Water Resources (1949, 1950), California Department of Water Resources (1957, 1958, and 1959), and Monterey County Flood Control and Water Conservation District (1959-70).

The cause of the disparity between model and prototype is unknown, and, concomitantly, the precision of the storage-coefficient values used in the two-dimensional ground-water model is also unknown. An ameliorating factor is that, all other things being equal, the storage coefficient used in the model affects only the timing of model-generated water-level changes and not the ultimate water level. Perhaps this can be better seen from the following example. The Salinas Valley ground-water basin was in the primordial steady state prior to the start of ground-water pumping in about 1900. Ground-water pumping disturbed the primordial steady state. The ground-water basin, however, has adjusted to the disturbance caused by ground-water pumping, and a new steady state has been established. If the model were to be used to simulate the transition from the primordial steady state to the new steady state, and if the storage-coefficient values used in the model were too small, the model would predict a shorter transition period than would actually occur, but the steady-state model-generated water level at the end of the transition period would not be affected. Therefore, given the uncertainty in the precision of the storage-coefficient values used in the model, the steady-state response of the ground-water basin to the prolonged (and steady) application of specified ground-water recharge and discharge should be better predicted by the model than the path by which the ground-water basin reached that steady state.

Unfortunately, the ability of the two-dimensional ground-water model to predict steady-state water level was not tested by the model verification. This was because the steady-state condition existing in 1970 was used to calibrate the model for transmissivity values. As might have been expected from the model verification, the model reproduced measured water level for autumn 1970 about as well as it did for the model calibration. The cumulative distribution of the deviation at the end of the verification period of model-generated water levels from measured water level is shown for each ground-water area in figure 50. The median deviations for the areas range from 4 to 7 ft, and the maximum deviations range from 20 to 42 ft, which is probably indicative of the predictive reliability of the two-dimensional ground-water model for long-term simulations.

Streamflow.--Comparisons of annual mean computed discharge and annual mean measured discharge for the Salinas River near Spreckels are shown in figure 51 for the verification period, 1945-70. For this period the river model overestimated discharge for the Salinas River by about 25 percent, which is probably indicative of the predictive reliability of the river model for long-term simulations. The computed mean discharge was 367 ft<sup>3</sup>/s, and the measured mean discharge was 300 ft<sup>3</sup>/s.

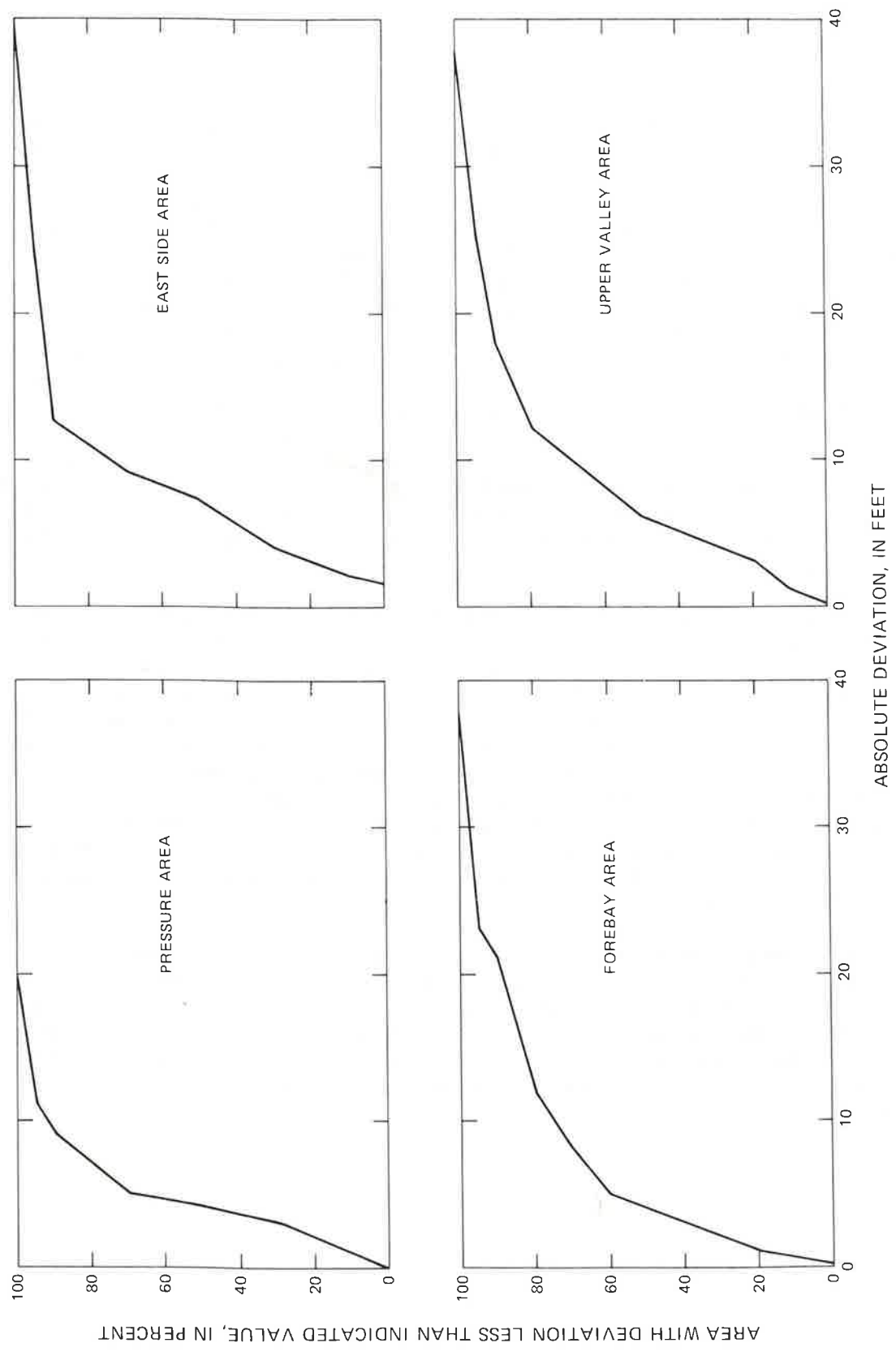


FIGURE 50.--Cumulative distribution, for each of the ground-water areas, of the deviation of transient-state water level generated by the two-dimensional ground-water model from measured water level for autumn 1970.

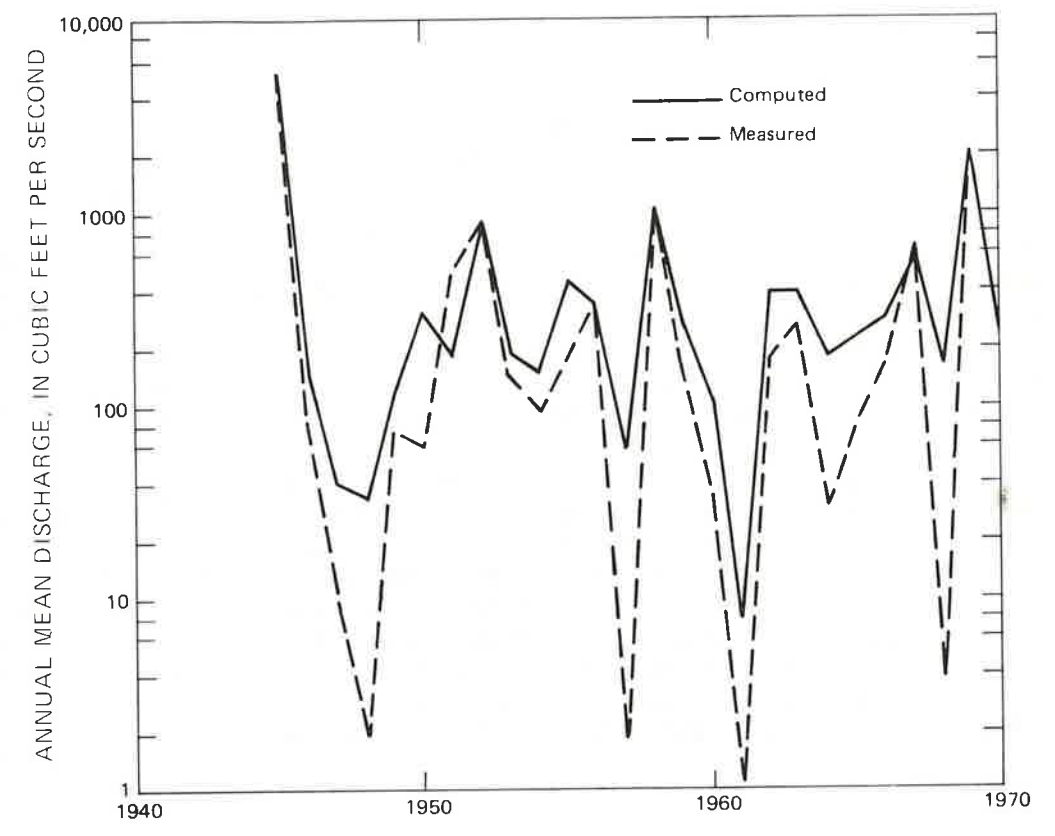


FIGURE 51.--Comparison of annual mean discharge computed by the river model and annual mean measured discharge for the Salinas River near Spreckels.



The long-term computed discharge for the Salinas River is closely related to the mass balance maintained by the two-dimensional ground-water model. The computed mass balance for the ground-water basin is in turn affected by the storage-coefficient values used in the model. Recalling that the precision of these storage-coefficient values is uncertain, and considering the largest plausible range of storage-coefficient values for the prototype, the disparity between computed and measured discharge for the Salinas River cannot be accounted for by lack of precision in the storage-coefficient values used in the two-dimensional ground-water model. Therefore, the cause of the disparity must lie elsewhere. Although the actual cause of the disparity cannot be identified, other areas where the difficulty may lie are either too much tributary inflow used in the river model or too little net discharge used in the two-dimensional ground-water model, both of which are estimated quantities.

Extension of results to three-dimensional ground-water model.--Given similar inputs, the response of the three-dimensional ground-water model is similar to the response of the two-dimensional ground-water model. Therefore, conclusions derived from the verification of the two-dimensional model should apply to the three-dimensional model. In particular, the three-dimensional model should predict steady-state hydraulic head with a median error of about 6 ft. The precision of the specific storage values used in the three-dimensional model is unknown, and, concomitantly, the precision of the timing of computed hydraulic-head changes also is unknown.

### THREE-DIMENSIONAL GROUND-WATER MODEL

#### Description of the Model

At most locations in the Pressure Area, the potentiometric surface for the 180-foot aquifer is higher than the potentiometric surface for the 400-foot aquifer. The hydraulic-head differential between these aquifers is due to differential pumping and recharge. Pumping from the 180-foot aquifer has been terminated in much of the area northwest of Salinas because of seawater intrusion. Water is pumped instead from wells perforated only in the 400-foot aquifer. The resulting head differential between the 180-foot and 400-foot aquifers ranges from 10 to 30 ft during summer months when pumping is greatest. During the spring the differential ranges from 5 to 10 ft.

South of Salinas in the Pressure Area, pumping is more evenly distributed between the two aquifers, and the hydraulic-head differential between the 180-foot and 400-foot aquifers is, for the most part, due to ground-water recharge to the 180-foot aquifer from the Salinas River. Head differentials in this area and seasonal variations of the differentials are not as great as in the area northwest of Salinas.

The two-dimensional ground-water model treats the ground-water basin as a single-aquifer system, and consequently it does not simulate vertical hydraulic-head differentials between the 180-foot and 400-foot aquifers. Several proposed ground-water management alternatives for the Salinas Valley involve separate alterations of pumpage in the 180-foot and 400-foot aquifers. To simulate the effect that these alterations would have on the potentiometric surfaces for the aquifers, a three-dimensional ground-water model was developed for the Pressure and East Side Areas. This model treats the ground-water basin as a three-dimensional continuum, and it simulates both the geographic and vertical hydraulic-head distribution.

The equation that describes ground-water flow in a three-dimensional continuum is (Bear, 1972, p. 204)

$$\frac{\partial}{\partial x} \left( K_{xx} \frac{\partial h}{\partial x} \right) + \frac{\partial}{\partial y} \left( K_{yy} \frac{\partial h}{\partial y} \right) + \frac{\partial}{\partial z} \left( K_{zz} \frac{\partial h}{\partial z} \right) - S_s \frac{\partial h}{\partial t} - W = 0 \quad (24)$$

where  $K_{xx}$ ,  $K_{yy}$ , and  $K_{zz}$  are the principal components of the hydraulic conductivity tensor;  $x$ ,  $y$ , and  $z$  are the principal directions;  $h$  is the hydraulic head,  $S_s$  is specific storage; and  $W$  is the discharge of a source or sink.

Approximate solutions to the ground-water-flow equation were obtained using the Galerkin finite-element method. Segol (1976) gives a mathematical description of the application of the method to three-dimensional problems. The computer program used to approximate solutions to the ground-water-flow equation is a Galerkin finite-element program developed by Genevieve Segol (written commun., 1975). The program employs isoparametric hexahedral elements.

The element configuration used for the three-dimensional model is shown in figures 56 through 58. As for the two-dimensional model, the geometrical relations in the ground-water basin are specified in the three-dimensional model through the configuration of elements. The element grid has three-dimensional form, and it expresses both geographical and depth relations in the prototype. Within the Pressure Area, the top layer of elements corresponds to the 180-foot aquifer and the third layer of elements from the top corresponds to the 400-foot aquifer. Outside the Pressure Area, the element layers do not correspond to specifically named aquifers but represent sections of water-bearing material in the basin. The local water-bearing properties of the ground-water basin are specified in the model by assigning parameter values to the element. These values represent the prototype vertical and horizontal hydraulic conductivity and specific storage. The model uses these specifications to compute hydraulic heads that mathematically satisfy the three-dimensional ground-water-flow equation for the sources and sinks applied, for the boundary conditions imposed, and for the system parameters specified.

## Source and Sink Discharge

### Agricultural and Municipal Pumpage

The geographic distribution of pumpage that was used in the two-dimensional model (figs. 27 and 29) was also used in the three-dimensional model. Additionally to be compatible with the nature of the three-dimensional model, the vertical distribution of the pumpage also was estimated.

In the development of the vertical distribution of pumpage, the pumpage from a given layer for a well was assumed to be proportional to the perforated interval of the well in the layer. For example, if 10 percent of the total perforated interval of a well was in a given layer, 10 percent of the total pumpage from the well was assumed to be derived from that layer. A more theoretically satisfying approach would consider the hydraulic conductivity of the layer. This approach, although desirable, is unworkable because in most cases data on pumpage from individual wells cannot be cross referenced with data on the perforated interval. With the employed approach, data on well perforations and on pumpage can be analyzed separately and then combined without reference to specific wells.

Given the assumption about how pumpage was distributed vertically, the method of estimating the distribution is as follows. The average distribution was developed for each quarter township in the Pressure and East Side Areas. The pumpage from a layer in the quarter township equaled the cumulative footage for all wells of perforated interval in that layer divided by the cumulative footage of perforated interval for all wells in all layers. The layers used were based on the finite-element grid for the three-dimensional model. The distributed pumpage from the prototype is aggregated in the model to the nearest node in the finite-element grid. Histograms, for selected quarter townships, illustrating the vertical distribution of pumpage are shown in figures 52 and 53.

### Ground-Water Recharge From Irrigation-Return Water

As described for the two-dimensional model, applied irrigation water that is not consumed by crops mostly percolates past the root zone and in most locations returns to the ground-water basin. In the two-dimensional model the irrigation return locally cancels part of the pumpage, and the input to the model was the pumpage minus the irrigation return. In the three-dimensional model, pumpage is withdrawn from nodes at various depths, and irrigation return is applied at nodes on the upper surface of the finite-element grid. Although the net pumpage from the ground-water basin remains the same overall, in the three-dimensional model local recycling of irrigation-return water is simulated.

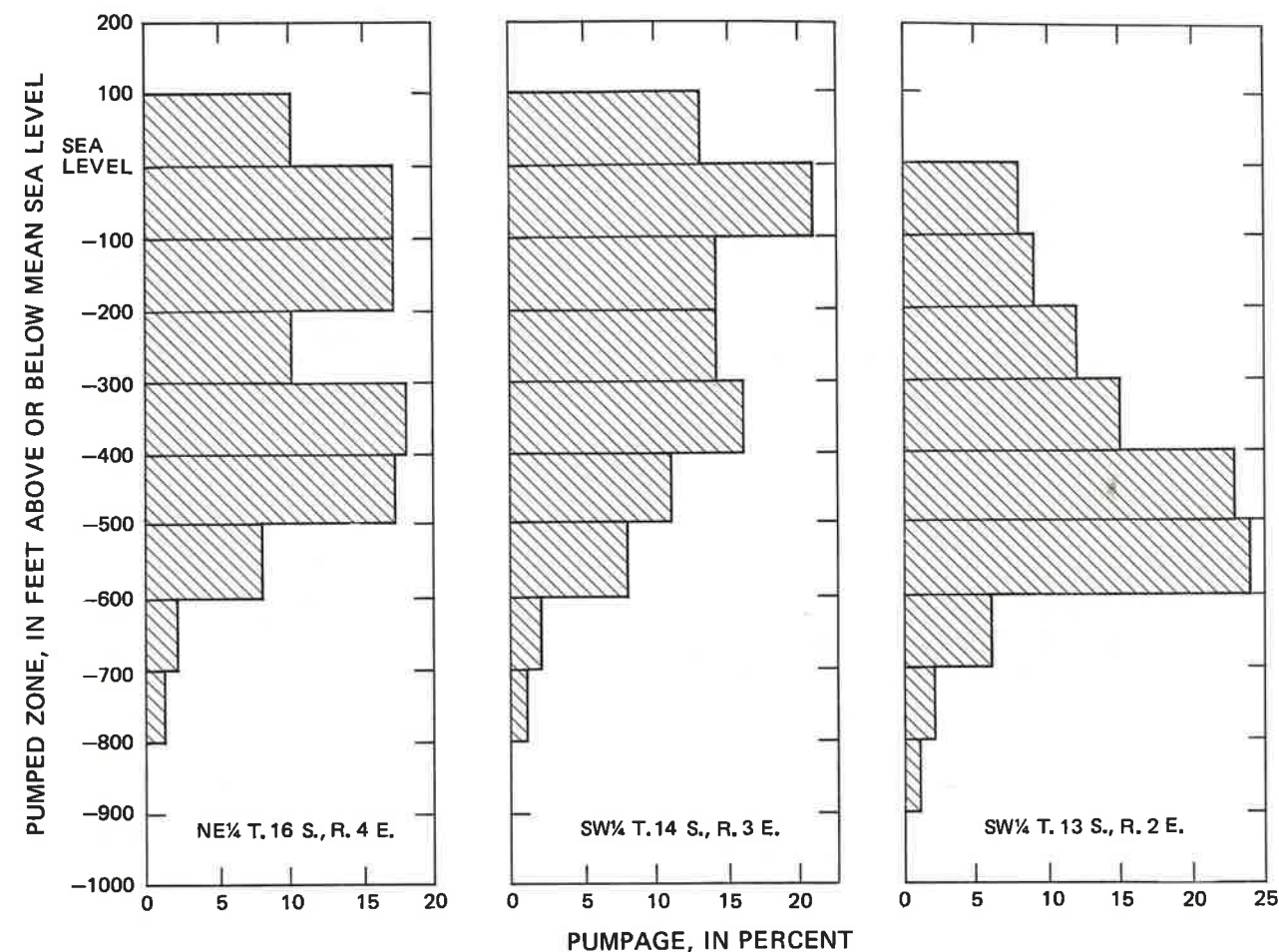


FIGURE 52.--Histograms of the vertical distribution of pumpage that was used in the three-dimensional ground-water model, for representative quarter townships in the Pressure Area.

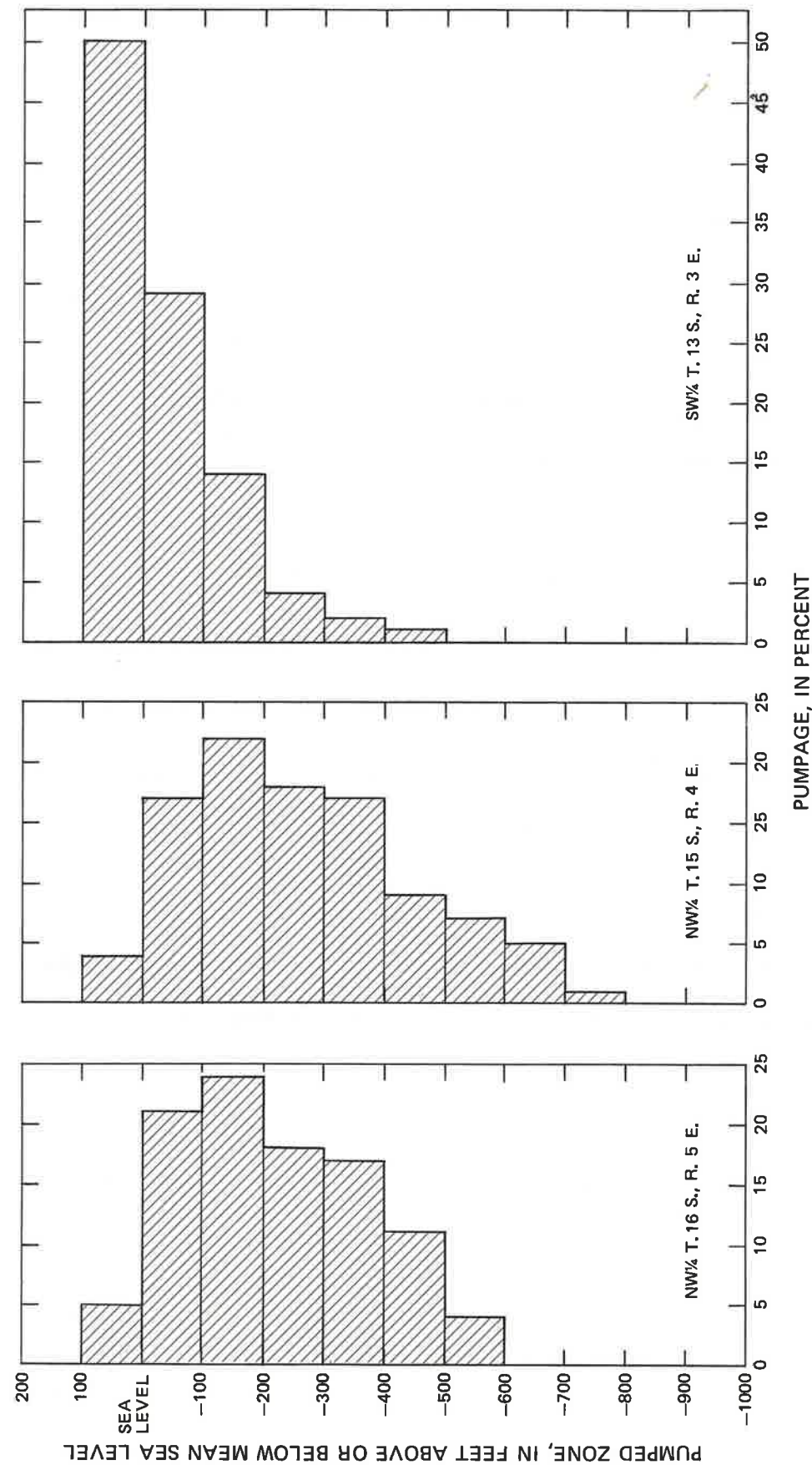


FIGURE 53.--Histograms of the vertical distribution of pumpage that was used in the three-dimensional ground-water model, for representative quarter townships in the East Side Area.

## Natural Ground-Water Recharge and Discharge

Natural ground-water recharge refers to recharge from small streams, precipitation, and the Salinas River. Natural discharge refers to the ground-water consumed by the riparian vegetation on the bottomlands along the Salinas River. The local rate of natural recharge or discharge used in the two-dimensional model (figs. 30 and 31) was also used in the three-dimensional model. The mechanisms that cause natural recharge and discharge act at the water table in the prototype, and in the three-dimensional model natural recharge and discharge were applied only to nodes on the upper surface of the finite-element grid.

### Boundary Conditions

The boundaries of the two-dimensional model are lines that enclose a planar region. The boundaries of the three-dimensional model are surfaces that enclose a solid region. The boundary conditions used on these surfaces are similar to those used on the lines representing the boundaries of the two-dimensional model. The boundary conditions are specification of hydraulic head on the boundaries and specification of discharge across them.

### Specified-Head Boundaries

The geographic area included in the three-dimensional model extends about 6 mi offshore beneath Monterey Bay. Offshore, the ground-water system is in contact with the water in Monterey Bay on the upper surface of the ground-water basin, which is coincident with the bottom of the bay. The hydraulic head on this surface was assumed to be identical with the time-averaged hydraulic head in the bay. The two-dimensional model extends only to the shore of Monterey Bay, and the approximately equivalent boundary condition on the two-dimensional model was the specification of constant hydraulic head along the shoreline.

Specified-head boundary conditions were also used on the vertical surface that bounds the southern end of the three-dimensional model near Gonzales. This is not a natural boundary of the ground-water basin. Ground water moves freely across this boundary into the area covered by the three-dimensional model, in response to recharge and pumpage on both sides of the boundary. Hydraulic head on the boundary cannot be specified directly, and the two-dimensional model was used to generate the boundary conditions. Therefore, along this boundary the hydraulic head on the three-dimensional model exactly matches those from the two-dimensional model.

A small disparity results from this method of generating boundary conditions. From the two-dimensional model only the average hydraulic head is given for this boundary. The imposition of depth-invariant hydraulic-head specifications in the boundary distorts the hydraulic-head distribution computed by the three-dimensional model for the area adjacent to the boundary. Vertical hydraulic head differentials in the prototype at this location are probably not greater than 5 ft for any two points on the boundary surface, and the distortions of computed hydraulic head are probably small and extend less than 1 mi away from the boundary.

#### Specified-Discharge Boundaries

The boundary surfaces without specified hydraulic head are impermeable boundaries. This boundary condition occurs on the subhorizontal surfaces that delineate the bottom of the ground-water basin and, except in the area offshore beneath Monterey Bay, the top of the ground-water basin. The impermeable-boundary condition also occurs on the vertical surfaces that delineate the geographic extent of the ground-water basin. These boundaries, where coincident with corresponding boundaries of the two-dimensional model, represent the same boundary conditions used locally on the two-dimensional model.

#### Initial Conditions

The procedure that was used for generating initial conditions for the two-dimensional model was also used for generating initial conditions for the three-dimensional model. First, steady-state water levels were computed for the steady annual mean pumping and recharge rates. The appropriate boundary conditions were obtained from similar computations using the two-dimensional model. Second, transient-state water levels were generated by the model for a 1-year cycle of transient pumpage and recharge using the steady-state model-generated water level as initial conditions. The model-generated water levels representing the end of the 1-year cycle were the initial conditions in the model.

#### System Parameters

The system parameters for the three-dimensional model are the horizontal and vertical hydraulic conductivity and specific storage. The available field data do not directly define the distribution of these parameters. If some reasonable assumptions regarding the general nature of the distribution of the parameters are accepted, however, the available data indirectly define their distribution.

#### Hydraulic Conductivity

Equivalent hydraulic conductivity.--The properties of the porous media making up the ground-water basin are highly heterogeneous on a small scale, and the available field data do not define this heterogeneity. In the development of transmissivity estimates for the two-dimensional model, this problem was ameliorated by making assumptions regarding the general nature of the distribution of transmissivity. For the three-dimensional model, similar assumptions were made regarding the distribution of hydraulic conductivity.

The equivalent average hydraulic conductivity for the solid region enclosed by an element in the finite-element grid is required for the three-dimensional model. When the ground-water system is composed of distinct horizontal layers, the equivalent hydraulic conductivity of the system can be determined for some simple flow cases. In the two-dimensional model, a binary system consisting of alternating beds of coarse-grained and fine-grained lithologies was considered. That system is also considered here.

Then, where flow is parallel to the beds, the equivalent hydraulic conductivity  $\bar{K}^h$  (where the superscript h is added to indicate flow parallel to the beds) is as given before by (Bear, 1972, p. 152)

$$\bar{K}^h = K_c^h (1-P) + K_f^h P \quad (25)$$

where  $K_c^h$  and  $K_f^h$  are the horizontal hydraulic conductivities of the coarse-grained and fine-grained beds, respectively, and P is the portion of a vertical interval occupied by fine-grained beds. The basis for this relation is that the same discharge will be conducted through the same aquifer thickness under the same gradient.

A second simple case is that where flow is perpendicular to the beds. The relation for the equivalent hydraulic conductivity  $\bar{K}^V$  (where the super-script v is added to indicate flow perpendicular to the beds) is given by (Bear, 1972, p. 154)

$$\bar{K}^V = \frac{K_c^V K_f^V}{K_f^V (1-P) + K_c^V P} \quad (26)$$

where  $K_c^V$  and  $K_f^V$  are the vertical hydraulic conductivities of the coarse-grained and fine-grained beds respectively. It is of interest to note that for  $K_f^V$  much smaller than  $K_c^V$ , the equivalent vertical hydraulic conductivity tends toward  $K_f^V/P$ ; while for  $K_f^h$  much smaller than  $K_c^h$ , the equivalent horizontal hydraulic conductivity tends toward  $K_c^h (1-P)$ .

The relations given for equivalent average hydraulic conductivity for the cases of flow parallel to beds and flow perpendicular to beds are exact. For the more general case of arbitrarily directed flow, exact relations cannot be developed. Bear (1972, p. 157), however, shows that a layered aquifer is equivalent in its average behavior to an anisotropic aquifer with principal

hydraulic conductivities  $\bar{K}^h$  and  $\bar{K}^V$ . For this statement to be valid, though, the individual layers must be thin with respect to the overall dimensions of the ground-water basin, which is a condition satisfied by the Salinas Valley ground-water basin.

Ratio of horizontal to vertical hydraulic conductivity.--The bedded character of alluvium imparts a strong anisotropy to the deposits if the average properties of large volumes are considered. Anisotropy is not so marked but is still present in small samples tested in the laboratory. Johnson, Moston, and Morris (1968) report both the horizontal and vertical hydraulic conductivities of laboratory samples of alluvium from the San Joaquin Valley, Calif. Figure 54 shows the cumulative distribution of the ratio of horizontal to vertical hydraulic conductivity for both coarse-grained and fine-grained samples. The horizontal hydraulic conductivity was greater than or equal to the vertical hydraulic conductivity for 72 percent of the coarse-grained samples and 69 percent of the fine-grained samples. As a measure of central tendency, the median ratio of horizontal to vertical hydraulic conductivity was about 2 for both sample types.

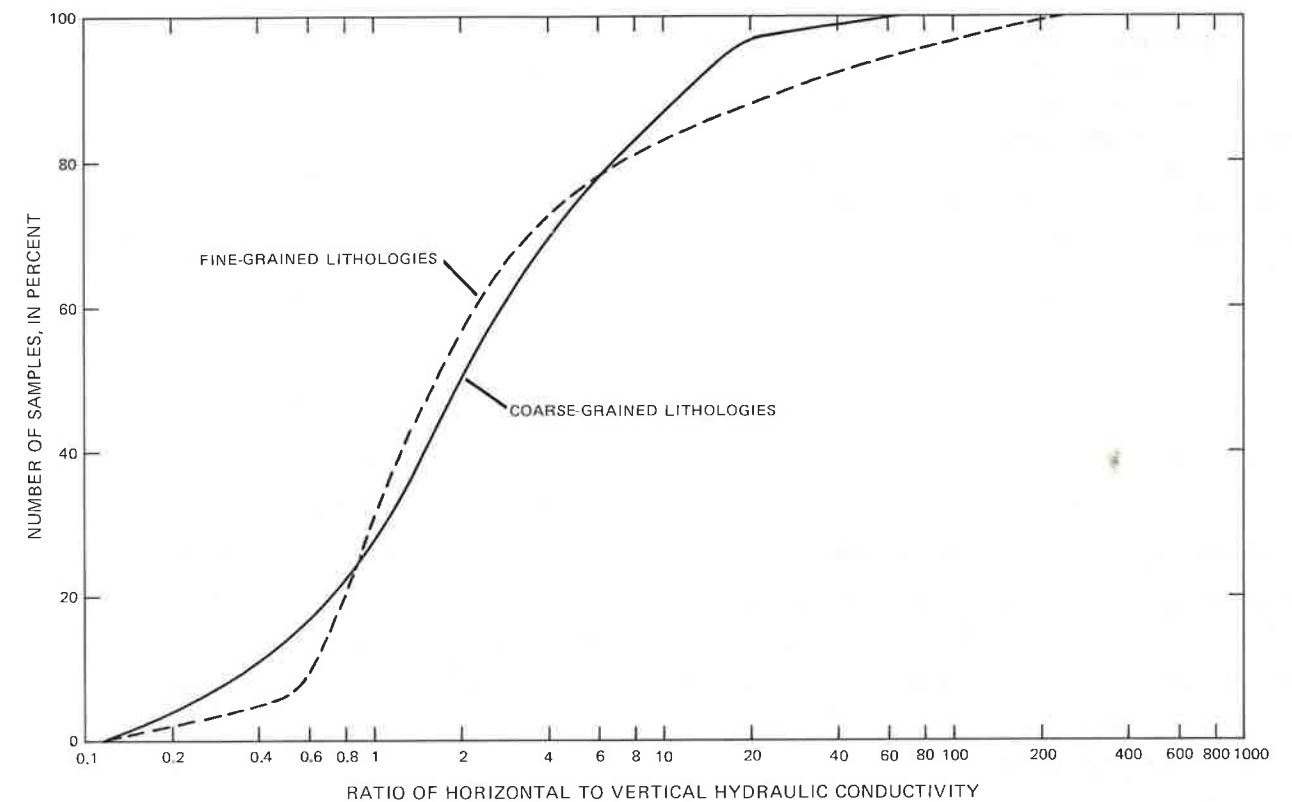


FIGURE 54.--Cumulative distribution of the ratio of horizontal to vertical hydraulic conductivity for laboratory samples of alluvium from the San Joaquin Valley, Calif. Based on data from Johnson, Moston, and Morris (1968).

The degree of anisotropy for the materials that make up the Salinas Valley ground-water basin is unknown. Given similarities, however, between the lithologies of the San Joaquin and Salinas Valleys, the degree of anisotropy in the hydraulic conductivity for the Salinas Valley is probably similar to that exhibited in samples from the San Joaquin Valley. In the development of estimates of hydraulic conductivity for the three-dimensional model, the assumption was made that the horizontal hydraulic conductivity was twice the vertical conductivity for both coarse-grained and fine-grained beds. Symbolically,

$$K_c^h = 2K_c^v \quad (27)$$

and

$$K_f^h = 2K_f^v. \quad (28)$$

Spatial relations.--Two spatial relations were assumed for hydraulic conductivity. The first relation was that  $K_c^h$  and  $K_c^v$  decrease linearly with depth (fig. 32). The rate of decrease was such that at a depth of 1,200 ft, these quantities were equal to one-half the value at the upper surface of the ground-water basin. The second relation is that  $K_f^h$  and  $K_f^v$  are invariant throughout the ground-water basin. Parallel relations were used in the two-dimensional model.

Calibration results.--Given expressions for equivalent average hydraulic conductivity, relations between horizontal and vertical hydraulic conductivity, and spatial relations for hydraulic conductivity in general, the problem of estimating the distribution of hydraulic conductivity can be reduced to the problem of estimating a single value of the vertical hydraulic conductivity for the fine-grained beds and of estimating the geographic distribution of the horizontal hydraulic conductivity for the coarse-grained beds. These quantities were estimated from a trial-and-error calibration using a steady-state simulation. Pumpage and autumn water-level measurements for 1970 were used in the steady-state simulation, as was done for the two-dimensional model.

Ground-water levels in the basin were computed by the model, using initial estimates of hydraulic conductivity. These model-generated water levels deviated locally as much as 40 ft from measured water levels. Again, as for the two-dimensional model, the objective of the calibration procedure was to iteratively reduce the local deviations to a reasonable level by adjusting the hydraulic conductivity. The net effect of these adjustments was to decrease the hydraulic conductivity about 15 percent from the initial estimates. The adjusted vertical hydraulic conductivity of the fine-grained beds was 0.5 ft/d. The adjusted horizontal hydraulic conductivity, at the upper surface of the ground-water basin, of the coarse-grained bed ranged from 20 to 100 ft/d and is shown in figure 55.

The estimated horizontal hydraulic conductivity for the three-dimensional model is about 15 percent larger than the estimated hydraulic conductivity for the two-dimensional model. This disparity is due principally to the occurrence of a vertical component of ground-water flow in the prototype. Observed lateral hydraulic-head differentials represent the cumulative head loss along the path of flow. Because the path of flow is not everywhere in a horizontal plane, head losses are, in part, related to the vertical hydraulic conductivity of the ground-water system. In the two-dimensional model, lateral hydraulic-head differentials are simulated through horizontal flow. The hydraulic conductivity used in the model must reflect the effects of both horizontal and vertical ground-water flow. Therefore, the hydraulic conductivity used in the two-dimensional model should be smaller than that used in the three-dimensional model, which better reflects the actual flow paths in the ground-water basin and the resistance to flow along those paths.

Figures 56, 57, and 58 show the steady-state model-generated water levels in the Pressure and East Side Areas that were computed by the three-dimensional model, using the hydraulic conductivities shown in figure 55. The fit of model-generated water level to measured water level is about the same as that obtained for the two-dimensional model (fig. 37). Cumulative distributions of the deviation of model-generated water level from the prototype water level for the East Side Area and for the 180-foot and 400-foot aquifers in the Pressure Area are shown in figure 59. The median deviations range from 5 to 6 ft, and the maximum deviations range from 17 to 48 ft.

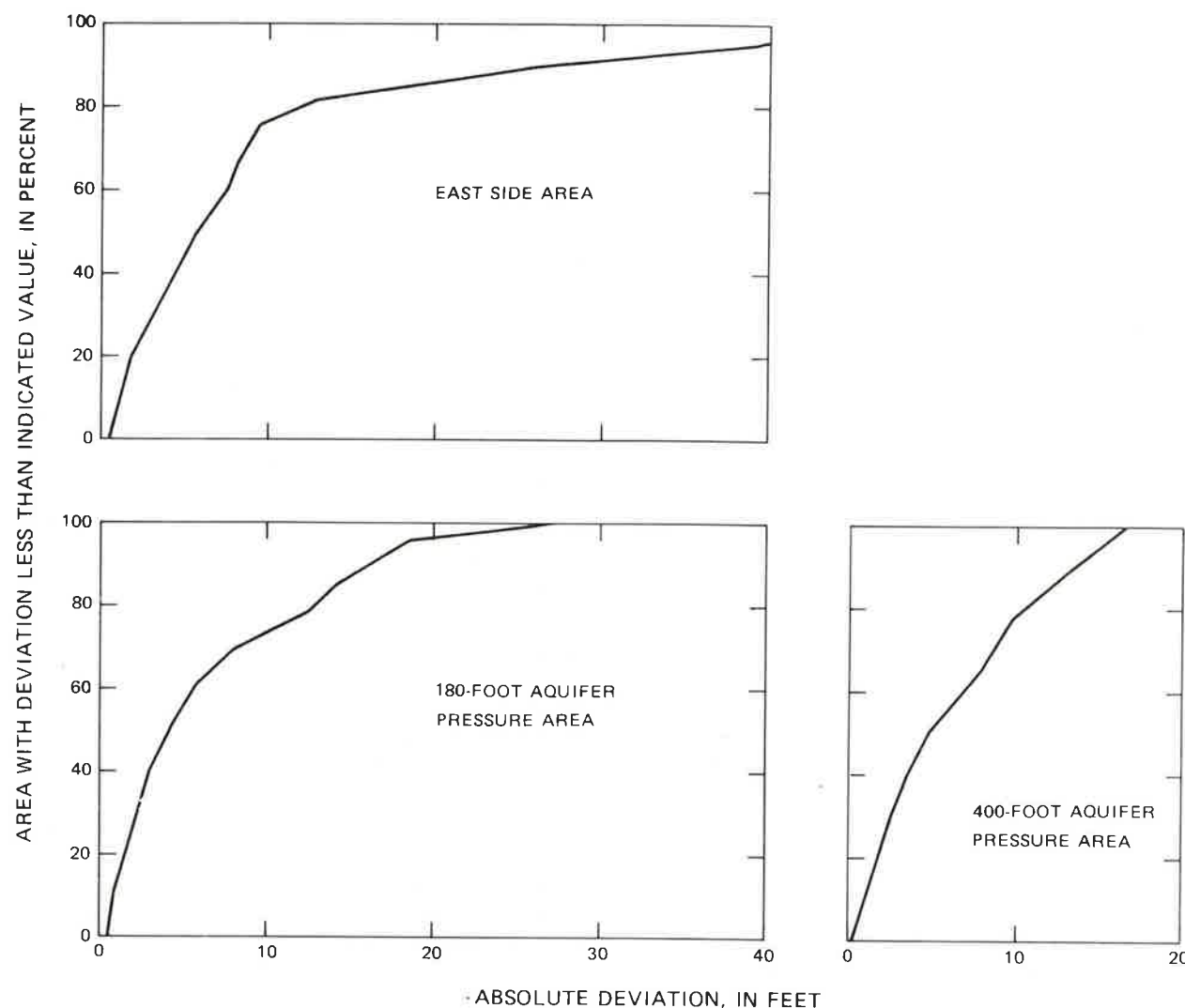


FIGURE 59.--Cumulative distribution of the deviation of steady-state water level generated by the three-dimensional ground-water model from measured water level for autumn 1970, for the East Side Area and the 180-foot and 400-foot aquifers in the Pressure Area.

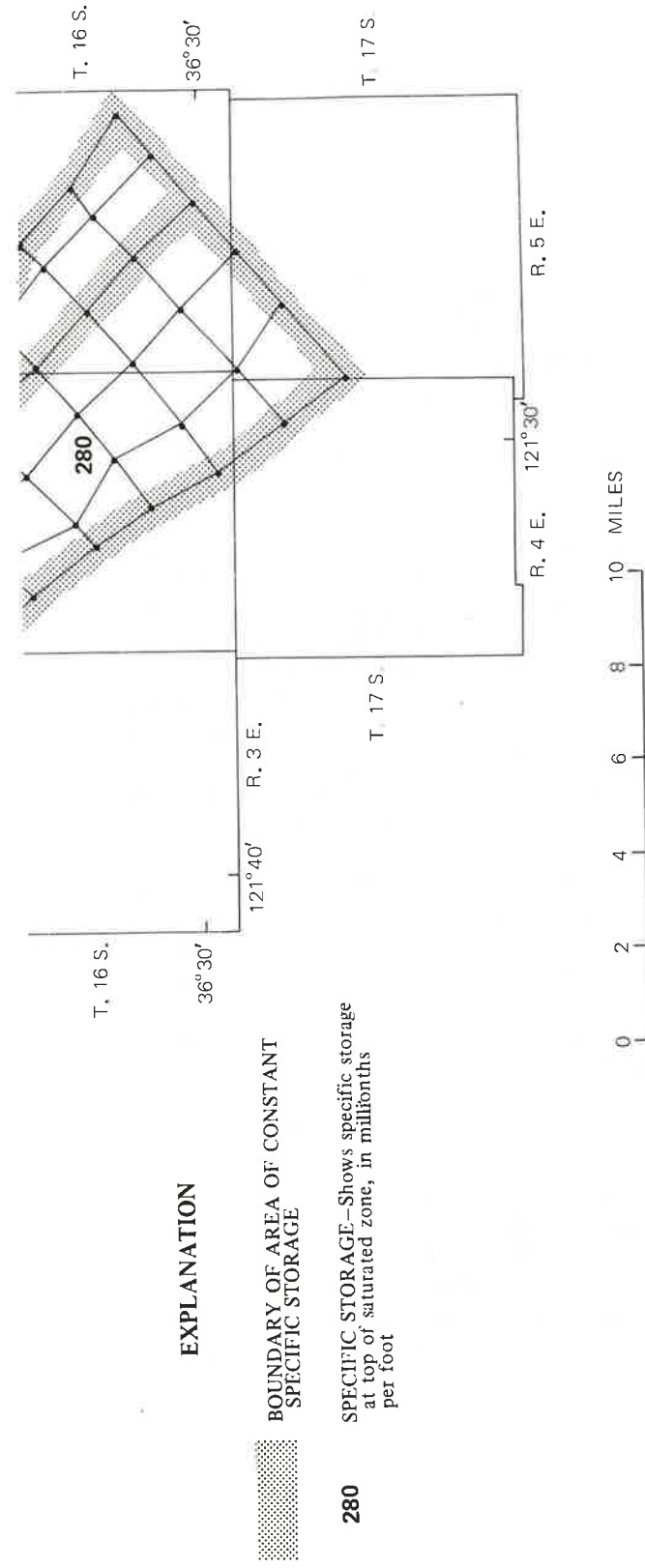
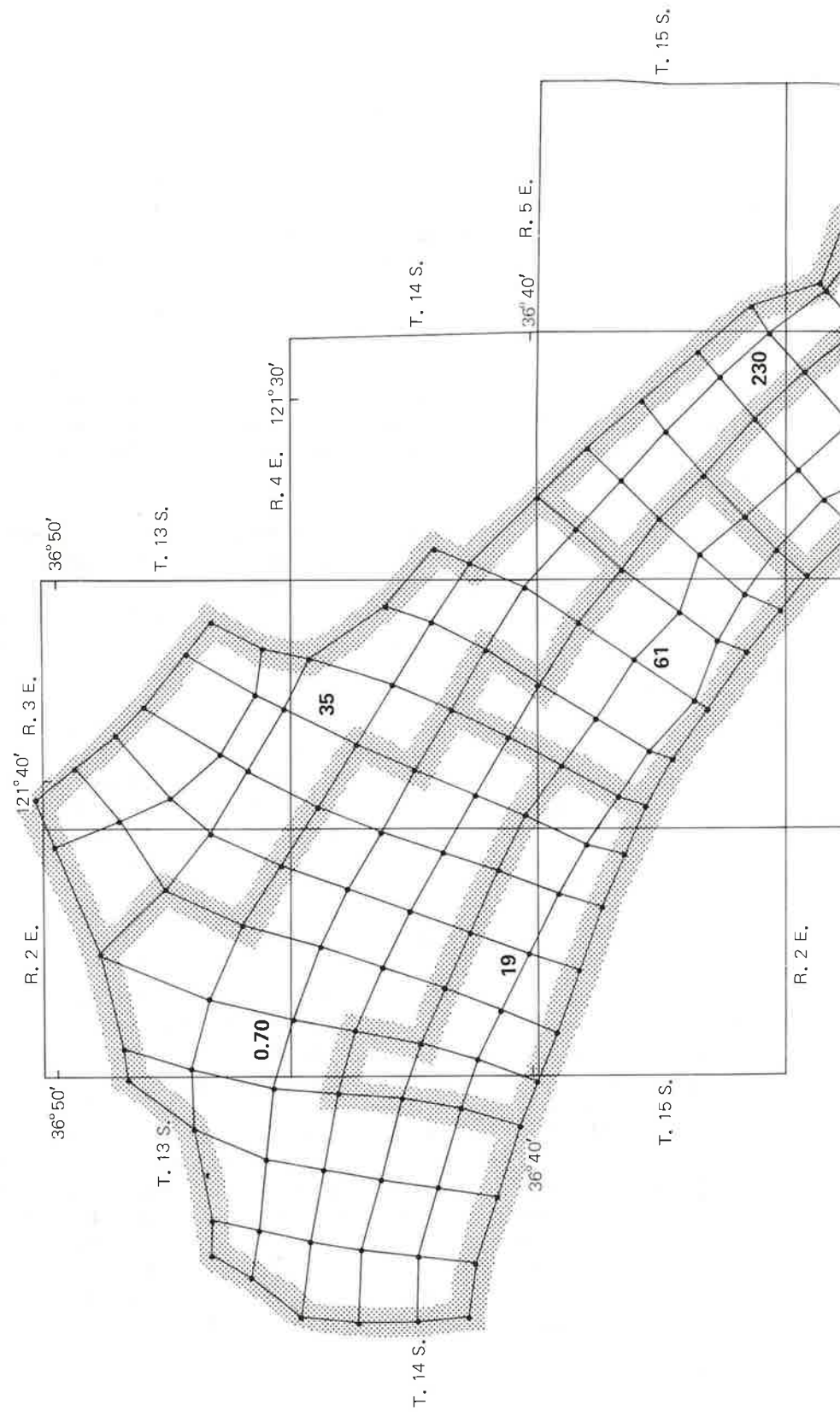
## Specific Storage

A transient-state simulation was used to calibrate specific storage values. In problems of three-dimensional transient flow in a compressible ground-water system, it is necessary to consider the amount of water released from or taken into storage per unit volume of the porous medium. The specific storage is the volume of water released from or taken into storage per unit volume of the porous medium per unit change in head (Lohman and others, 1972).

Spatial relations.--The available field data do not define the three-dimensional distribution of specific storage. To impose some rationality on the estimated distribution of specific storage, several assumptions regarding the spatial relations for this parameter were involved. These assumptions are described below.

In areas of confined ground water, the water derived from storage with a decline in head comes from expansion of the water and compression of the aquifer; similarly, water added to storage with a rise in head is accommodated partly by compression of the water and partly by expansion of the aquifer. The compressibility of the porous media (and of the water) may be more or less constant with depth. Johnson, Moston, and Morris (1968) report the compression index (which is the difference in void ratio for one logarithmic increment of load) for laboratory samples of alluvium from the San Joaquin Valley, Calif. The compression index for these samples, which is an approximate index of their specific storage, has a somewhat limited range for material of similar lithology. Concomitantly, the porous media that make up the Salinas Valley ground-water basin probably has limited vertical variability in compressibility on a macroscopic scale. Owing to this property of the porous media, in the development of specific-storage estimates for the three-dimensional model, specific storage was assumed to be invariant with depth in areas of confined ground water.

In areas of unconfined ground water, the quantity of water derived from or added to the aquifer due to the compressibility of the porous media and water generally is negligible compared to that involved in gravity drainage or filling of pores from the desaturation or resaturation of the porous media. Below the water table the compressibility of the porous media should be similar to that in areas of confined ground water, and the relation between head changes and storage changes is properly accounted for by the compressibility of the porous media. At the water table, however, the relation between head changes and storage changes is given by the specific yield of the porous media. To account for these two conditions, the specific storage used in the three-dimensional model was assumed to equal specific yield in the elements in the top of the finite-element grid and to equal the specific storage of a confined aquifer in other elements below.



**FIGURE 60. -- Finite-element grid for the three-dimensional ground-water model and geographic distribution of specific storage.**



**Calibration results.**--The calibration procedure was started by making initial estimates of specific storage using storage-coefficient values from the two-dimensional model (fig. 38). Specific storage of upper elements in the finite-element grid was set equal to the corresponding storage-coefficient values. The lower elements were assigned initial specific-storage values equivalent to the storage coefficient in the two-dimensional model for the area of confined ground water northwest of Salinas. The hydraulic-conductivity estimates obtained from the steady-state simulation (fig. 55) were used in the transient-state simulation, and these values remained unchanged during the calibration of specific storage. Specific storage was adjusted during the calibration, so that the computed head matched, to a reasonable degree, the seasonal variations of measured water level for the period December 1968-November 1971, which was the same period used to calibrate the storage coefficient for the two-dimensional model.

Figure 60 shows the final estimates of specific storage for the upper elements of the finite-element grid. These values range from 0.0000007 to 0.00028 per foot. The specific storage of other elements is 0.0000007 per foot. The storage coefficients equivalent to this distribution of specific storage are similar to the distribution of storage coefficient obtained for the two-dimensional model (fig. 38). In general, however, the equivalent storage coefficients for the three-dimensional model are about 15 percent larger than the storage coefficients for the two-dimensional model. This difference is such that the hydraulic diffusivity, which is transmissivity divided by storage coefficient (Lohman and others, 1972), is nearly equal in the models.

To obtain estimates of specific storage, the model-generated water level was fitted to hydrographs of measured water level for 37 wells. Comparisons between model-generated water level and measured water level for selected wells are shown in figures 61 through 63. The measure of goodness-of-fit between computed and measured hydrographs was the deviation between the corresponding amplitudes of the hydrographs representing the model and the prototype. The cumulative distribution of this deviation is shown in figure 64 for the East Side Area and for the 180-foot and 400-foot aquifers in the Pressure Area. The median deviations range from 8 to 11 ft, and the maximum deviations range from 28 to 32 ft.

Figures 65, 66, and 67 show model-generated water level in the Pressure and East Side Areas that were computed by the three-dimensional model for the end of the calibration period. Cumulative distributions of the deviation of model-generated water level from measured water level for the East Side Area and for the 180-foot and 400-foot aquifers in the Pressure Area are shown in figure 68. The median deviations range from 4 to 8 ft, and the maximum deviations range from 22 to 26 ft.

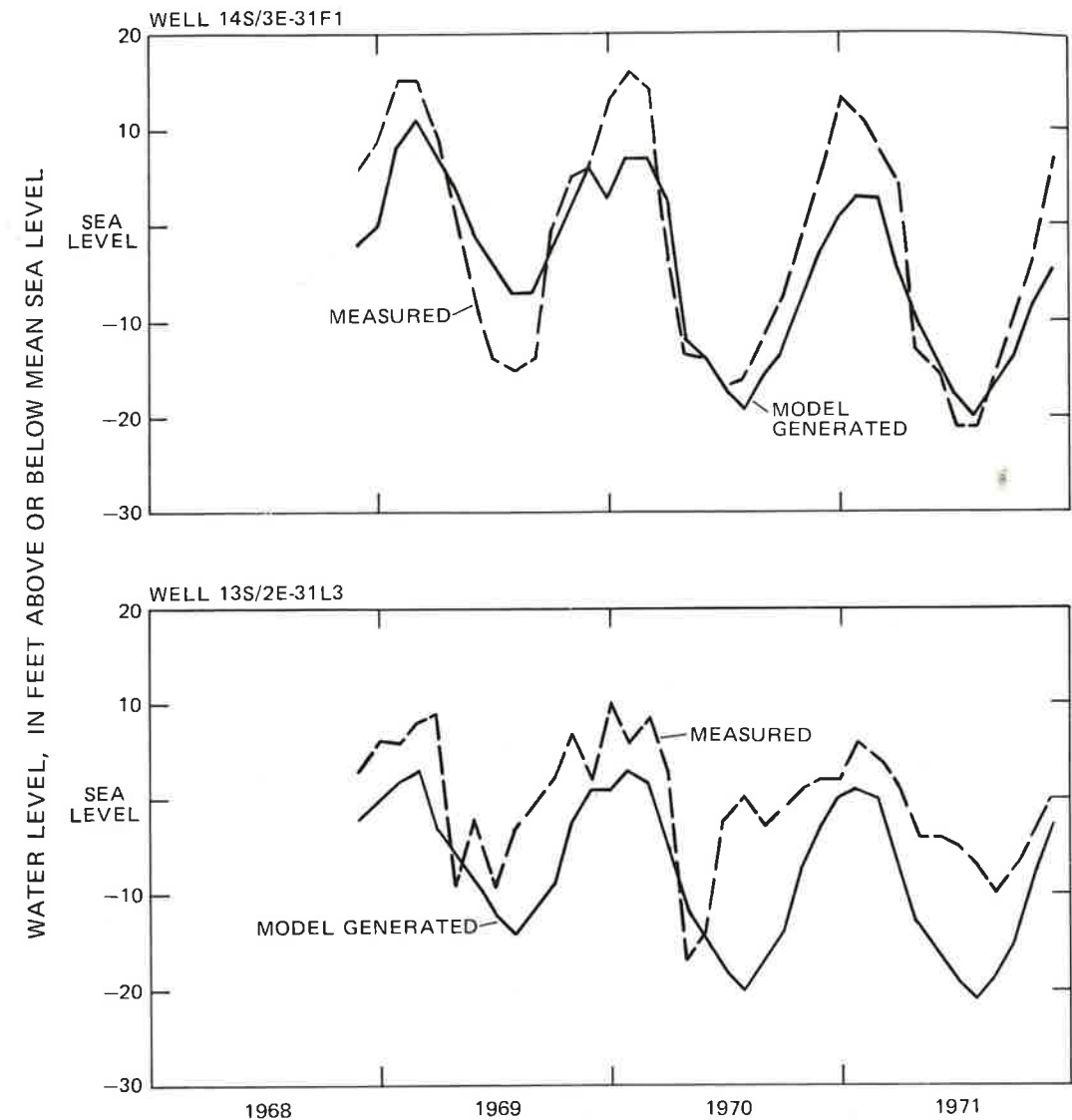


FIGURE 61.--Comparison of water level generated by the three-dimensional ground-water model and measured water level for wells 13S/2E-31L3 and 14S/3E-31F1 in the 180-foot aquifer of the Pressure Area.

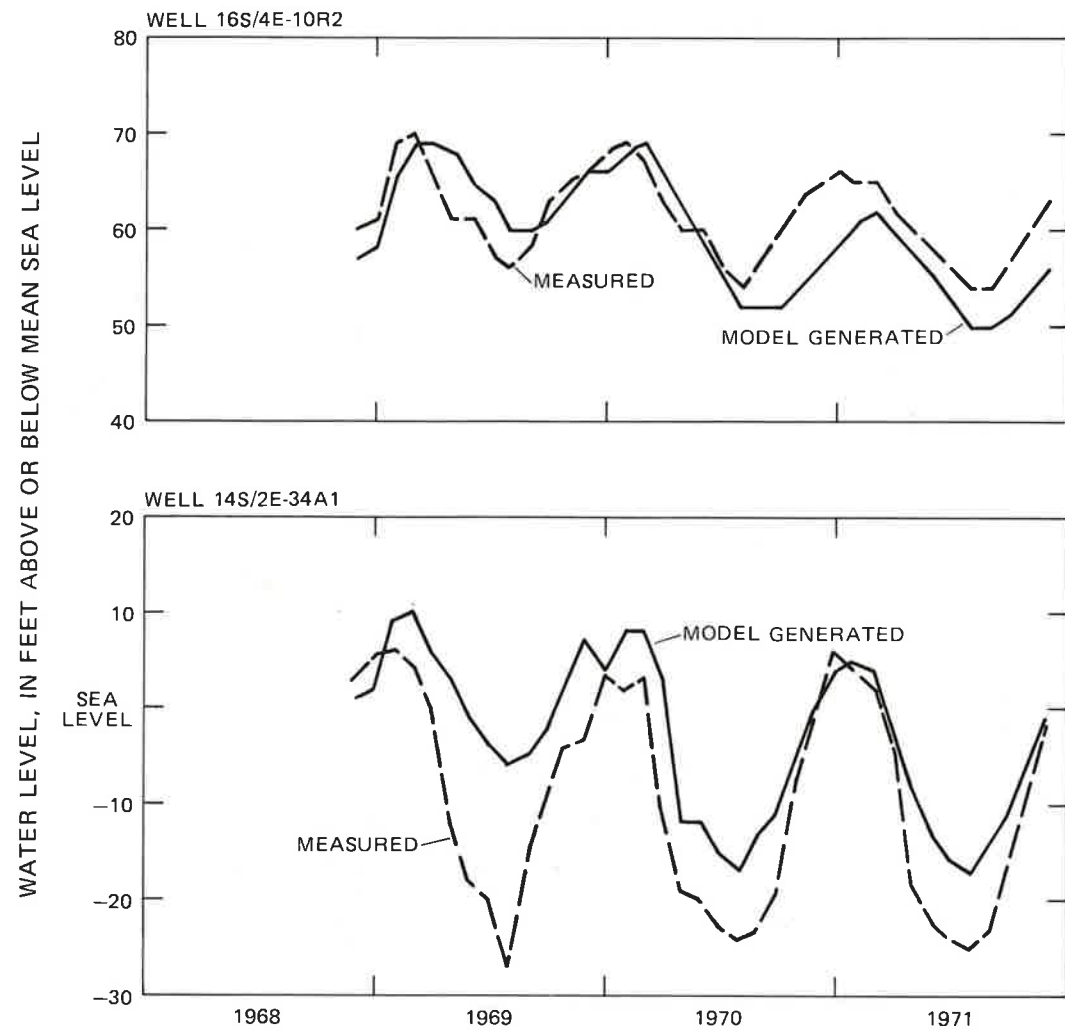


FIGURE 62.--Comparison of water level generated by the three-dimensional ground-water model and measured water level for wells 14S/2E-34A1 and 16S/4E-10R2 in the 400-foot aquifer of the Pressure Area.

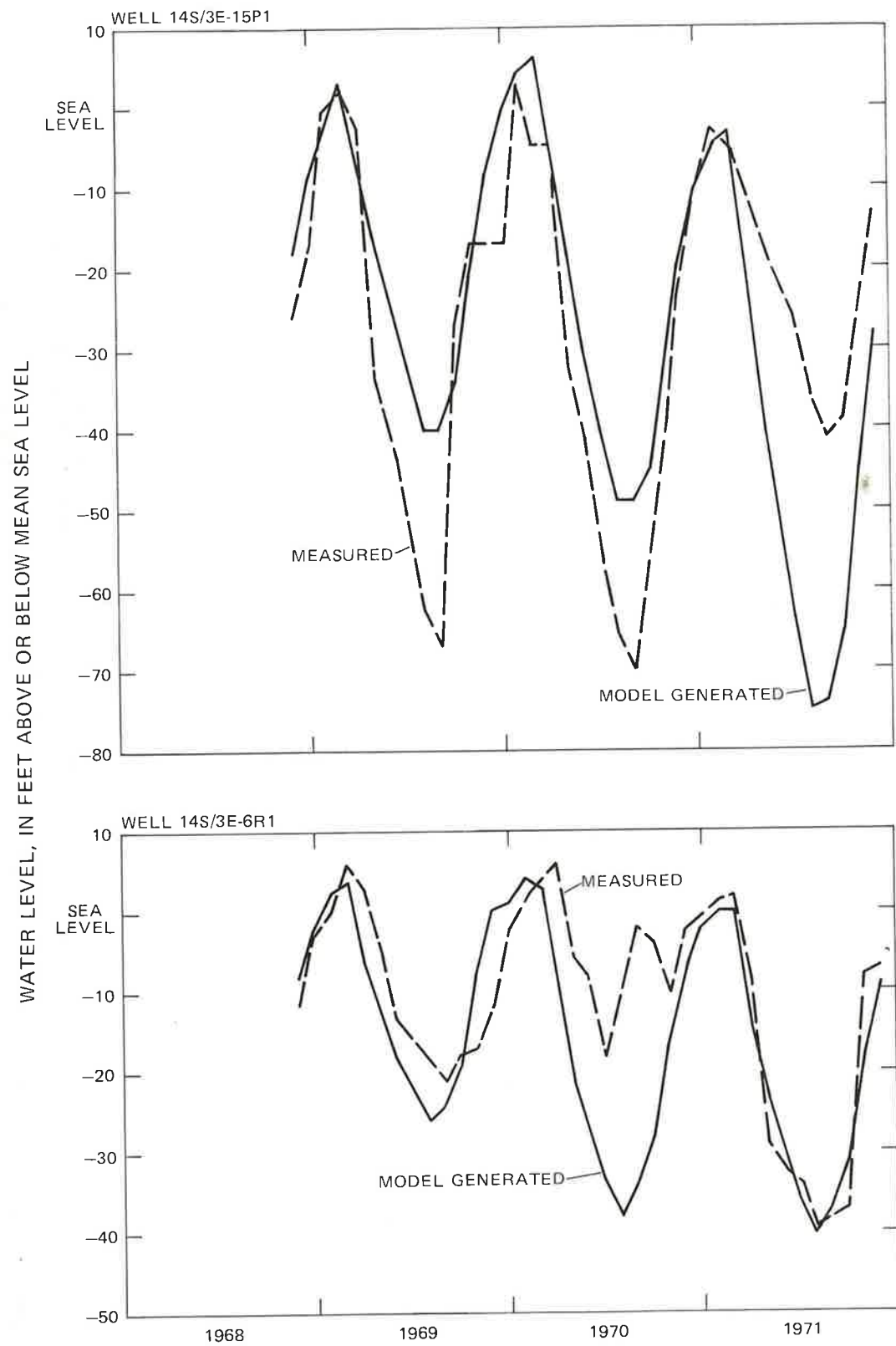


FIGURE 63.--Comparison of water level generated by the three-dimensional ground-water model and measured water level for wells 14S/3E-6R1 and 14S/3E-15P1 in the East Side Area.

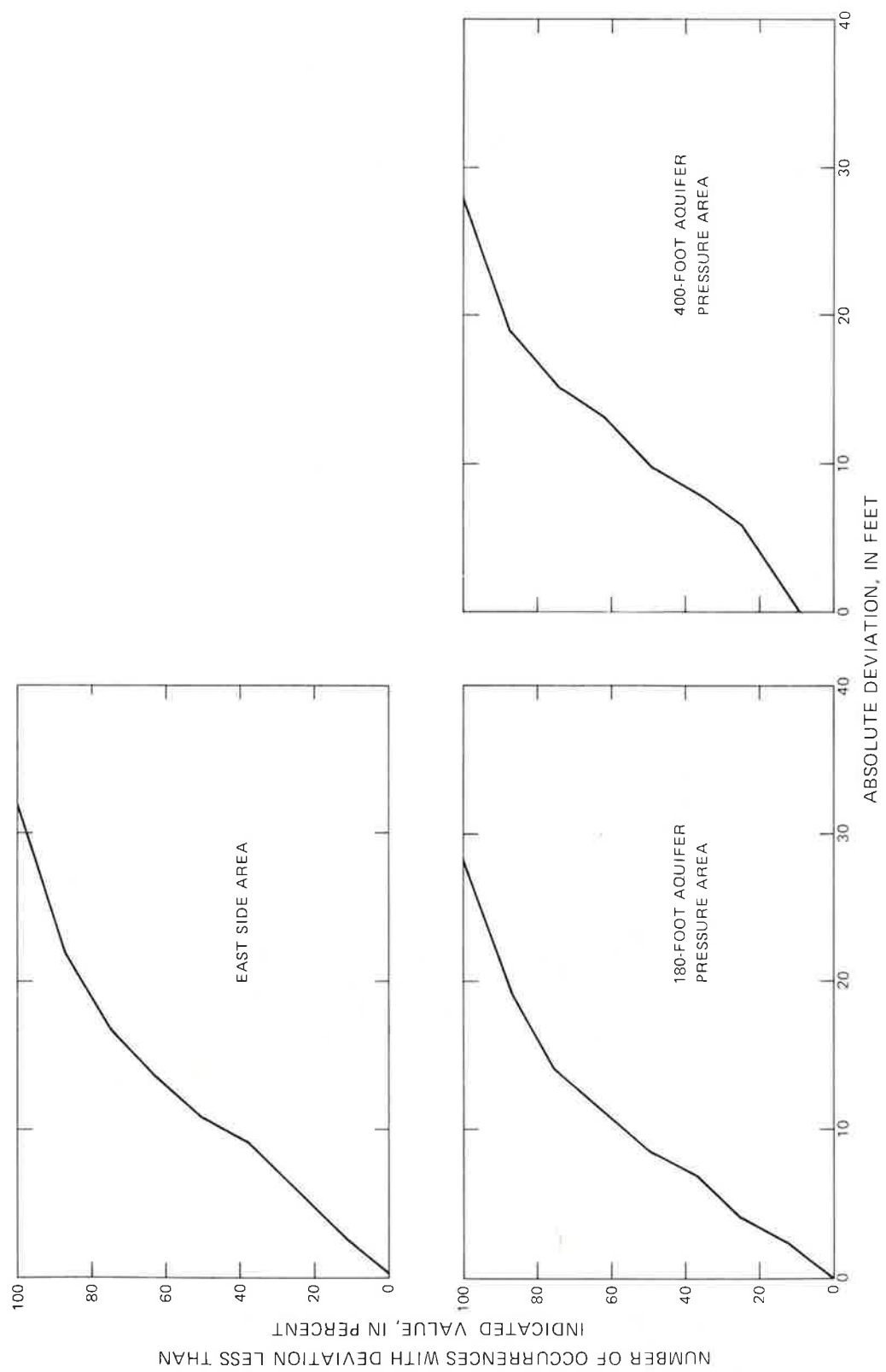


FIGURE 64.--Cumulative distribution of the deviation of the amplitude of seasonal fluctuations of water level generated by the three-dimensional ground-water model from the amplitude of measured water level, for the East Side Area and the 180-foot and 400-foot aquifers in the Pressure Area.

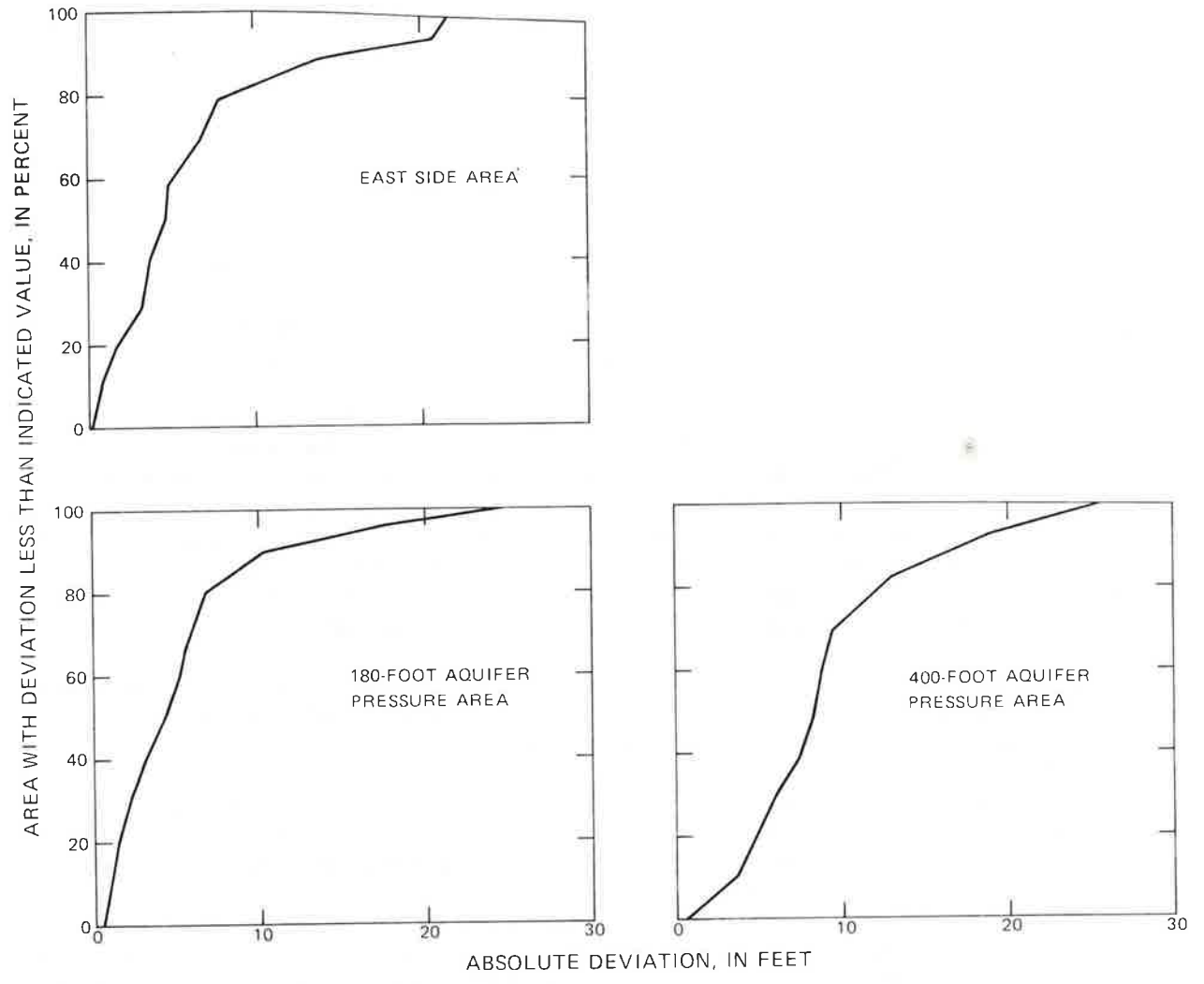


FIGURE 68.--Cumulative distribution of the deviation of transient-state water level generated by the three-dimensional ground-water model from measured water level for autumn 1971, for the East Side Area and the 180-foot and 400-foot aquifers in the Pressure Area.

## MODELING ERRORS

### Sources of the Deviation of Model-Generated Water Levels from Measured Water Levels

The observed deviation of the model-generated water levels from the prototype water levels (figs. 37, 44, 46, 50, 59, 64, 68) is the result of errors associated with the conceptual model, the computational scheme, the system parameters, the input data, the initial conditions, and the prototype water levels.

Conceptual model.--The errors associated with the conceptual models result mainly from the simplifying assumptions used in the conceptualization of the prototype. Although errors of conceptualization are probably not large compared to other errors in the models, these errors result from the assumption that ground-water flow is strictly horizontal in the two-dimensional model and from the spatial relation for hydraulic conductivity and specific storage that were imposed on the three-dimensional model.

Computational scheme.--Errors associated with the computational scheme are errors resulting from the numerical approximation of the solution to the governing equations. The numerical solution converges to the true solution as the elements are reduced to zero area (Hutton and Anderson, 1971). The use of elements with other than zero area results in the departure of the numerical solution from the true solution, especially where large changes in hydraulic-head gradients are involved. The computational scheme is probably not a serious source of error in the models, however.

System parameters.--The system parameters consist of the transmissivity and storage coefficient of the two-dimensional model and of the hydraulic conductivity and specific storage of the three-dimensional model. Prior estimates of these parameters are changed during the calibration of the model. The objective of the calibration is to identify parameter values that minimize the deviation of the model-generated water levels from the measured water levels while keeping the parameter values within physically reasonable limits. It is difficult to recognize when minimum-deviation parameter values have been found, however, and the calibration procedure is usually terminated prematurely. The presumption always remains that, if additional calibration runs had been made, perhaps the fit of the model to the prototype water levels could have been improved.

In using the model to make predictions of the response of the prototype to specific inputs, errors associated with the system parameters result from the deviation of the system parameters from their true values. Relatively small adjustments were made to the system parameters during the calibration of the steady-state and transient-state models. A consistency exists between estimates of the system parameters obtained from field data and estimates obtained from the calibration procedures. Consequently, the probability is greater that the system parameters used in the model are close to the true parameters than if that consistency did not exist.

If different estimates of the source and sink discharges had been used in the calibration, different estimates of the system parameters probably would have been obtained. Figures 69 and 70 show the effects of changes in the system parameters for the two-dimensional model on the predictions of hydraulic head that are made with the model. Figure 69 shows the effects on the computed hydraulic heads of relative changes in the storage-coefficient values. The measure of the effect on the computed hydraulic heads is the relative deviation of the computed changes in hydraulic heads at the end of a 5-year simulation period. The relative deviation (D) is defined by the relation

$$D = \left| \frac{\Delta h_o - \Delta h}{\Delta h_o} \right| \quad (29)$$

where  $\Delta h_o$  is the computed hydraulic-head change during the 5-year simulation period using the hydraulic conductivity values shown in figure 35 and the storage coefficient values shown in figure 38, and  $\Delta h$  is the computed hydraulic-head change using perturbed storage coefficient values. The 90-percentile and the median deviation are indicated in figure 69. (The 90-percentile deviation is the deviation value such that 10 percent of the deviations are smaller than that value.) Correspondingly, figure 70 shows the effects on computed hydraulic heads of relative changes in the hydraulic conductivity values.

The 90-percentile relative deviation is quite sensitive to changes in the system parameters. The 90-percentile relative deviation, however, is generally associated with areas that have smaller head changes. The median deviation is less sensitive to changes in the system parameters than is the 90-percentile deviation. This is especially true for changes in hydraulic conductivity.

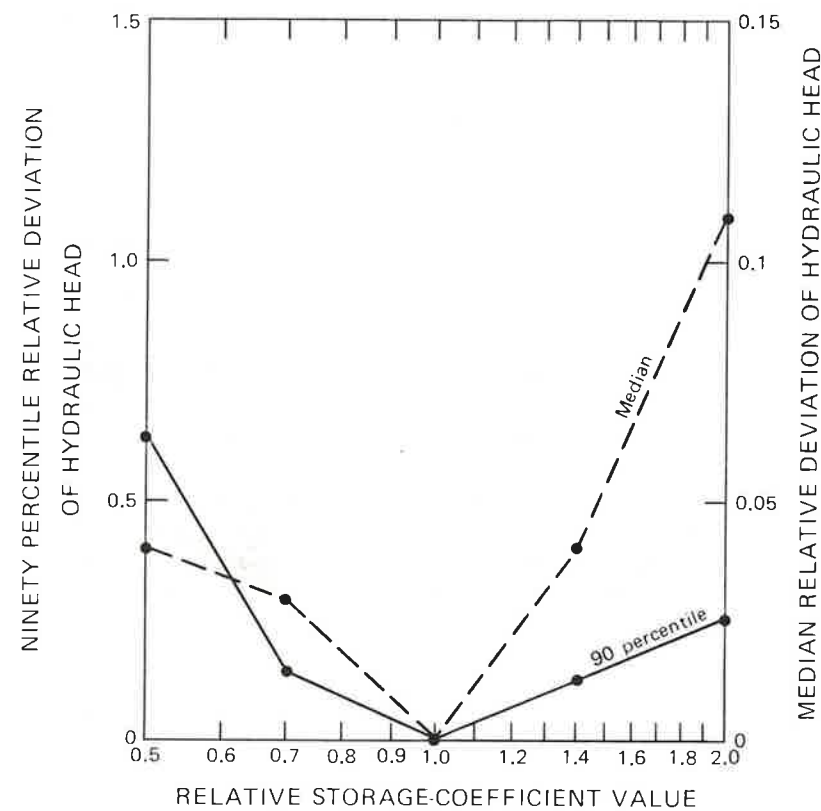


FIGURE 69.--Sensitivity of hydraulic heads computed by the two-dimensional ground-water model to changes in the storage-coefficient values used in the model.

Input data.--Errors associated with the input data result from the estimation of source and sink discharges. Techniques used to obtain these estimates typically bias the estimates, and the bias is for the most part transferred to the system parameters during the calibration process. This may be a relatively important source of error.

Initial conditions.--Transient-state simulations with the models require specification of initial water levels. Errors in the initial water levels produce errors in the model-generated water levels. In general, however, these errors become less important as the duration of the period of simulation increases.

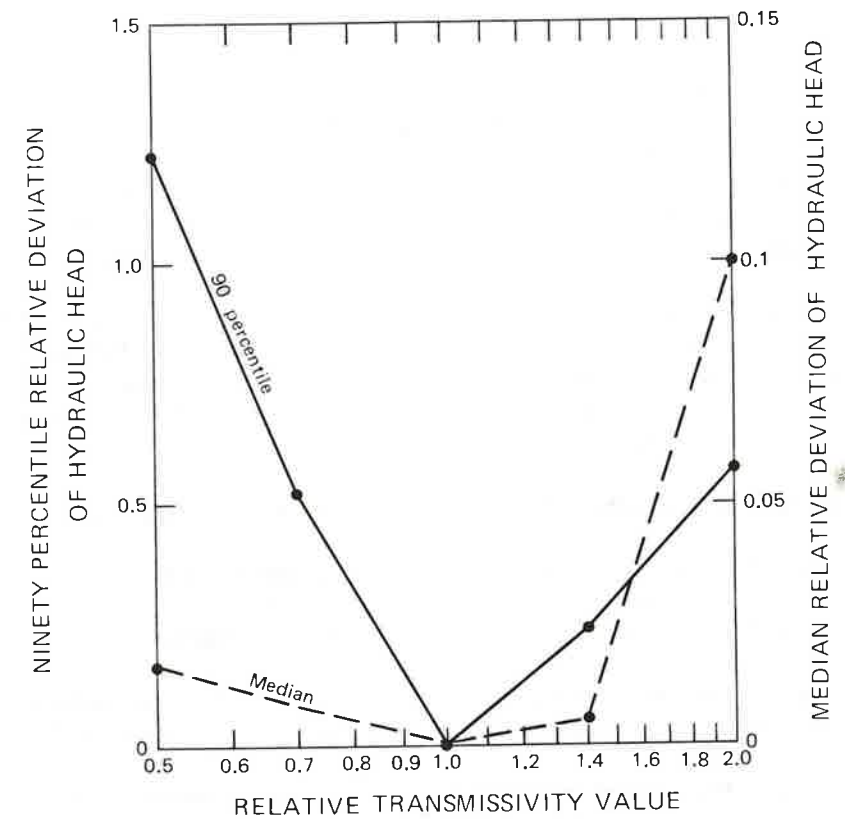


FIGURE 70.--Sensitivity of hydraulic heads computed by the two-dimensional ground-water model to changes in the hydraulic-conductivity values used in the model.

Prototype water levels.--Errors associated with the prototype water levels are errors of measurement, sampling, and interpretation. The largest errors of measurement probably result from locating wells incorrectly and thereby incorrectly estimating the altitude of the land surface at the well from topographic maps. Some water-level measurements may not be representative of the aquifer. Measurement of water levels in wells that are being affected by local pumping or in wells tapping perched aquifers, for example, will not be representative of aquifer conditions. These are sampling errors. Interpretation errors arise where field data are contoured or extrapolated to areas without any data. Prototype water levels probably are a serious source of local error.

The predictive accuracy of the model, when measured in terms of the deviation of the model-generated water levels from the prototype water levels, is directly proportional to the magnitude and duration of pumping. The greater the pumpage or the longer the duration of pumping, the greater will be the probable errors in computed hydraulic heads. If the future magnitude and duration of pumping are similar to those used in the verification of the two-dimensional model, the deviations of the model-generated water levels from the prototype water levels that were obtained from the verification of the two-dimensional model are probably indicative of the predictive accuracy of both the two-dimensional and three-dimensional models for long-term simulations. It may be possible, however, to improve the predictive accuracy of the models by selective use.

Consider three questions that can be asked about model predictions:

1. What will be the future pumpage and what will be the response of the prototype to that pumpage?
2. What will be the response of the prototype to any specified pumpage?
3. What will be the differential response of the prototype to two specified pumpages that are defined to be mutually exclusive?

The answer to the first question will contain errors that result from errors in the conceptual model, errors in the system parameters, errors in the initial conditions, and errors in the pumpage. The answer to the second question, however, will not contain errors resulting from errors in the pumpage. The third question eliminates initial conditions from consideration, and the answer to this question will not contain errors that result from either pumpage or initial conditions.

The elimination of pumpage errors from the second question will improve the probable accuracy of the answer to this question relative to the accuracy of the answer to the first question. The additional elimination of initial-condition errors from the third question will improve the probable accuracy of the answer to this question relative to the accuracy of the answers to both the first and second questions. Therefore, the best predictions are made with the models for interrogations involving the differential response of the prototype.

The Salinas Valley ground-water basin includes the area between Monterey Bay and San Ardo that is underlain by unconsolidated deposits. The unconsolidated deposits consist of the Paso Robles Formation, which is of Pleistocene and Pliocene age and locally is as much as 2,000 ft thick, and the alluvial fan, river, and windblown sand deposits, which are of Holocene and Pleistocene age and locally are collectively as much as 500 ft thick. Ground water occurs in a fairly continuous ground-water system in these deposits. Most of the water that is stored in the ground-water basin is in the Paso Robles Formation, but the principal water-bearing zones are in the alluvium.

Natural recharge to the Salinas Valley ground-water basin occurs mostly by infiltration of streamflow. The Salinas River is the principal source of ground-water recharge from streamflow. The annual recharge from the river was 156,000 acre-ft for the pumping rate existing in 1970. Small streams tributary to the Salinas River also contributed ground-water recharge. The cumulative mean annual recharge from these tributaries is 96,000 acre-ft.

Another source of ground-water recharge is subsurface inflow to the ground-water basin. Between King City and San Ardo, ground-water recharge occurs by subsurface inflow from the east. Precipitation on outcrops of older marine rocks that underlie this area infiltrates permeable soils that have formed on these rocks, percolates downward to the water table, and, by lateral movement, eventually enters the Salinas Valley ground-water basin as subsurface inflow. The mean annual recharge by this mechanism is 21,000 acre-ft.

Seawater intrusion from Monterey Bay is a source of ground-water recharge, although an undesirable source. The annual recharge from seawater was 10,000 acre-ft for conditions existing in 1970.

Ground-water discharge from the Salinas Valley ground-water basin occurs from pumpage and the consumptive use of ground water by riparian vegetation along the Salinas River. In 1970 the agricultural and municipal pumpage was 482,000 acre-ft. About 45 percent of this pumpage returns to the ground-water system, and in 1970 the annual return was 217,000 acre-ft. The riparian vegetation, which consists mostly of willows and cottonwoods, consumes 25,000 acre-ft of water annually.

A group of interacting hydrologic models was developed for the Salinas Valley. These models include the small-stream model, river model, two-dimensional ground-water model, and three-dimensional ground-water model. The small-stream model simulates ground-water recharge from tributaries of the Salinas River that cross the ground-water basin. The river model simulates ground-water recharge from and discharge in the Salinas River. The two-dimensional ground-water model simulates depth-averaged hydraulic head in the ground-water basin. The three-dimensional ground-water model simulates the depth variations of hydraulic head.

Each of the models employs a fixed set of mathematical expressions that were adapted to the Salinas Valley by selecting the proper set of numerical values for certain parameters within the mathematical expressions. Values for these parameters were selected by a calibration procedure that involved the trial-and-error adjustment of the parameter values until the model reproduced some selected behavior of the prototype to an acceptable level.

The critical parameters of the small-stream model were coefficients relating to the flow width and infiltration rate. These parameters were adjusted so that the model reproduced selected streamflow events for the Arroyo Seco.

The parameters of the river model were flow width, flow depth, and channel-bed leakage coefficients. These parameters were adjusted so that the model would simulate the discharge of the Salinas River at selected gaging stations and the hydraulic head differential between the river and the ground-water system. With the final parameter values, the river model reproduced annual mean discharge with an error not larger than 33 percent of the measured discharge.

The parameters of the two-dimensional ground-water model are transmissivity and storage coefficient. The model was calibrated by comparing the model-generated water level to corresponding prototype water level for both steady-state and transient-state simulations. For the steady-state simulation, which was used to calibrate transmissivity, the median deviation of water level generated by the model from measured water level for autumn 1970 was about 6 ft. For the transient-state simulation, which was used to calibrate storage coefficient, the median deviation of water level generated by the model for the end of a 3-year simulation period from measured water level for autumn 1971 was about 6 ft.

Parameters for the two-dimensional ground-water model were estimated, using data from the period December 1968-November 1971. To test the behavior of the model for longer simulation periods, the model was verified using the period December 1944-November 1970. Model verification involves using the model parameters derived from the calibration period to simulate water level for some period not involved in model calibration and comparing the model-generated water level with measured water level. At the end of the verification period, the median deviation of water level generated by the two-dimensional ground-water model from measured water level for autumn 1970 was about 6 ft.

The parameters of the three-dimensional ground-water model were hydraulic conductivity and specific storage. This model was also calibrated with both steady-state and transient-state simulations. For the steady-state simulation, which was used to calibrate hydraulic conductivity, the median deviation of model-generated water level from measured water level for autumn 1970 was about 5 ft. For the transient-state simulation, which was used to calibrate specific storage, the median deviation of model-generated water level from measured water level for autumn 1971 was about 6 ft.

The data used to calibrate the ground-water models contained errors. These errors in part caused the previously described deviation of model-generated water level from measured water level. The errors contained both systematic and random components. In general, the systematic errors were probably transferred to the estimates of transmissivity and storage coefficient for the two-dimensional ground-water model and to the estimates of hydraulic conductivity and specific storage for the three-dimensional ground-water model during the calibration procedure.

Predictions made with the ground-water models will be in error because of the transfer of data errors to the model parameters. The predictions will also contain errors that can be related to the initial conditions and assumed future pumpage. If these three types of errors are present, the median error of hydraulic-head prediction will probably be about the same as that obtained from the verification of the two-dimensional ground-water model, or about 6 ft if a similar magnitude and duration of pumpage are considered.

## REFERENCES CITED

- Bear, Jacob, 1972, Dynamics of fluids in porous media: New York, American Elsevier Publishing Co., 764 p.
- Bishop, C. C., and Chapman, R. H., 1967, Bouguer gravity map of California, Santa Cruz sheet: California Division of Mines and Geology, scale 1:250,000.
- Blaney, H. F., 1954, Consumptive use of ground water by phreatophytes and hydrophytes, International Union of Geodesy and Geophysics, Paper, 10th General Assembly, Rome, Italy: International Association of Scientific Hydrology Publication 37, v. 2, p. 53-62.
- Blaney, H. F., and Criddle, W. D., 1962, Determining consumptive use and irrigation water requirements: U.S. Agricultural Research Service Technical Bulletin 1275, 59 p.
- Blaney, H. F., Taylor, C. A., and Young, A. A., 1930, Rainfall penetration and consumptive use of water in Santa Ana River valley and coastal plain: California Department of Public Works, Division of Water Resources Bulletin 33, 162 p.
- Bramlette, M. N., 1946, [1947], The Monterey Formation of California and the origin of its siliceous rocks: U.S. Geological Survey Professional Paper 212, 57 p.
- California Department of Public Works, Division of Water Resources, 1946, Salinas Basin investigation: California Department of Public Works Bulletin 52, 230 p.
- \_\_\_\_\_, 1949, Salinas Basin investigation basic data: California Department of Public Works Bulletin 52-A, 426 p.
- \_\_\_\_\_, 1950, Salinas Valley investigation basic data: California Department of Public Works Supplement to Bulletin 52-A, 20 p.
- California Department of Water Resources, 1957, Salinas Valley investigation basic data: California Department of Water Resources Supplement to Bulletin 52-A, 89 p.
- \_\_\_\_\_, 1958, Salinas Valley investigation basic data: California Department of Water Resources Supplement to Bulletin 52-A, 68 p.
- \_\_\_\_\_, 1959, Salinas Valley investigation basic data: California Department of Water Resources Supplement to Bulletin 52-A, 75 p.
- \_\_\_\_\_, 1969, Special investigations, Salinas River Basin: California Department of Water Resources memorandum report, 67 p.
- \_\_\_\_\_, 1970, Sea-water intrusion, lower Salinas Valley: Progress report 1968-69: California Department of Water Resources, 28 p.
- \_\_\_\_\_, 1973, Sea-water intrusion, lower Salinas Valley, Monterey County: California Department of Water Resources, 91 p.
- \_\_\_\_\_, 1975, Sea-water intrusion in California, Inventory of coastal ground water basins: California Department of Water Resources Bulletin 63-5, 394 p.
- California Water Resources Board, 1955, Water utilization and requirements of California: California Water Resources Board Bulletin 2, v. 1 (text), 227 p., v. 2 (appendix and plates), p. 229-358.
- Compton, R. R., 1966, Granitic and metamorphic rocks of the Salinian block, California Coast Ranges: California Division of Mines and Geology Bulletin 190, p. 277-287.
- Dibblee, T. W., 1971a, Geologic map of the San Ardo quadrangle, California: U.S. Geological Survey open-file map, scale 1:62,500.
- \_\_\_\_\_, 1971b, Geologic map of the King City quadrangle, California: U.S. Geological Survey open-file map, scale 1:62,500.
- \_\_\_\_\_, 1972a, Geologic map of the Jamesburg quadrangle, California: U.S. Geological Survey open-file map, scale 1:62,500.
- \_\_\_\_\_, 1972b, Geologic map of the Greenfield quadrangle, California: U.S. Geological Survey open-file map, scale 1:62,500.
- \_\_\_\_\_, 1972c, Geologic map of the Soledad quadrangle, California: U.S. Geological Survey open-file map, scale 1:62,500.
- \_\_\_\_\_, 1973a, Geologic map of the Gonzales quadrangle, California: U.S. Geological Survey open-file map, scale 1:62,500.
- \_\_\_\_\_, 1973b, Geologic map of the Salinas quadrangle, California: U.S. Geological Survey open-file map, scale 1:62,500.
- Dibblee, T. W., and Clark, J. C., 1973, Geologic map of the Monterey quadrangle, California: U.S. Geological Survey open-file map, scale 1:62,500.
- Durham, D. L., 1974, Geology of the southern Salinas Valley area, California: U.S. Geological Survey Professional Paper 819, 111 p., map, scale 1:125,000.
- Durham, D. L., and Addicott, W. O., 1964, Upper Miocene and Pliocene marine stratigraphy in southern Salinas Valley, California: U.S. Geological Survey Bulletin 1194-E, 7 p.
- Environmental Data Service, 1966-75, Climatological data annual summary, Nevada: Environmental Data Service, annual issue.
- Fairbanks, H. W., 1898, Geology of a portion of the southern Coast Ranges [California]: Journal of Geology, v. 6, no. 6, p. 551-576.
- Fairborn, J. W., 1963, Gravity survey and interpretation of the northern portion of the Salinas Valley: Stanford, Calif., Stanford University, M.S. thesis, 33 p.
- Gatewood, J. S., Robinson, T. W., Colby, B. R., Hem, J. D., and Halpenny, L. C., 1950, Use of water by bottom-land vegetation in lower Safford Valley, Arizona: U.S. Geological Survey Water-Supply Paper 1103, 210 p.
- Greene, H. G., 1970, Geology of southern Monterey Bay and its relationship to the ground-water basin and seawater intrusion: U.S. Geological Survey open-file report, 50 p.
- Greene, H. G., Lee, W. H. K., McCulloch, D. S., and Brabb, E. E., 1973, Faults and earthquakes in the Monterey Bay region, California: U.S. Geological Survey Mineral Investigation Field Studies Map MF-518.
- Hamlin, Homer, 1904, Water resources of Salinas Valley, California: U.S. Geological Survey Water-Supply Paper 89, 91 p.
- Hickey, J. J., 1968, Hydrogeologic study of the Soquel-Aptos area, Santa Cruz County, California: U.S. Geological Survey open-file report, 48 p.



- Hutton, S. G., and Anderson, D. L., 1971, Finite element method: A Galerkin approach: American Society of Civil Engineers, Journal of the Engineering Mechanics Division, v. 7, no. 5, p. 1503-1520.
- Jenkins, O. P., 1943, Geomorphologic provinces of California: California Division of Mines Bulletin 118, p. 83-88.
- Johnson, A. I., 1966, Specific yield--Compilation of specific yields for various materials (rev. ed.): U.S. Geological Survey open-file report, 119 p.
- Johnson, A. I., Moston, R. P., and Morris, D. A., 1968, Physical and hydrologic properties of water-bearing deposits in subsiding areas in central California: U.S. Geological Survey Professional Paper 497-A, 71 p.
- Jorgensen, L. N., Rose, M. A., Busch, R. D., and Bader, J. S., 1971, California streamflow characteristics--Volume 1: Colorado River Basin, southern Great Basin, and Pacific Slope Basins excluding Central Valley: U.S. Geological Survey open-file report, 657 p.
- Leopold, L. B., and Maddock, Thomas, Jr., 1953, The hydraulic geometry of stream channels and some physiographic implications: U.S. Geological Survey Professional Paper 252, 57 p.
- Leopold, L. B., and Miller, J. P., 1956, Ephemeral streams--Hydraulic factors and their relation to the drainage net: U.S. Geological Survey Professional Paper 282-A, 37 p.
- Leopold, L. B., Wolman, M. G., and Miller, J. P., 1964, Fluvial processes in geomorphology: San Francisco, W. H. Freeman and Co., 522 p.
- Lohman, S. W., 1972, Ground-water hydraulics: U.S. Geological Survey Professional Paper 708, 70 p.
- Lohman, S. W., and others, 1972, Definitions of selected ground-water terms--Revisions and conceptual refinements: U.S. Geological Survey Water-Supply Paper 1988, 21 p.
- Martin, B. D., 1964, Monterey submarine canyon, California: Genesis and relationships to continental geology: Los Angeles, University of Southern California, Ph. D. thesis, 249 p.
- McClelland, E. J., 1963, Aquifer-test compilation for the Central Coastal region, California: U.S. Geological Survey open-file report, 53 p.
- Meinzer, O. E., 1927, Plants as indicators of ground water: U.S. Geological Survey Water-Supply Paper 577, 95 p.
- Metcalf and Eddy, Engineers, 1976, Land application of wastewater in the Salinas-Monterey Peninsula area: Metcalf and Eddy, Engineers (San Francisco), report to U.S. Army Corps of Engineers, 140 p.
- Monterey County Flood Control and Water Conservation District, 1959-67, Basic data and operation report: Monterey County Flood Control and Water Conservation District, annual issue.
- \_\_\_\_\_, 1967, A study of underground hydraulic properties in selected areas of Salinas Valley: Monterey County Flood Control and Water Conservation District, 30 p.
- \_\_\_\_\_, 1968-75, Ground water and climatology: Monterey County Flood Control and Water Conservation District, annual issue.
- \_\_\_\_\_, 1968a, Arroyo Seco River Project--Conservation, flood control, and recreational potential of water storage reservoirs: Monterey County Flood Control and Water Conservation District, 61 p.
- \_\_\_\_\_, 1968b, Investigation of an East Side canal project, Salinas Valley [California]: Monterey County Flood Control and Water Conservation District, 41 p.

- Muir, K. S., 1973, Ground-water pumpage in part of Monterey County, California, 1968-71, U.S. Geological Survey open-file report, 3 p.
- Muskat, Morris, 1937, The flow of homogeneous fluids through porous media: Ann Arbor [Mich.], J. W. Edwards, Inc., 763 p.
- Pinder, G. F., and Frind, E. O., 1972, Application of Galerkin's procedure to aquifer analyses: Water Resources Research, v. 8, no. 1, p. 108-120.
- Piper, A. M., 1933, Notes on the relation between moisture equivalent and specific retention of water-bearing materials: Transactions of the American Geophysical Union, v. 14, p. 481-487.
- Piper, A. M., Gale, H. S., Thomas, H. E., and Robinson, T. W., 1939, Geology and ground-water hydrology of the Mokelumne area, California: U.S. Geological Survey Water-Supply Paper 780, 229 p.
- Rantz, S. E., 1968, A suggested method for estimating evapotranspiration by native phreatophytes: U.S. Geological Survey Professional Paper 600-D, p. 10-12.
- \_\_\_\_\_, 1969, Mean annual precipitation in the California region: U.S. Geological Survey basic-data compilation, map.
- \_\_\_\_\_, 1974, Mean annual runoff in the San Francisco Bay region, California, 1931-70: U.S. Geological Survey Miscellaneous Field Studies Map MF-613, 2 sheets, scale 1:500,000.
- Robinson, T. W., 1958, Phreatophytes: U.S. Geological Survey Water-Supply Paper 1423, 84 p.
- Segol, Genevieve, 1976, A three-dimensional Galerkin finite element method for the analysis of contaminant transport in variably saturated porous media: Department of Earth Sciences, University of Waterloo, Waterloo, Ontario, 243 p.
- Sieck, H. C., 1964, A gravity investigation of the Monterey-Salinas area, California: Stanford, Calif., Stanford University, M.S. thesis, 40 p.
- Smith, R. E., 1972, The infiltration envelope: Results from a theoretical infiltrometer: Journal of Hydrology, v. 17, p. 1-21.
- Starke, C. W., and Howard, A. D., 1968, Polygenetic origin of Monterey submarine canyon: Geological Society of America, v. 79, no. 7, p. 813-826.
- Thorup, R. R., 1976, Report on Castroville irrigation project, deep test hole and freshwater bearing strata below the 400-foot aquifer, Salinas Valley, California: Richard R. Thorup, Monterey, Calif., Report to Monterey County Flood Control and Water Conservation District, 59 p.
- Tinsley, J. C., III, 1975, Quaternary geology of northern Salinas Valley, Monterey County, California: Stanford, Calif., Stanford University, Ph.D. thesis, 194 p., map, scale 1:62,500.
- U.S. Army Corps of Engineers, 1975, Plan of study for the Salinas-Monterey Bay area [California], urban water resources and wastewater management study: U.S. Army Corps of Engineers, San Francisco District, 94 p.
- U.S. Bureau of the Census, 1971, 1970 census of population, number of inhabitants, California: U.S. Bureau of the Census report PC(1)-A6, 71 p.
- U.S. Soil Conservation Service, 1975, Soil survey of Monterey County, California: U.S. Soil Conservation Service interim report, 305 p.

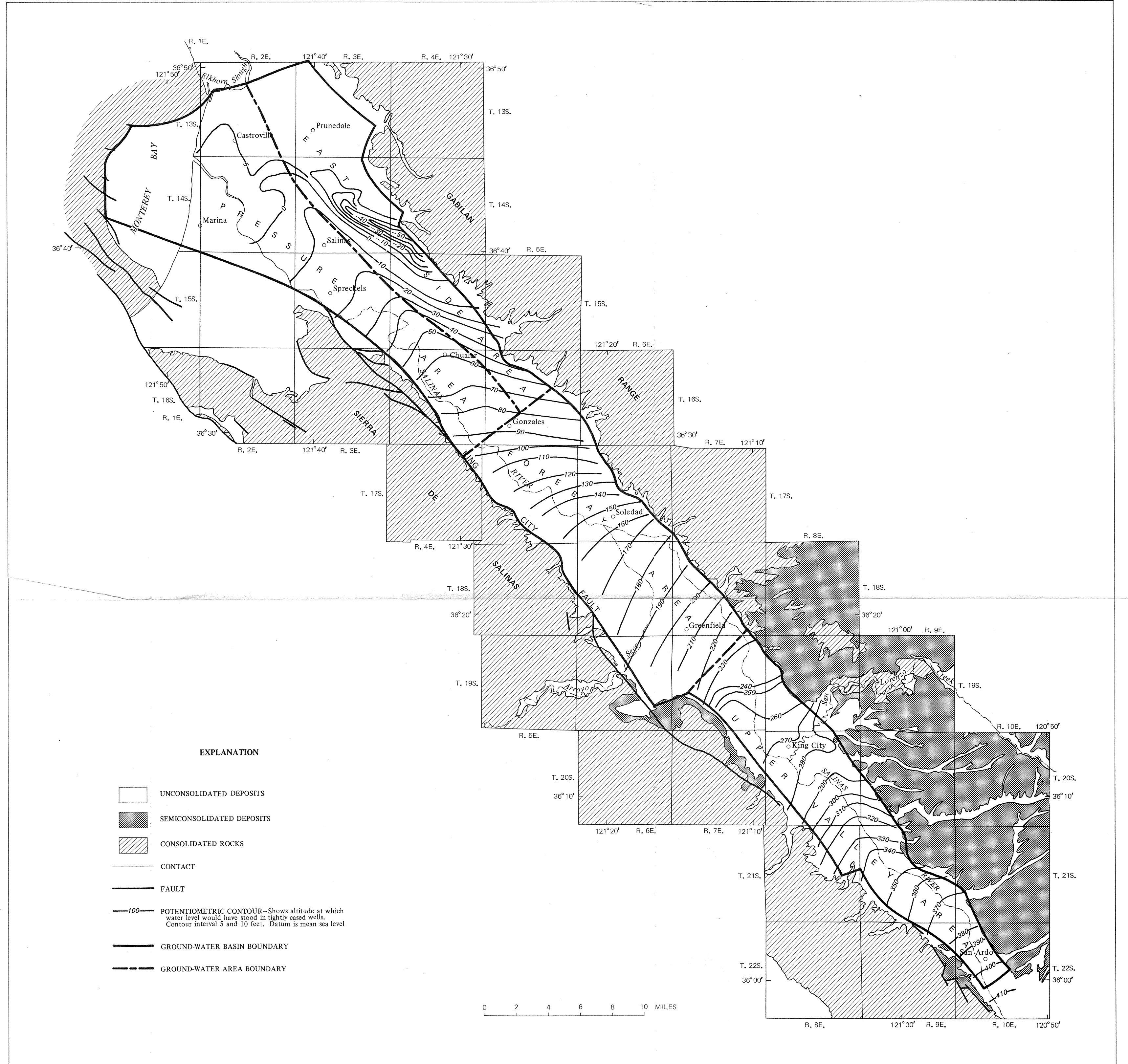
U.S. Weather Bureau, 1955, Climatic summary of the United States--  
Supplement for 1931 through 1952, California: U.S. Weather Bureau  
Climatography 11-22.

\_\_\_\_ 1961-65, Climatological data, annual summary, California: U.S. Weather  
Bureau, annual issue.

\_\_\_\_ 1965, Climatic summary of the United States--Supplement for 1951 through  
1960, California: U.S. Weather Bureau Climatography 86-22, 42 p.

Wolman, M. G., 1955, The natural channel of Brandywine Creek,  
Pennsylvania: U.S. Geological Survey Professional Paper 271, 56 p.

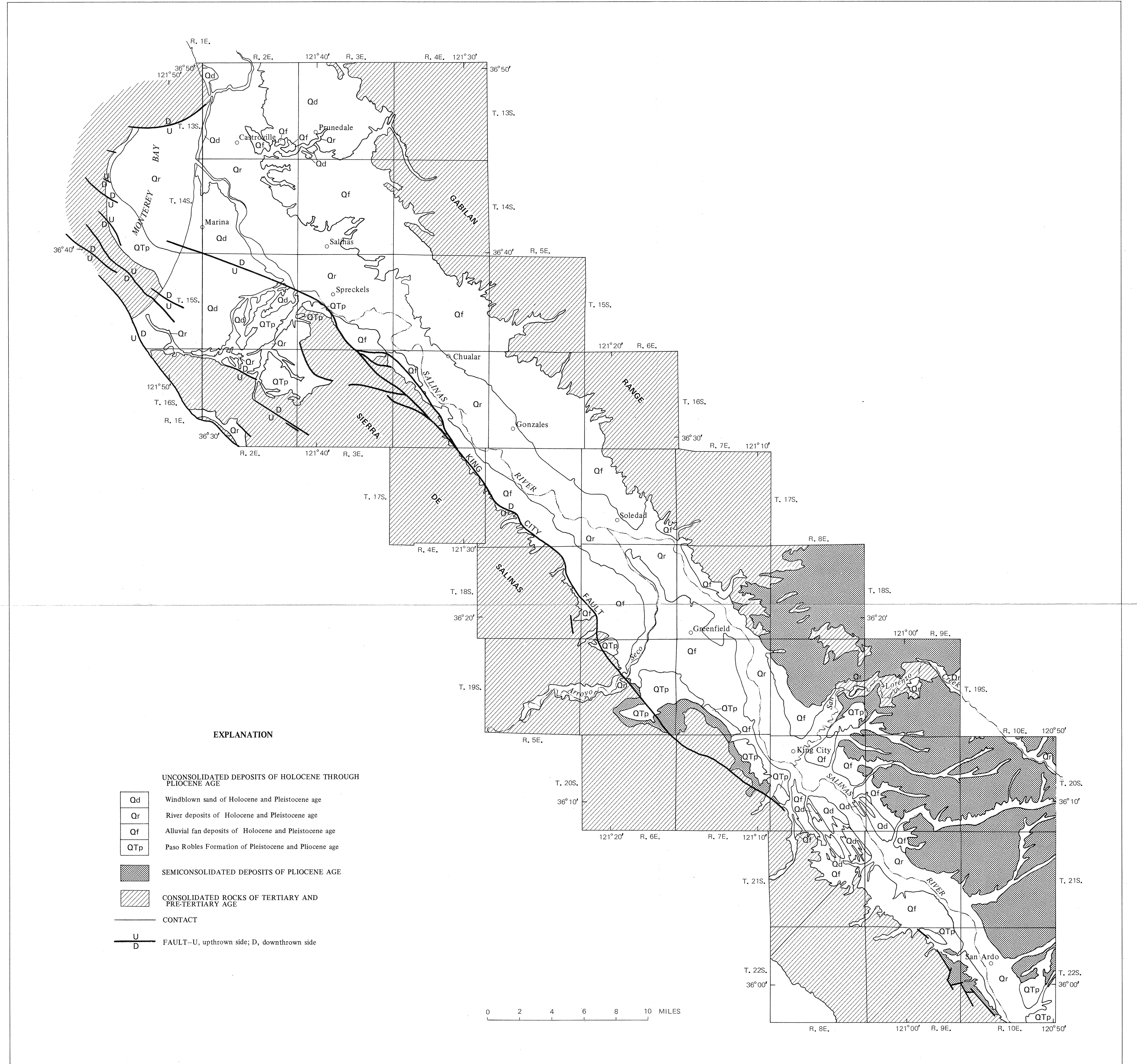
Wolman, M. G., and Brush, L. M., Jr., 1961, Factors controlling the size  
and shape of stream channels in coarse noncohesive sands: U.S.  
Geological Survey Professional Paper 282-G, p. 183-210.



Base from U. S. Geological Survey 1:62,500 quadrangles

Geology modified from D. I. Durham (1974), H. G. Greene (1970), J. C. Tinsley (1975), T. W. Dibblee (1971a, 1971b, 1972a, 1972b, 1972c, 1973a, and 1973b), and T. W. Dibblee and J. C. Clark (1973)

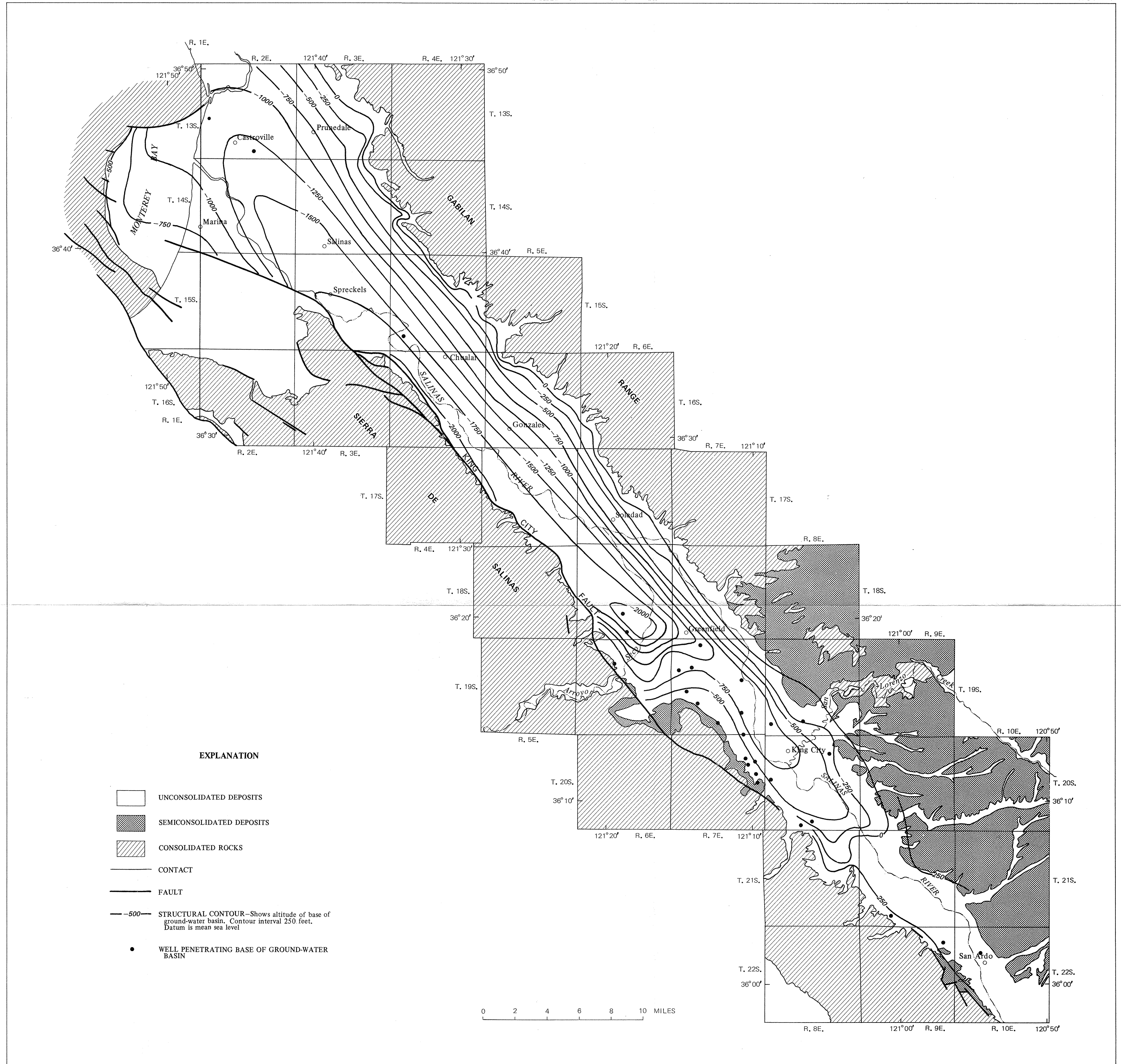
MAP OF SALINAS VALLEY, CALIFORNIA, SHOWING GROUND-WATER AREAS, GROUND-WATER BASIN, AND POTENTIOMETRIC CONTOURS FOR AUTUMN 1970



Base from U. S. Geological Survey 1:62,500 quadrangles

Geology modified from D. L. Durham (1974), H. G. Greene (1970), J. C. Tinsley (1975), T. W. Dibblee (1971a, 1971b, 1972a, 1972b, 1972c, 1973a, and 1973b), and T. W. Dibblee and J. C. Clark (1973)

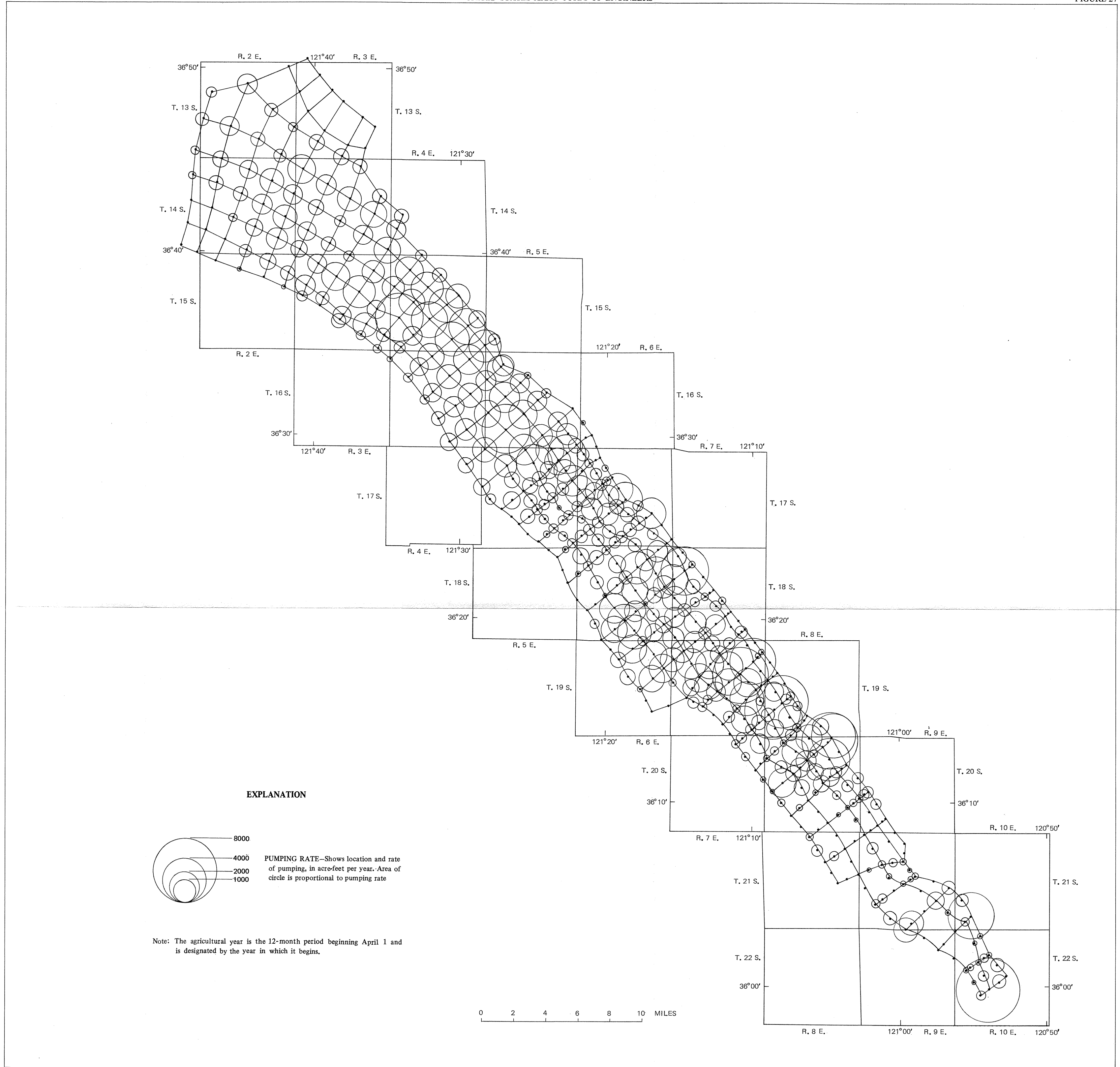
MAP SHOWING GENERALIZED GEOLOGY OF THE SALINAS VALLEY, CALIFORNIA



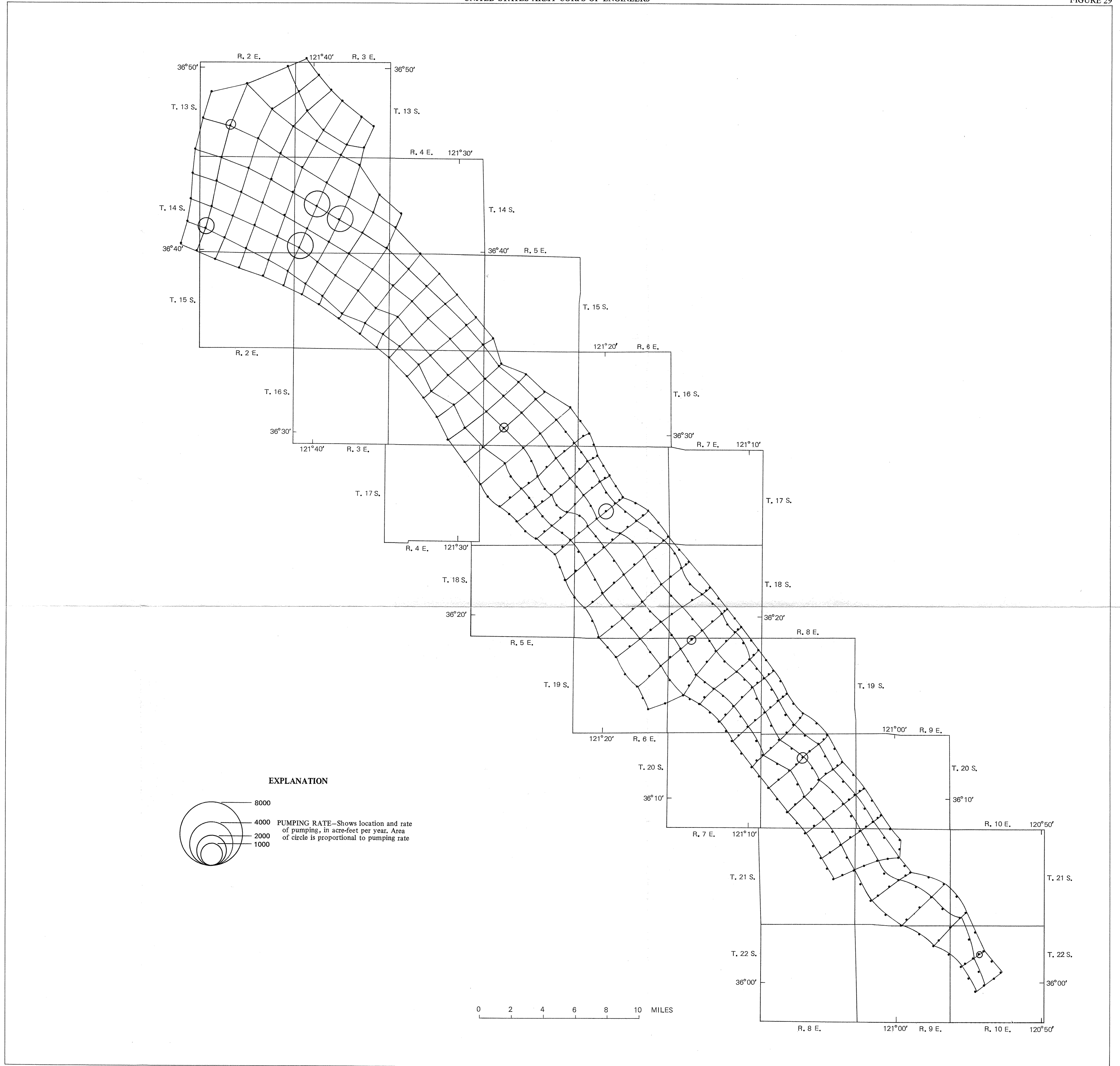
Base from U. S. Geological Survey 1:62,500 quadrangles

Geology modified from D. L. Durham (1974), H. G. Greene (1970), J. C. Tinsley (1975), T. W. Dibblee (1971a, 1971b, 1972a, 1972b, 1972c, 1973a, and 1973b), and T. W. Dibblee and J. C. Clark (1973)

MAP OF SALINAS VALLEY, CALIFORNIA, SHOWING ALTITUDE OF THE BASE OF THE GROUND-WATER BASIN

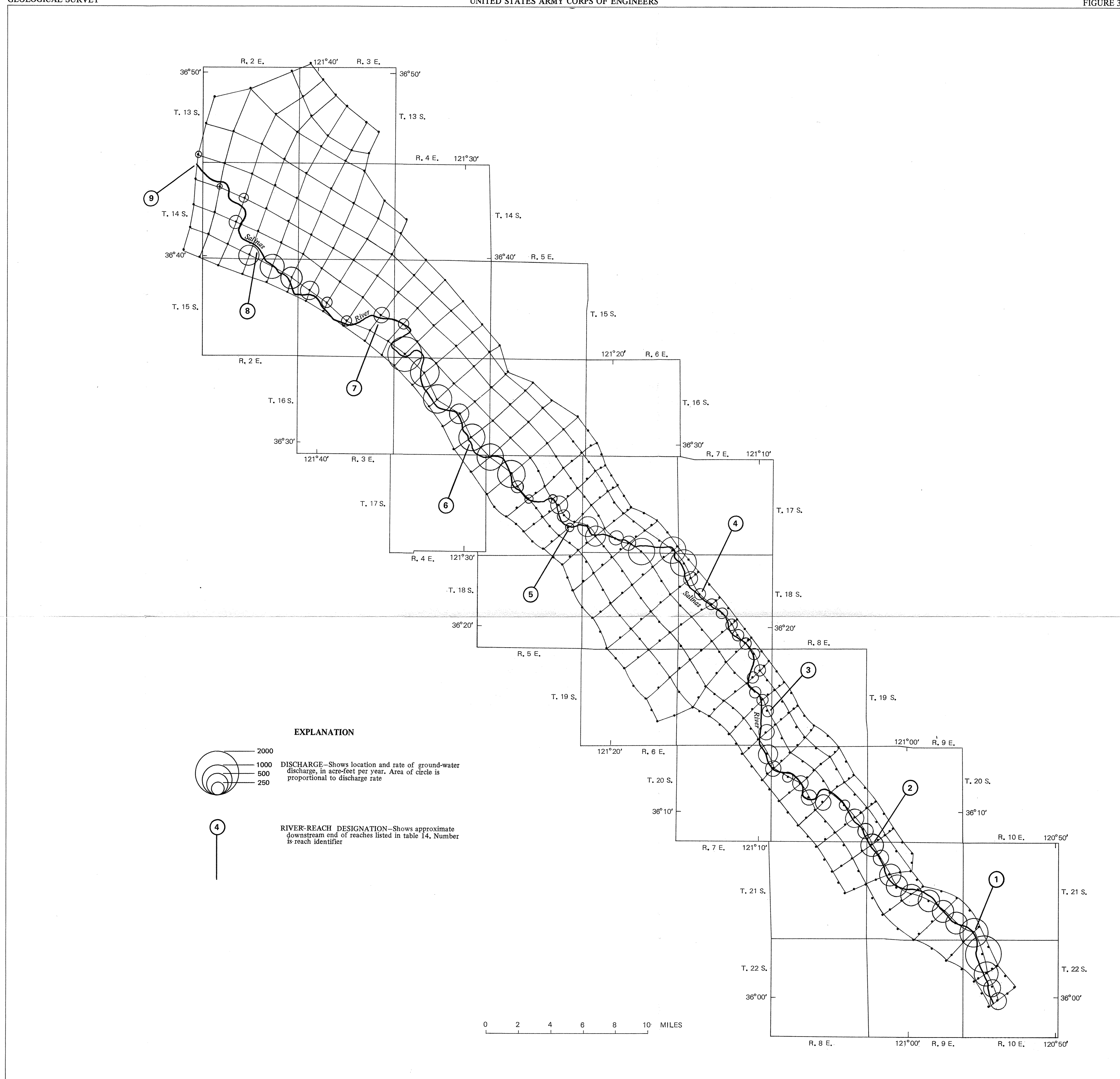


Base from U.S. Geological Survey 1:62,500 quadrangles  
MAP OF THE SALINAS VALLEY GROUND-WATER BASIN, CALIFORNIA, SHOWING FINITE-ELEMENT GRID FOR THE TWO-DIMENSIONAL GROUND-WATER MODEL AND GEOGRAPHIC DISTRIBUTION OF AGRICULTURAL PUMPAGE FOR AGRICULTURAL YEAR 1970



Base from U.S. Geological Survey 1:62,500 quadrangles

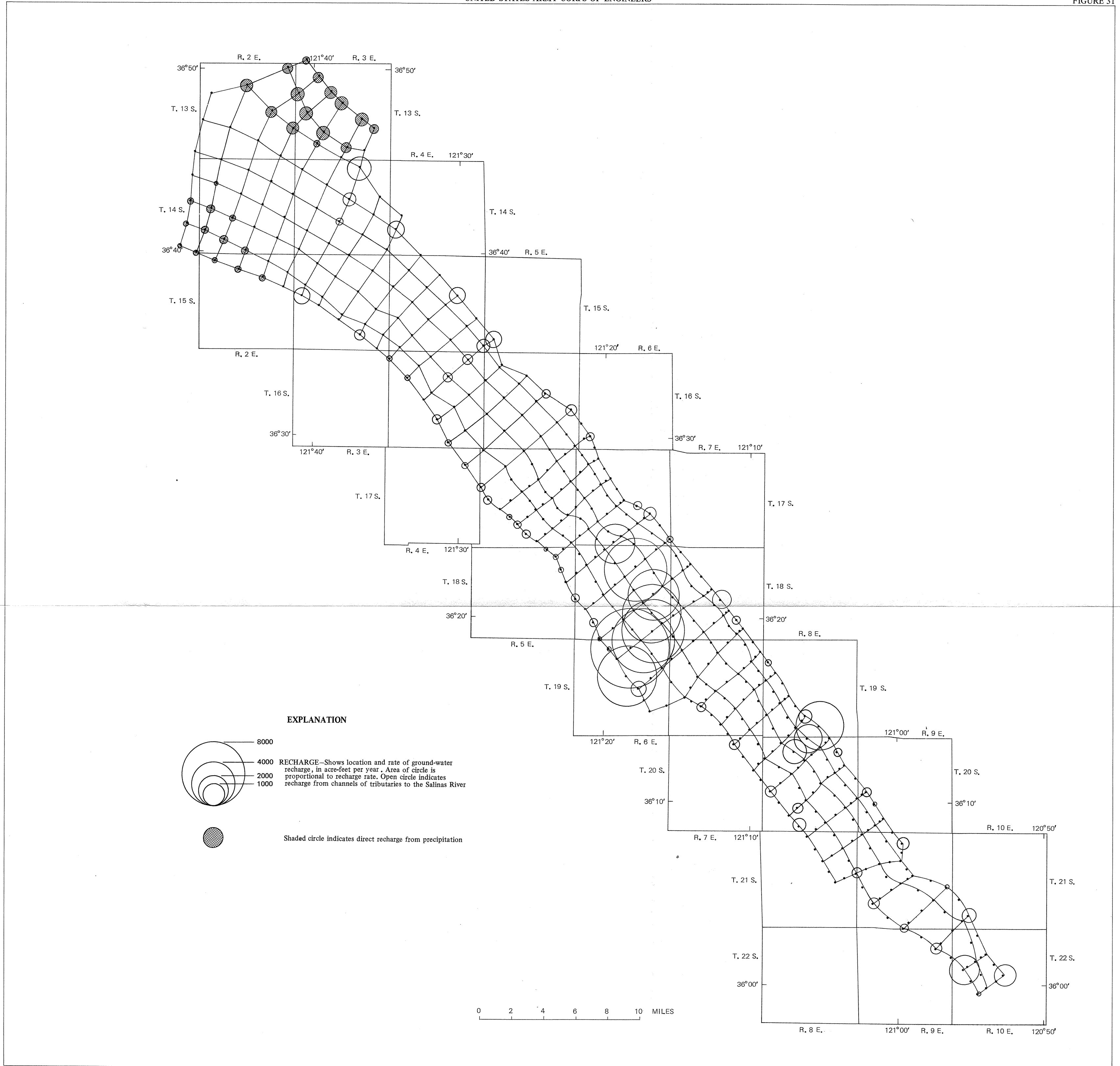
MAP OF THE SALINAS VALLEY GROUND-WATER BASIN, CALIFORNIA, SHOWING FINITE-ELEMENT GRID FOR THE TWO-DIMENSIONAL GROUND-WATER MODEL AND GEOGRAPHIC DISTRIBUTION OF MUNICIPAL PUMPAGE FOR 1970



Base from U.S. Geological Survey 1:62,500 quadrangles

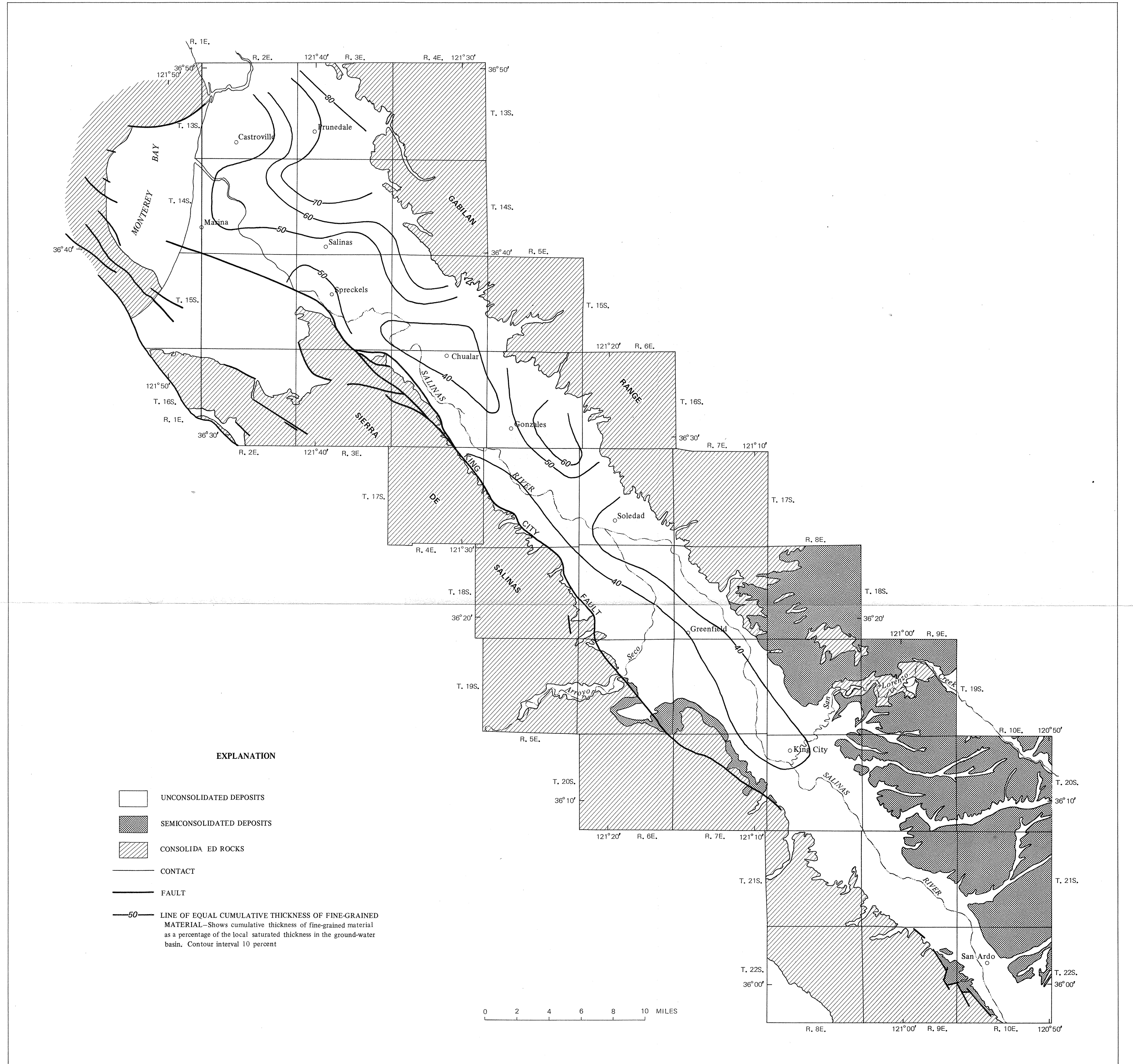
MAP OF THE SALINAS VALLEY GROUND-WATER BASIN, CALIFORNIA, SHOWING FINITE-ELEMENT GRID FOR THE TWO-DIMENSIONAL GROUND-WATER MODEL AND GEOGRAPHIC DISTRIBUTION OF PHREATOPHYTE DISCHARGE





Base from U.S. Geological Survey 1:62,500 quadrangles

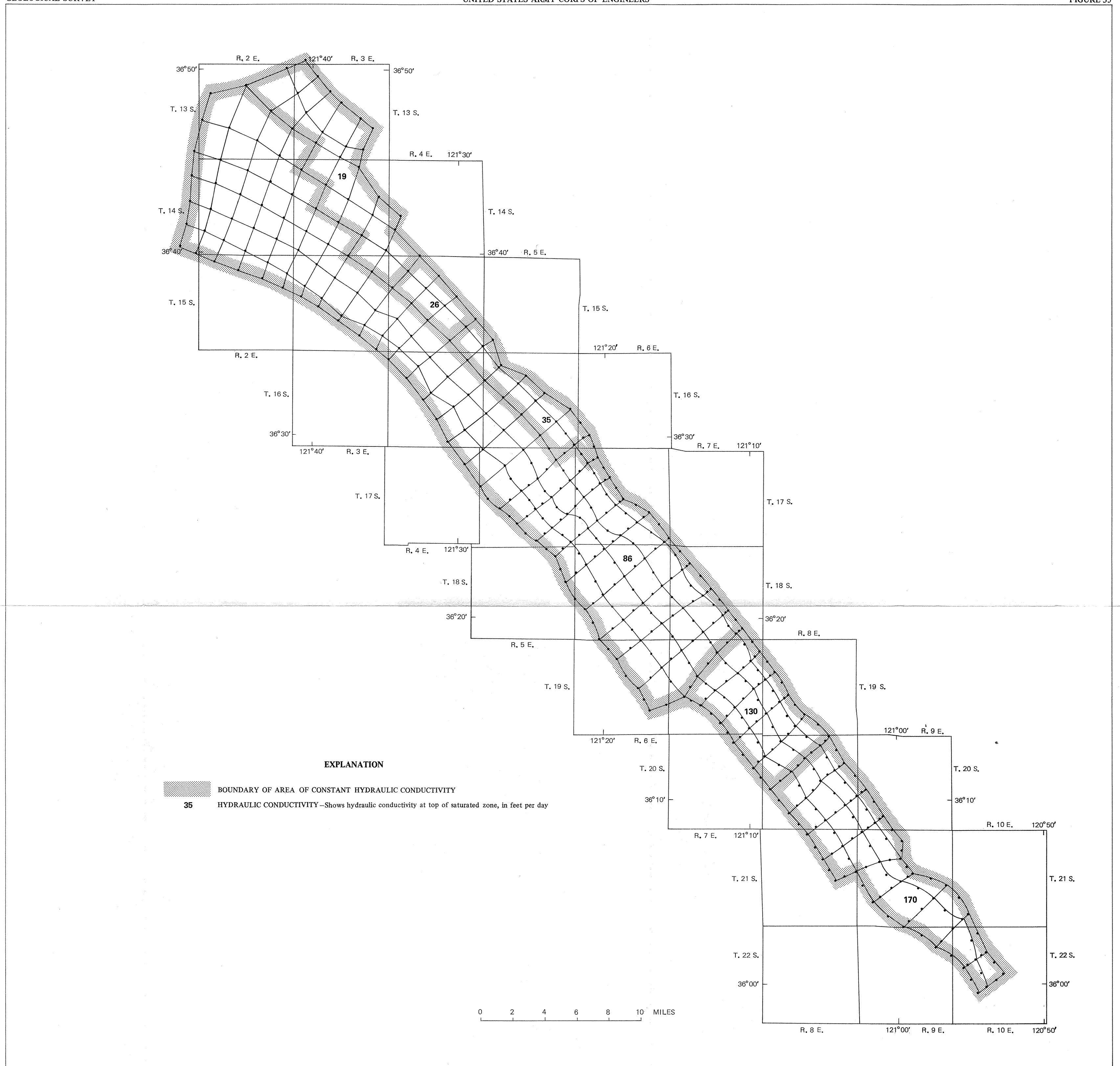
MAP OF THE SALINAS VALLEY GROUND-WATER BASIN, CALIFORNIA, SHOWING FINITE-ELEMENT GRID FOR THE TWO-DIMENSIONAL GROUND-WATER MODEL AND GEOGRAPHIC DISTRIBUTION OF GROUND-WATER RECHARGE FROM SMALL STREAMS AND DIRECT PRECIPITATION



Base from U. S. Geological Survey 1:62,500 quadrangles

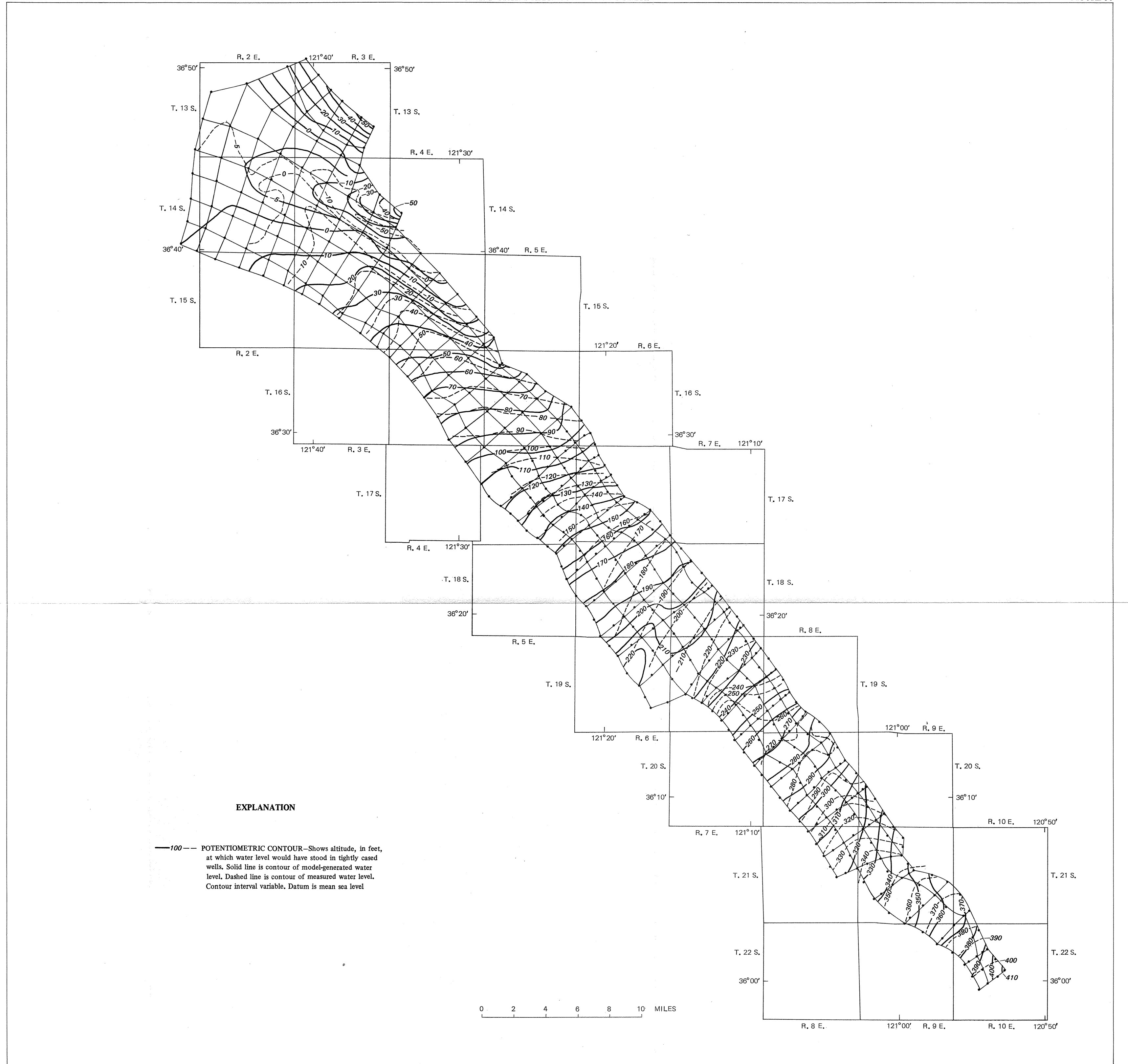
Geology modified from D. L. Durham (1974), H. G. Greene (1970), J. C. Tinsley (1975), T. W. Dibblee (1971a, 1971b, 1972a, 1972b, 1972c, 1973a, and 1973b), and T. W. Dibblee and J. C. Clark (1973)

MAP OF SALINAS VALLEY, CALIFORNIA, SHOWING CUMULATIVE THICKNESS OF FINE-GRAINED LITHOLOGIES



Base from U.S. Geological Survey 1:62,500 quadrangles

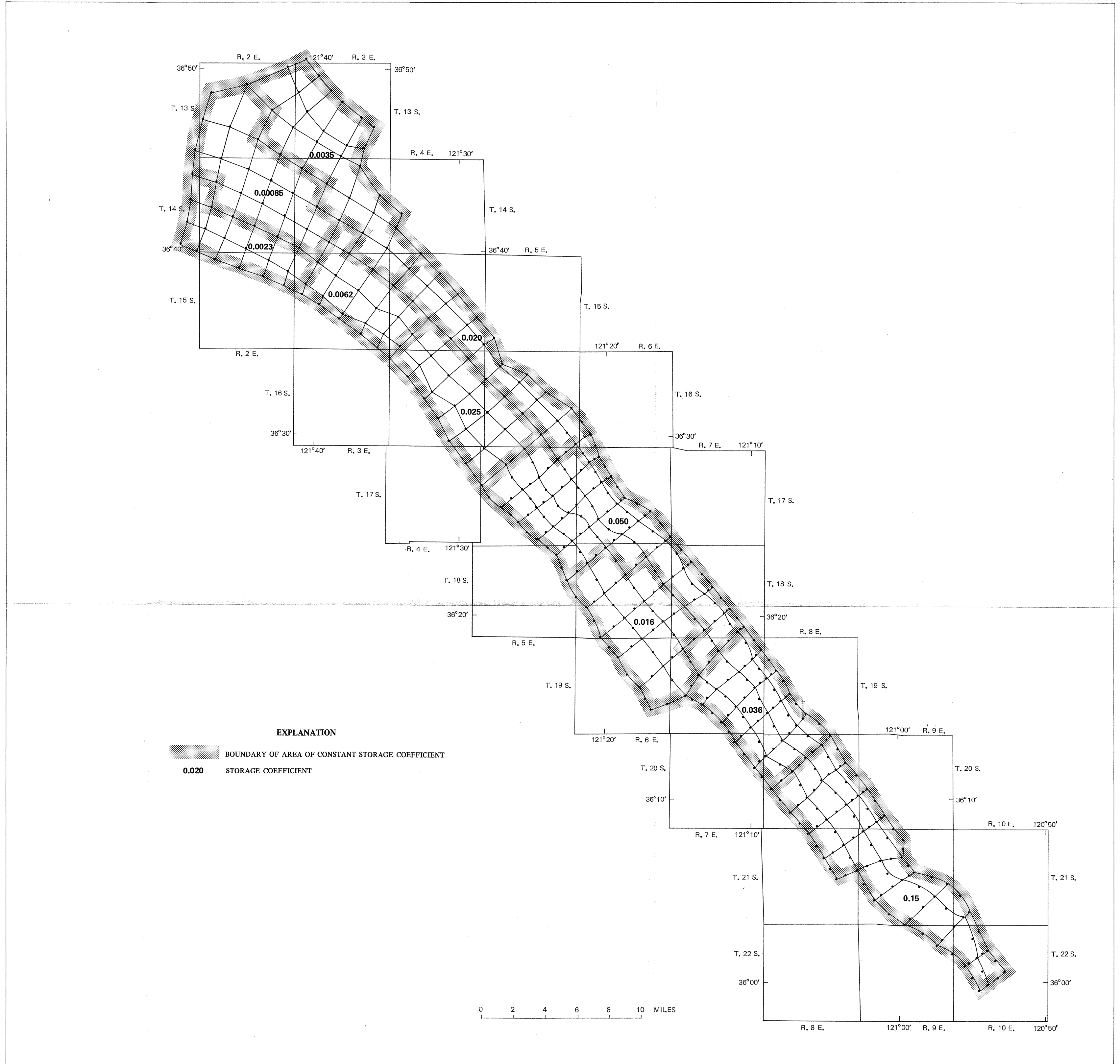
MAP OF THE SALINAS VALLEY GROUND-WATER BASIN, CALIFORNIA, SHOWING FINITE-ELEMENT GRID FOR THE TWO-DIMENSIONAL GROUND-WATER MODEL AND GEOGRAPHIC DISTRIBUTION OF HYDRAULIC CONDUCTIVITY



Base from U.S. Geological Survey 1:62,500 quadrangles

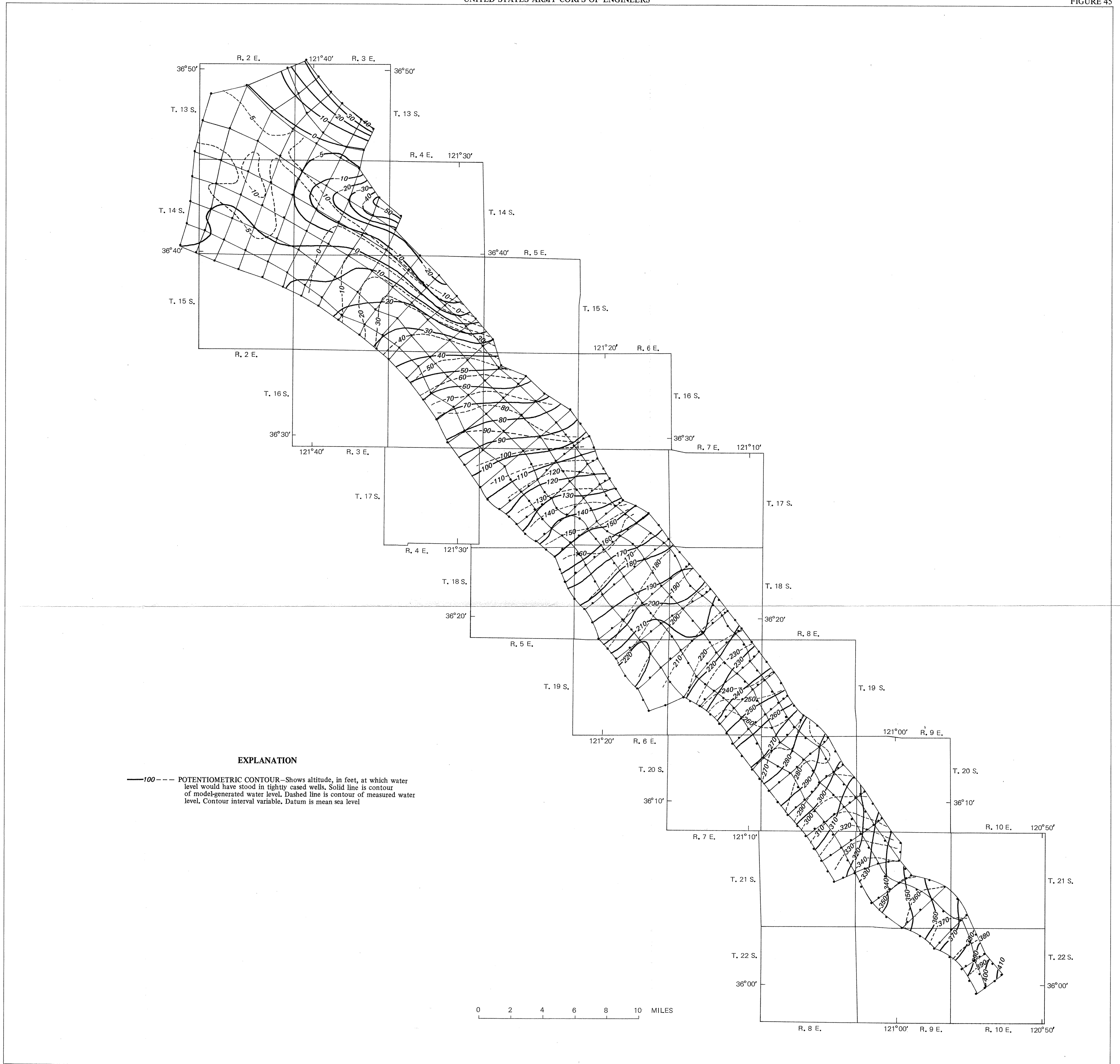
Measured water-level contours from Monterey County Flood Control and Water Conservation District (1970)

MAP OF THE SALINAS VALLEY GROUND-WATER BASIN, CALIFORNIA, SHOWING FINITE-ELEMENT GRID FOR THE TWO-DIMENSIONAL GROUND-WATER MODEL, STEADY-STATE WATER-LEVEL CONTOURS GENERATED BY THE MODEL, AND MEASURED WATER-LEVEL CONTOURS FOR AUTUMN 1971



Base from U.S. Geological Survey 1:62,500 quadrangles

MAP OF THE SALINAS VALLEY GROUND-WATER BASIN, CALIFORNIA, SHOWING FINITE-ELEMENT GRID FOR THE TWO-DIMENSIONAL GROUND-WATER MODEL AND GEOGRAPHIC DISTRIBUTION OF STORAGE COEFFICIENT



Base from U.S. Geological Survey 1:62,500 quadrangles

Measured water level contoured from data from Monterey County Flood Control and Water Conservation District (1971)

MAP OF THE SALINAS VALLEY GROUND-WATER BASIN, CALIFORNIA, SHOWING FINITE-ELEMENT GRID FOR THE TWO-DIMENSIONAL GROUND-WATER MODEL, TRANSIENT-STATE WATER-LEVEL CONTOURS GENERATED BY THE MODEL, AND MEASURED WATER-LEVEL CONTOURS FOR AUTUMN 1971

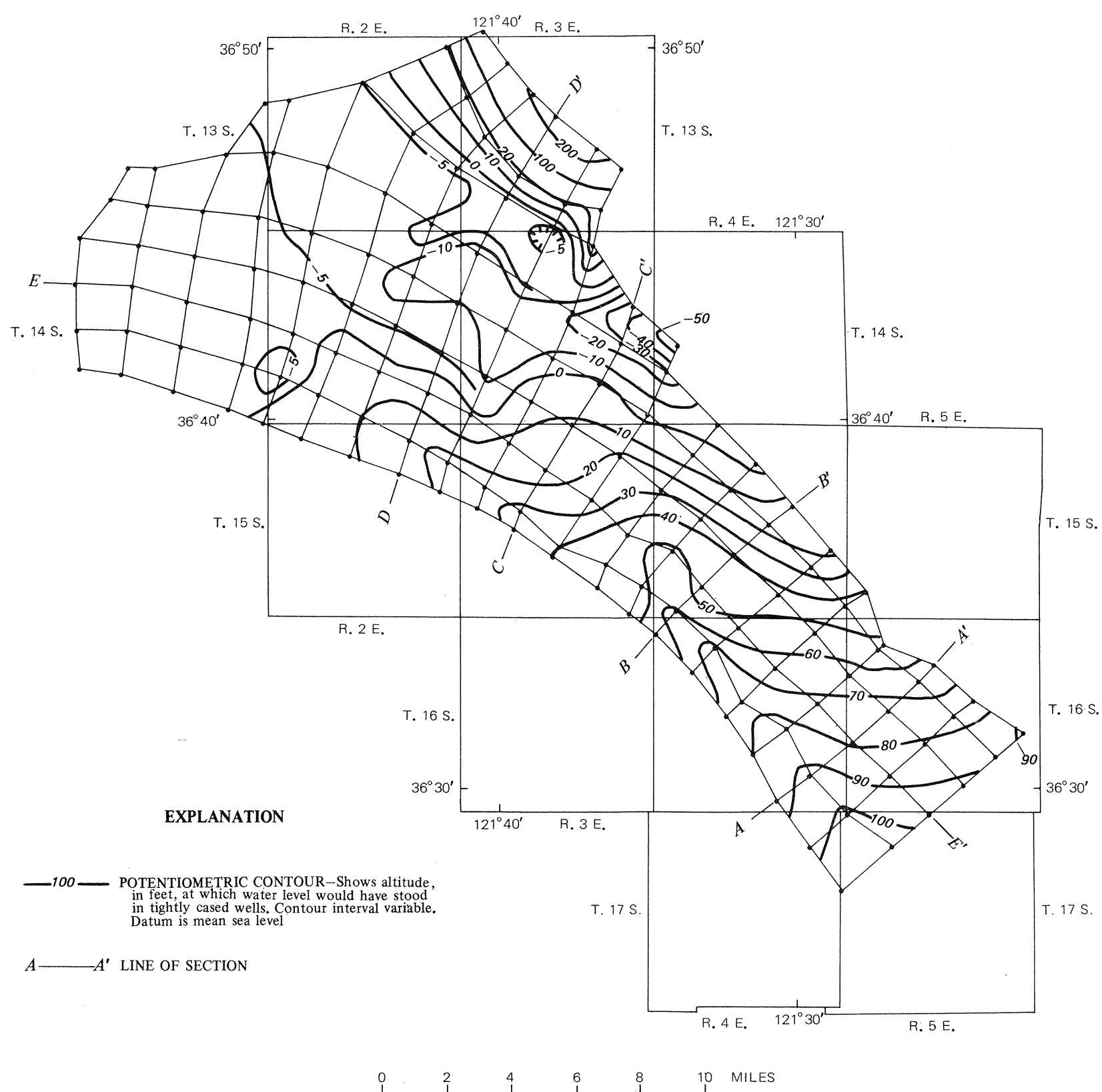


FIGURE 56.—FINITE-ELEMENT GRID FOR THE THREE-DIMENSIONAL GROUND-WATER MODEL AND STEADY-STATE WATER-LEVEL CONTOURS GENERATED BY THE MODEL FOR THE TOP LAYER OF ELEMENTS IN THE GRID. IN THE PRESSURE AREA, THE WATER LEVEL CORRESPONDS TO THAT IN THE 180-FOOT AQUIFER

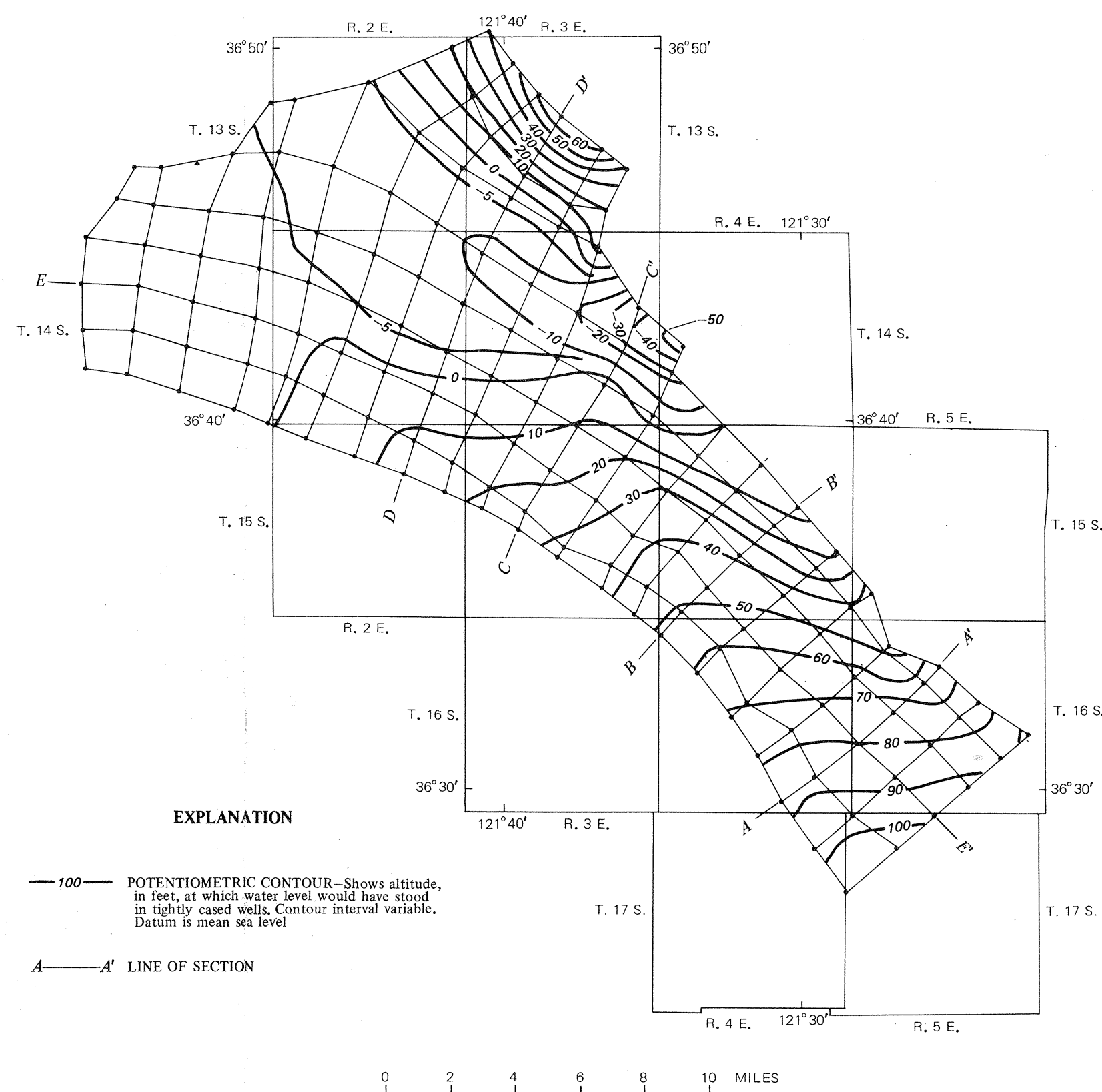


FIGURE 57.—FINITE-ELEMENT GRID FOR THE THREE-DIMENSIONAL GROUND-WATER MODEL AND STEADY-STATE WATER-LEVEL CONTOURS GENERATED BY THE MODEL FOR THE THIRD LAYER OF ELEMENTS IN THE GRID. IN THE PRESSURE AREA, THE WATER LEVEL CORRESPONDS TO THAT IN THE 400-FOOT AQUIFER

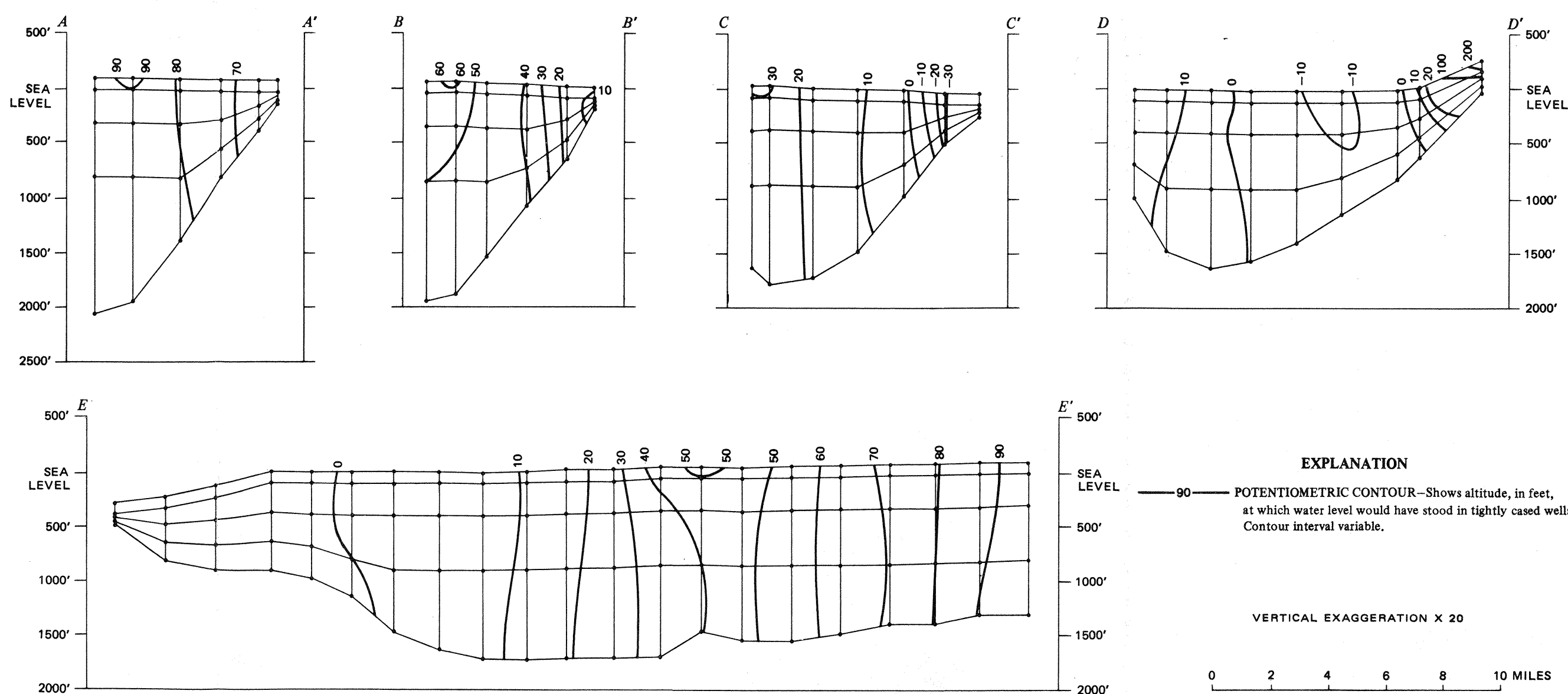


FIGURE 58.—SECTIONS SHOWING FINITE-ELEMENT GRID FOR THE THREE-DIMENSIONAL GROUND-WATER MODEL AND STEADY-STATE WATER-LEVEL CONTOURS GENERATED BY THE MODEL

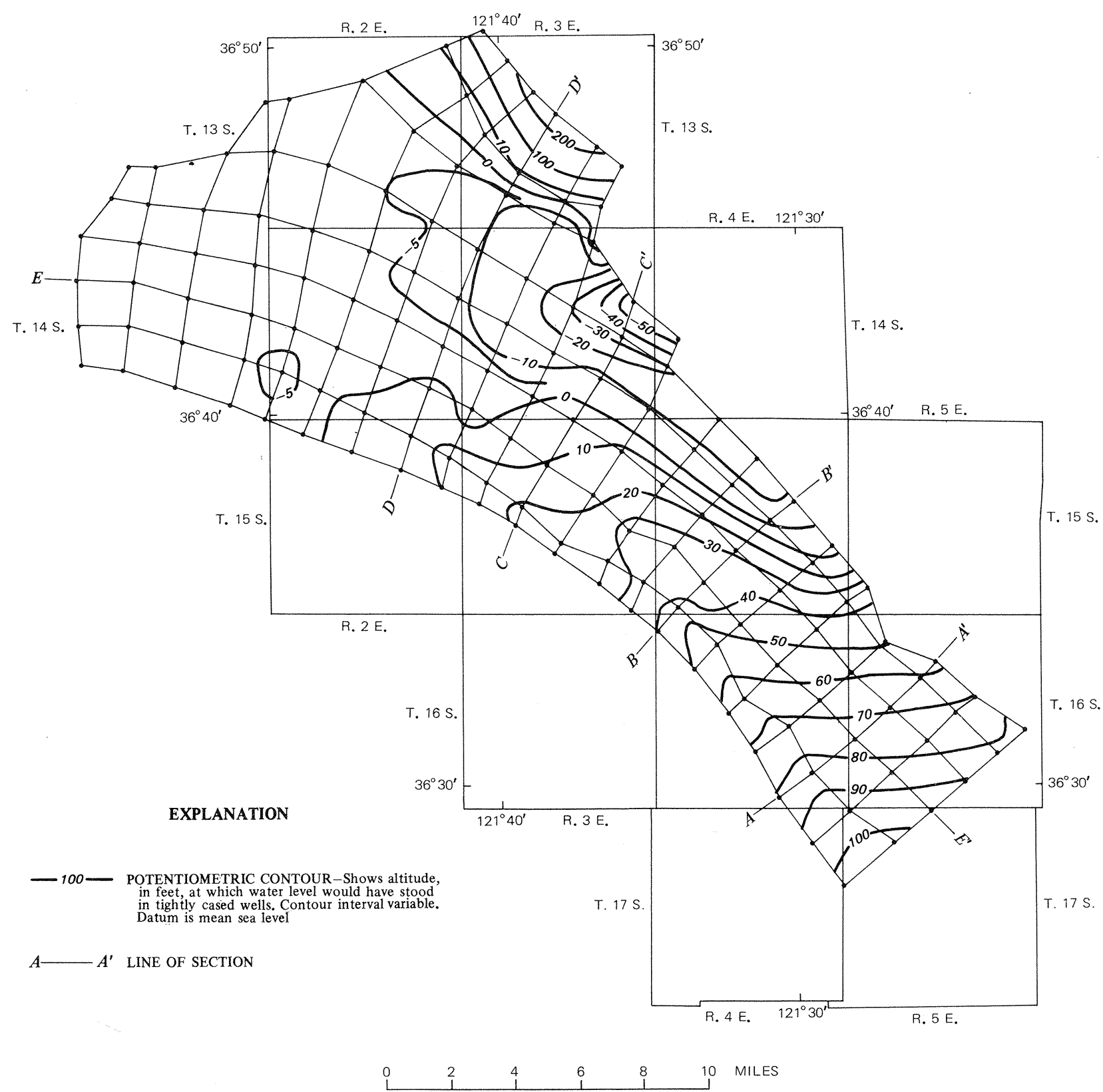


FIGURE 65.-- FINITE-ELEMENT GRID FOR THE THREE-DIMENSIONAL GROUND-WATER MODEL AND TRANSIENT-STATE WATER-LEVEL CONTOURS GENERATED BY THE MODEL FOR THE TOP LAYER OF ELEMENTS IN THE GRID. IN THE PRESSURE AREA, THE WATER LEVEL CORRESPONDS TO THAT IN THE 180-FOOT AQUIFER

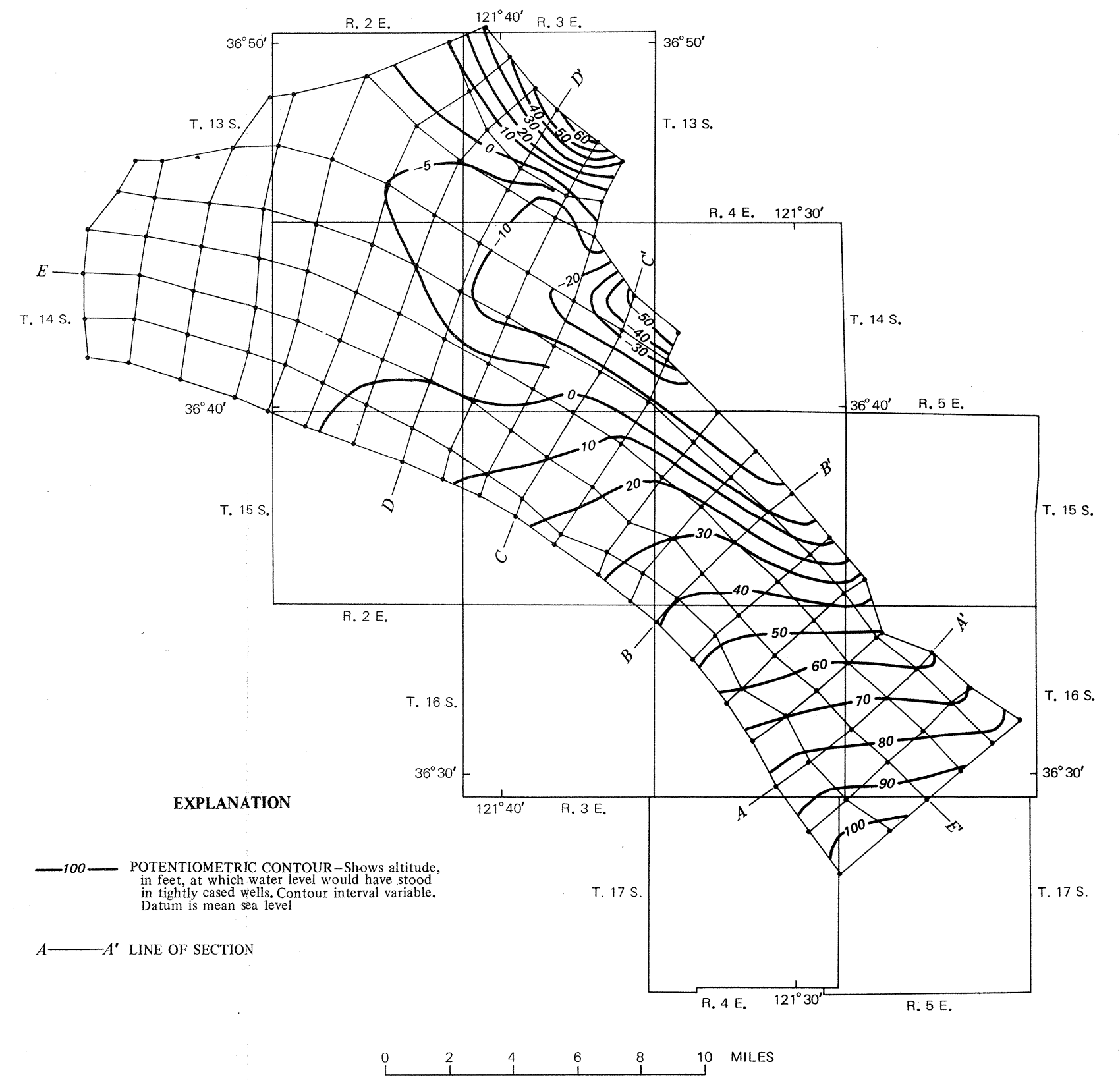


FIGURE 66.-- FINITE-ELEMENT GRID FOR THE THREE-DIMENSIONAL GROUND-WATER MODEL AND TRANSIENT-STATE WATER-LEVEL CONTOURS GENERATED BY THE MODEL FOR THE THIRD LAYER OF ELEMENTS IN THE GRID. IN THE PRESSURE AREA, THE WATER LEVEL CORRESPONDS TO THAT IN THE 400-FOOT AQUIFER

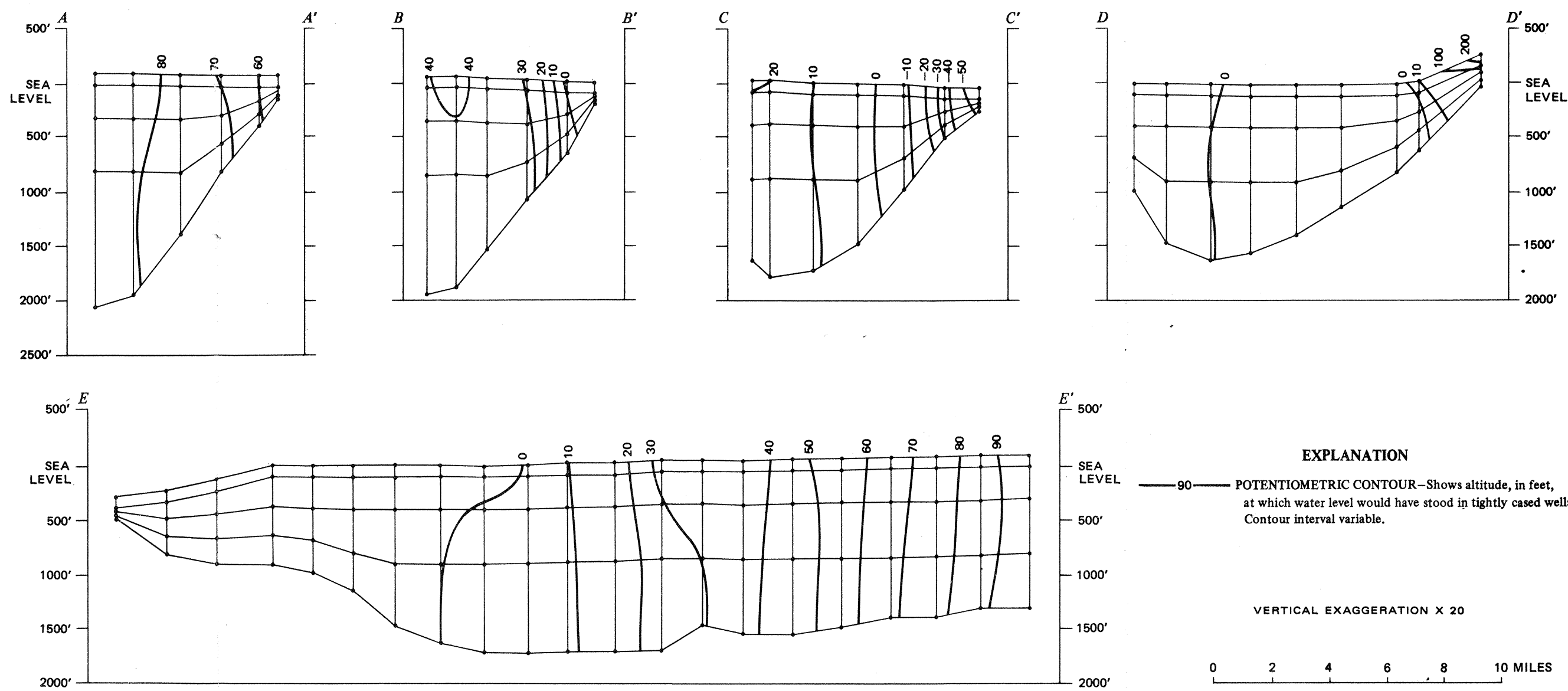


FIGURE 67.-- SECTIONS SHOWING FINITE-ELEMENT GRID FOR THE THREE-DIMENSIONAL GROUND-WATER MODEL AND TRANSIENT-STATE WATER-LEVEL CONTOURS GENERATED BY THE MODEL